IMPACT OF MAGNETIC FIELD ON HYBRID NANOFLUID FLOW IN THE PRESENCE OF CONVECTIVE BOUNDARY CONDITIONS

BY

ABDUL GHAFOOR

NATIONAL UNIVERSITY OF MODERN LANGUAGES

ISLAMABAD

December, 2023

Impact of Magnetic Field on Hybrid Nanofluid Flow in The Presence of Convective Boundary Conditions

BY

ABDUL GHAFOOR

MS Mathematics, National University of Modern Languages, Islamabad, 2023

A THESIS SUBMITTED IN PARTIAL FULFILMENT OF

THE REQUIREMENTS FOR THE DEGREE OF

MASTER OF SCIENCE

In **Mathematics**

To

FACULTY OF ENGINEERING AND COMPUTING

NATIONAL UNIVERSITY OF MODERN LANGUAGES ISLAMABAD

NATIONAL UNIVERSITY OF MODERN LANGUAGES FACULTY OF ENGINEERING & COMPUTER SCIENCE

THESIS AND DEFENSE APPROVAL FORM

The undersigned certify that they have read the following thesis, examined the defense, are satisfied with overall exam performance and recommend the thesis to the Faculty of Engineering and Computing for acceptance.

Thesis Title: Impact of Magnetic Field on Hybrid Nanofluid Flow in The Presence of Convective Boundary Conditions

Submitted By: Abdul Ghafoor **Registration #:** 35-MS/Math/F21

Master of Science in Mathematics (MS Math)
Title of the Degree

Mathematics
Name of Discipline

Dr. Anum Naseem _____
Name of Research Supervisor Signature of Research Supervisor

Dr. Sadia Riaz _____
Name of HOD (MATH) Signature of HOD (MATH)

Dr. Noman Malik _____
Name of Dean (FEC) Signature of Dean (FEC)

Date: December 6th, 2023

AUTHOR'S DECLARATION

I Abdul Ghafoor

Son of Muhammad Arif

Registration # 35-MS/Math/F21

Discipline Mathematics

Candidate of **Master of Science in Mathematic (MS Math)** at the National University of Modern Languages do hereby declare that the thesis **Impact of Magnetic Field on Hybrid Nanofluid Flow in the Presence of Convective Boundary Conditions** submitted by me in partial fulfillment of MS Math degree, is my original work, and has not been submitted or published earlier. I also solemnly declare that it shall not, in future, be submitted by me for obtaining any other degree from this or any other university or institution. I also understand that if evidence of plagiarism is found in my thesis/dissertation at any stage, even after the award of a degree, the work may be cancelled and the degree revoked.

_____

Signature of Candidate

Abdul Ghafoor

Name of Candidate

6th December 2023

Date

ABSTRACT

Title: Impact of Magnetic Field on Hybrid Nanofluid Flow in the Presence of Convective Boundary Conditions

This study aims to examine how the presence of an electrically conducting hybrid nanofluid affects the flow when the fluid is flowing over a porous surface. The study also takes into consideration the convective boundary conditions. The governing equations for the conservation of mass, momentum and energy for the hybrid nanofluid flow over the exponentially stretching surface are introduced. By employing the similarity transformation approach, the set of partial differential equations are transformed into a set of non-dimensional ordinary differential equations. The bvp4c method is utilized to solve these governing equations in order to obtain velocity and temperature profiles. The results indicate that solutions exist for cases involving the assisting and opposing flows. The study presents the findings of a boundary layer analysis considering different volume fractions of composite nanoparticles, suction/injection parameter, magnetic parameter, Eckert number and Biot number. The outcomes demonstrate that the presence of nanoparticles has a notable influence on drag force and Nusselt number within the boundary layer. Additionally, the study establishes the relationship between the variations in surface skin friction and heat transfer for both assisting and opposing flow scenarios.

TABLE OF CONTENTS

LIST OF TABLES

LIST OF FIGURES

LIST OF ABBREVIATIONS

MHD	Magnetohydrodynamics
PDEs	Partial differential equations
ODEs	Ordinary differential equations
RKF45	Runge Kutta Fehlberg
SWCNTs	Single Wall Carbon Nanotubes
MWCNTs	Multi Wall Carbon Nanotubes
Cu	Copper
Al_2O_3	Alumina / Aluminum oxide
MATLAB	Matrix Laboratory
BVP4C	Boundary Value Problem for 4^{th} Order Colocation
TiO_2	Titanium dioxide
Nu	Local Nusselt Number
Cf	Skin Friction Coefficient
SiO_2	Silicon dioxide
$C_2H_6O_2$	Ethylene glycol
Ag	Silver
H_2O	Water
KBM	Keller Box Method
GE	Governing Equation
HNF	Hybrid nanofluid

LIST OF SYMBOLS

x, y	Cartesian coordinates
$u,\ v$	Velocity components
T	Temperature
T_w	Temperature of the wall
T_∞	Ambient temperature of the hybrid nanofluid
ϕ_1	Concentration 1st nano-particle
ϕ_2	Concentration 2nd nano-particle
n_1	1st nano-particle
n_2	2nd nano-particle
ρ	Density
ρ_{n1}	Density 1st nano-particle
ρ_{n1}	Density 1st nano-particle
ρ_{nf}	Density of nanofluid
ρ_{hnf}	Density of hybrid nanofluid
μ	dynamic Viscosity
μ_{nf}	dynamic viscosity nanofluid
μ_{hnf}	dynamic viscosity hybrid nanofluid
ν	Kinematic viscosity
ν_{nf}	Kinematic viscosity nanofluid
ν_{hnf}	Kinematic viscosity hybrid nanofluid
k	Thermal conductivity
k_{n1}	Thermal conductivity of 1st nano-particle
k	Thermal conductivity of 2nd nano-particle

k_{nf}	Thermal conductivity of nanofluid
k_{hnf}	Thermal conductivity of hybrid nanofluid
c_p	Specific heat
$(\rho Cp)_{n1}$	Heat capacitance 1st nano-particle
$(\rho Cp)_{n2}$	Heat capacitance 2nd nano-particle
$(\rho Cp)_{nf}$	Heat capacitance of nanofluid
$(\rho Cp)_{hnf}$	Heat capacitance of hybrid nanofluid
β	Thermal expansion
$(\rho\beta)_{n1}$	Thermal expansion 1st nano-particle
$(\rho\beta)_{n2}$	Thermal expansion 2nd nano-particle
$(\rho\beta)_{nf}$	Thermal expansion nanofluid
$(\rho\beta)_{hnf}$	Thermal expansion hybrid nanofluid
σ	Electrical conductivity
σ_{n1}	Electrical conductivity 1st nano-particle
σ_{n2}	Electrical conductivity2nd nano-particle
σ_{nf}	Electrical conductivity nanofluid
σ_{hnf}	Electrical conductivity hybrid nanofluid
σ^*	Stefan Boltzmann constant
τ	Stress tensor
k	Thermal conductivity
B_0	Magnetic field constant
T_w	Temperature of the wall
T_∞	Ambient temperature of the hybrid nanofluid
T	Temperature
ρ_f	Density of the fluid

ν_f	Kinematic viscosity of the base fluid
q_r	Radiative heat flux
q'''	Heat generation constant
S	Suction parameter
&	And
n	Velocity index constraint
M	Magnetic field parameter
R	Thermal radiation
Ec	Eckert number
ς_1	Heat source parameter
ς_2	Heat sink parameter

ACKNOWLEDGMENT

I got no words to articulate my cordial sense of gratitude to Almighty Allah who is the most merciful and most beneficent to his creation.

I also express my gratitude to the last Prophet of Almighty Allah, Hazrat Prophet Muhammad (PBUH) the supreme reformer of the world and great educator for human being.

I extend my thanks to all those who supported and encouraged me during the course of this work. I would like to express my deep gratitude to my MS supervisor, Dr. Anum Naseem, for her valuable guidance and encouragement throughout the process of writing this thesis. Without her efforts, this undertaking would have remained incomplete. I would like to acknowledge all my teachers in the Department of Mathematics for their contributions to my education.

I offer a profound tribute to my parents for their prayers, unwavering support, encouragement, and appreciation. Their presence has been a constant source of strength and motivation.

Lastly, I would like to express my heartfelt gratitude to my father, mother, sisters, brothers and friends, who have provided me with unwavering support throughout my MS degree journey.

(Abdul Ghafoor)

DEDICATION

This thesis is dedicated to my parents, teachers, brothers and sister who always supported and nurtured me for achieving this goal. All of them have been a source of motivation and strength during moments of despair and discouragement.

CHAPTER 1

Introduction

1.1 Hybrid nanofluid

A designed fluid or suspension that blends two or more different kinds of nanoparticles with a base fluid is known as a hybrid nanofluid. Colloidal suspensions of tiny particles (also known as nanoparticles) spread in a base fluid, usually water or oil, are known as nanofluids in general. By adding nanoparticles with various compositions or qualities to produce particular desired traits or capabilities, hybrid nanofluids take this idea a step further. A few instances of hybrid nanofluids and their uses can be found in multifunctional fluids, biomedical applications, optical properties, energy storage and conversion, catalysis and environmental applications. A nanofluid is a liquid involving a base fluid with nanoparticles dispersed in it, and the nanoparticles are typically made of metallic elements, iron oxide, silicon carbide, etc. These fluids are created by adding engineered ionic concentrations of nanomaterials to the base liquid. Nanocrystals have unique properties that make them potentially useful in various thermal transfer applications, like nanoelectronics, pharmaceuticals, fusion motors, motor thermodynamic efficiency, household fridges, cooling systems, heat transfer, milling and machine tools. They offer better thermal conduction and convective heat transport than the base liquid. In 1995, Choi [1] was the first person to analyze the heat transfer capabilities of nanofluids and presented his research at the Argonne National Laboratory. This discovery led to the belief that nanofluids could be the next generation of heat transfer fluids, as they offered intriguing opportunities to enhance performance. This sparked the interest of many scientists who engaged in experimental and numerical discussions about nanofluids. However, modern times require enhanced thermal conductivity, leading to the development of hybrid nanofluids, which are currently undergoing intense investigation. These fluids have been proven to outperform traditional nanofluids in terms of effectiveness by adding two distinct nanoparticles

into water or kerosene liquids, which improves their thermal conductivities. Hybrid nanofluids showcase some of the outstanding characteristics of nanomaterials and have considerable potential for a wide range of heat exchangers, including coolants, generators, machinery, drug reduction and electronic systems. They are a synthetic mixture of ferrous, plastic, or non-metallic micro power with conventional fluids, aiming to increase the rate of heat transmission in various applications. Several researchers have shown physically and numerically that certain hybrid nanofluids have a higher rate of heat transmission compared to traditional working fluids. In terms of efficiency, experiments have shown that hybrid nanofluids perform better than nanofluids. The hybrid nanofluid brings out some remarkable properties of nanomaterials. Hybrid nanofluids have been around since the last decade **[**2, 3], and several studies have been conducted in the recent years to provide insight into their creation and application. Entropy formation of nanofluids and hybrid nanofluids in various thermal systems under various boundary conditions and physical circumstances was examined by Huminic *et al*. [4]. Entropy generation in mini-channels, entropy generation in macro-channels, and entropy generation in cavities were the three categories into which the pertinent publication was divided. Analysis was done on the impacts of temperature, flow regime, nanoparticle concentration and viscous dissipative, stream-wise, electromagnetic effects on entropy generation. The magneto-hydrodynamic flow of engine oil (base fluid) containing hybrid nanoparticles (MWCNT with MoS_4) and (SWCNT with Ag) was studied by Waqas *et al*. [5] with fluid flowing over a vertical stretching cylinder. Additionally considered are the effects of thermal radiation and viscous dissipation. To outline the physical issue, the Tiwari and Das [6] nanofluid model with the most recent thermo-physical properties and hybrid nanofluid features were taken into consideration. Moreover, contributions from numerous shape-factors were taken into account. The results of the transformed system were numerically computed using a bvp4c solver (shooting technique) in MATLAB.

1.2 Stagnation point

A point on the surface of a solid mass submerged in a stream of fluid where the stream lines diverge and face the stream is referred to as stagnation point. Fluid dynamics, aerodynamics, and engineering are just a few of the many domains where stagnation points have significant applications. Few of which are in aerodynamics, aircraft design, wind tunnel testing, heat transfer, jet engines, environmental fluid dynamics, hydrodynamics, ship design,

fluid measurement techniques and biomedical applications. The Naiver-Stokes equations governing the stagnation point flow were first investigated by Hiemenz [7] who showed how similarity transformation can reduced them to an ordinary differential equation of third order. No analytical solution to the reduced differential equation exact due to its nonlinearities, hence the nonlinear equation is often solved numerically under the guidance of two-point boundary conditions, one of which is set at infinity. Fay and Riddell [8] derived the boundary-layer equations for situations involving disassociated exterior flow. Specifically, the inclusion of molecule recombination and diffusion effects in the boundary layer was considered. The authors demonstrate that even if chemical reactions happen at a slow rate, preventing the boundary layer from reaching thermochemical equilibrium, it is possible to accurately simplify the equations at the stagnation point into a set of nonlinear ordinary differential equations. These stagnation point equations were numerically solved using two different approaches, equilibrium and non-equilibrium situation. The numerical outcomes were connected with the parameters used in the quantitative framework to reduce dependence on particular physiological hypotheses. Non-Newtonian fluids were a topic of discussion for many researchers. Thus, among the non-Newtonian fluids, the solution of the stagnation point flow for viscoelastic fluids has been given [9, 10]. Nath [11] examined the flow of a micro-polar fluid in a continuous, constant and incompressible laminar boundary layer around an endless wedge form and used fourth-order Runge-Kutta-Gill method numerically to solve the equations. The results demonstrate the influence of coupling, micro-rotation and pressure gradient parameters on the profiles of velocity and micro-rotation as well as the surface shear stress. The study also explored how the standard length of the micro-polar fluid influences the properties of the boundary layer. Hoogendoorn [12] investigated the effects of turbulence on stagnation zone using circular jets for heat transfer. The research focuses on nozzle-to-plate lengths that were close to zero. Liquid crystals had been used in a novel measurement method. The equation explained how jet roughness affected heat transfer near the stagnation point of cylinders, which is consistent with the established relationship found in the body of existing research. It was demonstrated that the corresponding increase for impinging jets at the point of stagnation was identical to that for cylinders in a stream free. Nazar *et al.* [13] investigated the stagnation point flow of a non-Newtonian micro-polar fluid with zero vertical velocity at the surface. Anuar *et al*. [14] quantitatively examined the impact of slip on stagnation point flow and heat transfer over an exponentially stretching/shrinking sheet filled with Copper-Alumina/water nanofluids and numerically resolved the system using MATLAB bvp4c function. On the flow pattern and heat transmission, the impacts of the nanoparticle volume

fraction, slip parameter and stretching/shrinking parameter have been investigated. In the case of a shrinking sheet, it was discovered that there are two possible hybrid nanofluid solutions. Copper nanoparticles and the slip parameter both contribute to a wider spectrum of solutions. In comparison to viscous fluid and other types of nanofluid, hybrid nanofluids transfer heat more quickly. The first solution was linearly stable and physically feasible, according to a stability analysis. Khashi'ie *et al.* [15] described the *Cu*-Al_2O_3/water hybrid nano-fluidic stagnation point flow with convection driven by a plate Riga. The Riga plate's electromagnet hydrodynamic (EMHD) force had an impact on the efficiency of heat transport and could be used to postpone boundary layer separation. To simplify the governing model, similarity transformation was applied and MATLAB software's bvp4c function was employed. In contrast to the buoyancy assisting and also opposing flows, which have two similar solutions, pure forced convection had a unique solution. The volumetric concentration of copper increased, which increased Nusselt number for assisting and also opposing flows.

1.3 Magneto hydrodynamic

A multidisciplinary scientific subject called magneto hydrodynamics (MHD) combines the principles of electromagnetism and fluid dynamics to explore how conducting fluids, typically plasmas or ionized gases behave when exposed to magnetic fields. MHD has uses in astrophysics, engineering, and plasma physics, among other fields. The main uses of magneto hydrodynamics can be found in astrophysical phenomena, fusion research, magnetohydrodynamic generators, plasma propulsion, geophysical phenomena, laboratory experiments and nuclear reactor safety. In the analysis of heat transfer in hybrid nanofluid flows, magnetohydrodynamics (MHD) plays a crucial role. The study done by Kandasamy *et al*. [16] looked at how the shape of the nanoparticles affects the compressed MHD movement of nanoparticles of metal in a solution made from water across a porous detector surface. In the vast majority of important investigations, three different types of nanoparticle shapes were taken into consideration. The results were determined by means of the RKF method through shooting approach. Solid volume fraction and nanoparticle shape had been found to strongly effect the squeeze flow phenomenon. When combined with a magnet field and thermal radiation energy, the use of a cylindrical *Cu*-water nanoscale and a cylinder-shaped SWCNTs-water nanoparticle enhances Nusselt number as compared to other tiny particles shapes in various flow circumstances. Hussain *et al.* [17] explored the magnetohydrodynamic flow of a

hybrid nanofluid and also took into account the thermal radiation. The bvp4c MATLAB programme was used to achieve the study's results, which involved both single- and multiwall nanofiber materials. Khan *et al.* [18] introduced hybrid nanofluids as new fluid subclasses with superior thermal properties that improve the performance of conventional fluids. The numerical calculations were carried out using the shooting method and the built-in MATLAB bvp4c function. The impact of non-linear radiation on the heat transfer characteristics of a rotating, three-dimensional, as well as magnetohydrodynamic flow of hybrid nanofluid was examined by Hassan *et al.* [19]. This flow model's surface is capable of both directions stretching. The increased energy transportation properties of hybrid liquids over mono-fluids were described by Babu *et al.* [20]. These fluids are utilized in solar collectors as well as in some military equipment's due to their improved thermal conductivity. The heat source/sink effect was discussed by Sulochana *et al.* [21] as well as regression modelling of hybrid nanofluid flow across an expanding and contracting surface. The main objective of the theoretical work is to identify the nanoparticle volume fraction that gives the highest heat transfer rate and best fits the regression model for the Nusselt number, one of the crucial factors in understanding heat exchange rate. The kinematics of a first-generation magnetohydrodynamic TiO_2 and *Ag* hybrid nanofluid flow across a porous medium were examined by Neethu *et al.* [22]. For the inquiry, heat transfer through radiation, heat dissipation, and polymerization were considered.

1.4 Mixed convection

Mixed convection is a combination of free and forced convection. Mixed convection is a type of heat transfer that occurs when both natural convection and forced convection are present in a fluid flow. Mixed convection is often encountered in practical engineering applications, such as in heat exchangers or electronic cooling systems. The characteristics of mixed convection depend on the relative strengths of the buoyancy and forced convection forces, as well as the geometry of the system and the properties of the fluid. In some cases, mixed convection can lead to more efficient heat transfer compared to purely forced or natural convection alone. However, the complexity of mixed convection can also make it difficult to predict and analyze, requiring sophisticated modeling techniques to totally comprehend its conduct. In a study, thermophoresis and Brownian motion were investigated in relation to the separation of layer flow across an exponentially stretched surface under a convective condition by Mustafa *et al*. [23]. Nadeem *et al.* [24] looked at the flow composed of water nanofluid in

three dimensions across a sheet that was geometrically extending. They discovered that the Nusselt number was reduced by the temperature exponent restriction and convection parameters increase the Nusselt number and temperature of nanofluids. Ghalambaz *et al.* [25] investigated the flow and heat transfer properties of a hybrid nanofluid made up of $Al_2O_3 - Cu$ particles in water over a plate that was vertical. *Cu-*Al_2O_3/water hybrid nanofluid was the main emphasis of Jamaludin *et al.* [26] and they studied the problem addressing conduction and convection stagnation point flow and heat transfer across a porous extending/lessening surface with the heat source/sink effects and magnetic field. The similarity transformations were used to change the mathematical models of the problem into simplified equations and then the ODEs were resolved precisely utilizing the MATLAB function bvp4c. Analysis of mixed convective and magnetohydrodynamic flow over a porous vertical surface was done by Wahid *et al.* [27]**.** Two different kinds of nanoparticles, namely copper and alumina, were hybridized for the study. With the help of the bvp4c scheme, the equation system was solved. In order to execute their flow research, Khan *et al.* [28] looked into thin film flow and examined a stretched surface. The major contributions of Marangoni convection, magnetohydrodynamics and viscous dissipation changed the flow properties and assisted in producing the desired outcomes. The flow assumptions result in improved heat transmission.

1.5 Thermal radiation

The thermal radiation is also termed as infrared radiation or heat radiation. It is considered to be form of radiation that can a material can emit if it as at a temperature beyond absolute zero. The thermal molecular motion can result into thermal radiation. It is a basic concept in the field of physics and its applications can be observed in wide variety of areas like engineering, environmental sciences or astronomy. Infrared thermography, infrared heating, remote sensing, medical imaging, space exploration and environmental monitoring are a few applications where thermal radiation can be seen. Yoo *et al*. [29] conducted a study on the heat transfer properties of TiO_2, Al_2O_3 and *Fe* nano-liquids, which revealed a notable enhancement in the heat transfer properties when compared to the base fluids. In a rotating system between two surfaces, Chamkha *et al.* [30] investigated heat transmission and MHD flow of a mixed convective nanofluid. The structure's upper and bottom plates were thought to be permeable and extensible. The significant effects of thermal radiation and Joule heating were taken into account. The significance of a thermally radiative hybrid nano-fluid moving across an extended

sheet in relation to the impact of a heat source or sink was examined by Waqas *et al.* [31]. A numerical description of a hybrid nanoparticle flow over a region that was enlarging and contracting while heat radiation took place was found by Mahabaleshwar *et al*. [32]. Salahuddin *et al.* [33] used the implicit finite difference method to analyze the thermal radiation impact of an incompressible hybrid nanofluid. The exceedingly difficult and nonlinear partial differential system's numerical solution proved that hybrid nanofluid outperformed mono nanoparticles in terms of thermal performance. Yasir *et al.* [34] looked at heat transmission as well as the flow properties of a hybrid nanofluid created by an extending/lessening sheet.

1.6 Contributions to the Thesis

In this thesis, a review study of Rehman *et al.* [80] has been presented and then the flow analysis has been extended with impact of MHD on hybrid nanofluid flow with convective boundary conditions. The main focus is the numerical analysis of MHD hybrid nano-liquid flow via an exponentially extending surface in the presence of a convective boundary conditions and magnetic field. Through the use of similarity transformations, the proposed nonlinear PDEs are transformed into a system of ODEs. The MATLAB software is utilized to construct the table and graphs which illustrate the numerical results. In-depth discussion is done by the effects of dimensionless factors on $f'(\eta)$, $\theta(\eta)$, $f"(0)$ and $\theta'(0)$. Tables and graphs are used to present the results.

1.7 Thesis Organization

The information below gives a quick summary of the thesis contents.

Chapter 1 is an introductory chapter and provides a brief overview of the important concepts used in the thesis and the research carried out on these concepts.

Chapter 2 covers the existing literature available on the ideas and assumptions that are a part of executed research work. This chapter delivers the previous studies done by the researchers based on the necessary concepts used.

Chapter 3 provides some fundamental definitions, dimensionless parameters, which are used during the research to obtain the numerical results of the flow problem.

Chapter 4 presents a complete review for the hybrid nanofluid flow via an exponentially stretching sheet with a heat generation/absorption and thermal radiation. MATLAB, bvp4c technique is utilized to find the numerical outcomes of the governing flow equations.

Chapter 5 extends the review work by considering the impact of magnetic field for hybrid nanofluid flowing due to a permeable surface which is stretching exponentially. The study has been performed by considering thermal radiation, heat sours/sink, convective boundary conditions and stagnation point. By utilizing similarity transformations, the set of governing nonlinear PDEs are transformed into the nonlinear ODEs. The results for various parameters are discussed through graphs and tables.

Chapter 6 gives the final remarks about the whole research work and the future work that can be performed from this research.

References consulted for this thesis are listed in the Bibliography.

CHAPTER 2

Literature Review

2.1 Hybrid nanofluid

When distinct nanoparticles are combined to form a hybrid nanofluid, a synergistic effect occurs where the unique qualities of the individual nanoparticles interact to produce improved or customized properties. The production of solar energy, electronic gadgets, heating systems, mechanical operations, etc. all benefits from the use of hybrid nanotubes. The numerical solutions for *Cu-*Al_2O_3/H_2O oblique flow of stagnation-point across a contracting surface was computed by Yahaya *et al.* [35] and the algorithm yields dual solutions utilizing the bvp4c solver. The stability analysis indicated that the initial solution had positive smallest eigenvalues, signifying stability. Furthermore, the introduction of Al_2O_3 nanoparticles into the *Cu-*H_2O nanofluid demonstrated a 4.798% increase in the local Nusselt number, while concurrently reducing the skin friction coefficient by 37.753%. Hussain *et al.* [36] investigated the flow's heat transmission characteristics. To achieve the desired results, a recently discovered concept of hybrid nanofluid was used. The flow of hybrid base nanoliquid through a rotating surface that was rapidly stretching was the subject of this work. The basic fluid is a (50%/50%) combination of ethylene glycol and water and the discussion of thermo-physical characteristics was executed. The analysis of related parameters reveals that hybrid base nanofluid performs better than nanofluid but the right choice of composition was essential. For TiO_2 and *CuO*-hybrid based fluid, graphical representation shows that the curve velocity declines when the rotation parameter was increased. Othman *et al.* [37] described the flow and heat transfer behaviors of a hybrid nanofluid with carbon nanotubes on a porous exponentially shrinking surface. In addition to this, the influences of a heat source/sink and magnetic field were examined. Employing a similarity solution to transform the PDEs model into ODEs and using MATLAB's bvp4c, these equations were numerically resolved. Wahid *et al.* [38] described a computational model and analysis used to examine the separation flow of a hybrid nanofluid and heat transfer caused by an exponentially permeable extending/lessening curved surface. The solution of ODEs was made easier by the bvp4c tool. The plots showing how

certain parameters affect physical quantities were also included, along with a comparison of the results for validation purposes. It was found that as the volume fraction coefficient for copper and curvature parameters increased, boundary layer separation was extended. Dual solutions were examined and the hybrid nanofluid flow's first solution was seen to be stable. The knowledge of nanomaterials with steady thermal effects was familiarized by Chu *et al.* [39]. For a two dimensional unstable flow caused by a porous extended sheet, the thermal assessment of a hybrid nanofluid including four different kinds of nanoparticles, subjected to inclined magnetic field and non-uniform heat source/sink had been numerically examined. Copper, titanium dioxide, silver and aluminum oxide nanoparticles, as four varieties had all been taken into account while using water as base fluid. The governing PDEs were transformed into the ODEs with the usage of similarity conversion. A numerical method identified as the KBM was utilized to solve these similarity equations. In general, the study of hybrid nanofluids offer hypothesis that scientists and engineers can use to guide parameter adjustments in order to meet their optimal goals for the relevant practical applications. Khashi'ie *et al.* [40] looked at the electro-magneto-hydrodynamic (EMHD) and heat generation affected USSP flow on a Riga plate. Al_2O_3 and *Cu* nanoparticles were also present in the fluid. The energy and momentum equations constituted the flow model. The similarity variables were then used to simplify these equations. The bvp4c function produces the numerical results, which were displayed in graphs and tables. Through an exponentially permeable extended sheet, a comparison was done for the flow of a $Al_2O_3 + Ag\ /H_2O$ hybrid nanofluid with a Al_2O_3-H_2O mono nanofluid based by Chakraborty *et al.* [41]. Under the influence of thermal radiations, fluctuating magnetic flux and uneven heat generation, the sheet was submerged in a non-Darcy absorbent medium. DTM was used to obtain the analytical solution, while fifth-order RKF with shooting process generated the numerical solution.

2.2 Stagnation point

According to the principles of fluid dynamics, a stagnation point is a particular location in a flowing fluid where the fluid's velocity falls to zero as a result of the opposing forces that are driving its motion. It is where the fluid temporarily stops moving or becomes stagnant. Stagnation points are frequently observed in the study of fluid flow around solid objects like airfoils, automobiles, and ships, where it is necessary to comprehend the fluid flow to forecast aerodynamic or hydrodynamic behaviors. Stagnation points are significant because they

frequently coincide with regions of high pressure. Arani *et al.* [42] investigated the hybrid *Ag-CuO/water* nanofluid stagnation-point flow across the lessening/extending surface. With suitable transformation, the complicated equations were converted to ODEs. The DEs were unraveled by means of the RKF45 method. This numerical investigation revealed the survival of dual solutions, which were related toward the particular values of the shrinkage rate. The study demonstrated that with the suction/injection parameter, the resistance factor of Ag/H_2O increased through around (35–50) %. According to time-dependent steadiness analysis, simply the top branch of results was steady in real physics, whereas the lower branch was unstable**.** According to Teh *et al.* [43] analysis, the hybrid nanofluid had a sizable number of real-world applications. In comparison to nanofluids containing a single type of nanoparticle, hybrid nanofluids had been discovered to have a superior capacity for heat transfer but with additional physical presumptions surrounding the fluid flow, it might be possible to further investigate the properties of heat transfer rate involving hybrid nanofluids in higher-dimensional space. The Tiwari-Das model was used to investigate the three dimensional hybrid flow with spinning extending/lessening sheets with the effects of magnetic field and joule heating. Abbasi *et al.* [44] discussed and compared the results stagnation point flow for hybrid model and conventional nanofluid model, improved hybrid nanoparticles heating. The thermal contrast of three diverse types of nanoparticles, including SiO_2,Al_2O_3 and TiO_2 in suspension with base liquid $C_2H_6O_2$. The numerical Keller box outcomes were achieved and used to execute the comparison. Alqahtani *et al.* [45] explored the stagnation point flow and energy transport for the nanofluid with the significant effect of magnetohydrodynamics and a nonlinear thermal radiation. The Brownian motion and in addition thermophoresis phenomena for the nano-fluidic model was a part of the study. The flow of ternary hybrid nanofluid for Homann stagnation-point was inspected by Sarfraz *et al.* [46]. The fluid was moving over an over a spiraling disk and the study was conducted with the effect of magnetic field.

2.3 Magneto hydrodynamics

MHD entails the investigation of the relationship between magnetic fields and ionized fluids. It explores how the magnetic field can interact with the phenomena of fluid. The Lorentz force, originates due to the moving charged particles and the magnetic field itself, thus giving rise to the significant magnetohydrodynamics. Aly *et al.* [47] described magnetohydrodynamics, suction and radiation effects used to study the flow of $Cu\text{-}TiO_2/H_2O$

across a nonlinear stretched sheet. The flow controlling PDEs using the suitable similarity conversions were converted to ODEs and a mathematical method, CPSDM was used to solve these equations. The features of a two dimensional uneven nanofluid flow across a transparent exponential elastic sheet were examined by Kumar *et al.* [48]. The effect of variables including the magnetization parameter, thermal rays, and the presence of a random heat source or sink was also investigated. The PDEs which are the dimensional equations were changed into ODEs by utilizing the suitable transformations. The reframed ODEs were mathematically solved using the computer programme MATLAB and the bvp4c package. The skin friction was found to increase when the magnetic field parameter improved in an absolute sense. *Cu-*Fe_3O_4 */*$C_2H_6O_2$ hybrid nanofluid flow across an elongating sheet with an angled thermal radiations, partial slip and magnetic field was studied by Unyong *et al.* [49] to determine the effects of the important parameters on the flow. A hypergeometric function was used to analytically solve the dimensionless form of the fluid model. The main findings of research paper include that the presence of inclined magnetic field can enhance the amount of heat conduction in *Cu-*Fe_3O_4 */*$C_2H_6O_2$ hybrid nanofluid. Joshi *et al.* [50] performed *Cu-Ag /*H_2O-$C_2H_6O_2$ hybrid nanofluid MHD flow via a pliable surface in Darcy Forchheimer absorbent medium as well as the mutual effects of heat radiation and suction/blowing were investigated. In the scientific modelling of principal equations, the boundary layer approximation and Cartesian coordinate structure were both employed and RKF technique was used to unravel the results. The graphs were used to scrutinize the physical influence of relevant limitations on the flow. Khan *et al.* [51] reflected the presence of two dimensional MHD, viscous dissipation, Joule heating and slip condition for an incompressible non-liquids flowing towards a permeable stretched sheet. The model also involved the utilization of the effects of convective conditions, mass suction and heat suction/blower. *Cu* nanoparticles were combined with H_2O to create the nanoliquid and the solution was found using the bp4c scheme. Based on various estimates of the relevant parameters, the various results the reduction of heat transfer rate with Hartman and Eckert numbers. Babu *et al.* [52] studied cross nano-fluid's radiative mobility through an exponentially stretchable sheet near the stagnation point through variable heat sources/sinks and handled the presence of magneto-hydrodynamics. It was assumed that thermophoresis & Brownian motion effects exist. The prevailing equations for this study were first transformed via similarity transformation as a system of ODEs. The effects of a number of important characteristics, such as regular profiles (temperature, velocity and concentration) were explained using the RK 4th order mechanism. According to the performed investigation, the magnetic field raised the temperature profile of the Cross nanofluid while lowering its velocity.

2.4 Mixed convection

The significant phenomena of mixed convection can be seen in numerous scientific and engineering applications. Its role in many purposes relates its thorough understanding for optimizing the performance, safety and efficiency of innumerable systems. Ellater *et al.* [53] addressed the continuous and mixed convective flow of hybrid nanofluid that conducts electricity across a stretchable impermeable sheet. The properties of changing magnetic fields, heat generation and chemical reactions were all taken into account in the flow distribution. In order to increase the competence and effectiveness of thermal energy transmission for a diversity of industrial and biotic reasons, a computational model was constructed. The working fluid water contains *Ag* and *MgO* nanomaterials in the hybrid nanofluid. A system of PDEs had been used to express the scenario which were then later simplified. The acquired first order DEs were evaluated by means of the computing method PCM. Aimed at consistency and validity checks, the results were compared to existing literature and the bvp4c package. Haq *et al.* [54] described a Newtonian hybrid nanofluid flow containing *Cu* and Al_2O_3 nanoparticles through a stretched surface and the flow had undergone mixed convection. Also taken into account were the velocity and thermal slip conditions. The fluid flow had been examined in terms of the effects of viscous dissipation, Brownian motion, thermophoresis diffusion, heat absorption and thermal radiation for the intended outputs. To further control the flow stream, a magnetic field was applied at an inclined angle. Hansda *et al*. [55] examined the involvement of thermo-solute mixed convection and magnetic field applied at an angle for a hybrid nanofluid flow. The flow was conducted in a wavy enclosure which was partially heated. A compact scheme was established to model the governing equations and the outcomes were shown as Sherwood number, Nusselt number and streamlines and the flow was studied for numerous parameters. The entropy generation for mixed convective flow of hybrid nanofluid was inspected by Mamun *et al*. [56]. The research was carried out by changing the magnetic fields and the flow was considered to be moving because of the rotating cylinders. The fluid comprises of water as base fluid and three different types of nanoparticles, *Cu*, *SWCNT* and Al_2O_3 were employed and their effects on the flow was recorded. Lone *et al.* [57] depicted mixed convection phenomena for hybrid nanofluid flow because of the rotating sphere with the addition of thermal radiation effect. The model equations for the flow was solved analytically via homotopy analysis method.

2.5 Thermal radiation

Thermal radiation is an important topic for the various fields including fluid dynaimcs. Its study leads to advanced solutions for numerous tasks. Wang *et al.* [58] performed the entropy-optimized analysis for thermally radiative Darcy-Forchhiemer nanofluid flow across a permeable medium. The stretching of the surface is responsible for initiating the flow and heat expression also included viscous dissipation. SiO_2 and *AlOOH* are regarded as nanoparticles and $C_3H_8O_2$ was regarded phase molten in this instance. Through the use of appropriate dimensionless variables, nonlinear ordinary dimensionless form was created. The ND-solve method was used to numerically solve the obtained dimensionless expressions. For SiO_2 & *AlOOH* nanoparticles, Bejan number, temperature, velocity profile & graphical features of entropy rate against flow variables were examined. The thermal transfer rate improved with an increase in radiation. According to research completed by Zainal *et al.* [59], the focus was on the flow near a porous extending/lessening Riga plate and Al_2O_3-*Cu/H₂O* was the considered nanofluid. The bvp4c procedure was used in the MATLAB system to solve the simplified mathematical model. Once the appropriate assumptions were made, this solution technique can generate several solutions. Wahid *et al.* [60] examined the *Al₂O₃+Cu /H₂O* mixed convective hybrid nanofluid flow via an angled lessening plate using thermally radiative magneto-hydrodynamic (MHD) theory. The PDEs of the flow model were transformed into ODEs via incorporating similarity revolutions. The mathematical solution of the mathematical model was implemented using bvp4c. There were two conceivable solutions because of the plate's motion. A stability investigation had determined that the first solution was stable. As a result, the first solution can be used in real practical applications. Arif *et al*. [61] considered base fluid to be engine oil and different nanoparticles exhibiting different shapes were dispersed, thus a tri hybrid nanofluid was constructed. The Jeffery fluid was set to motion due to a vertical plate within a rotating surrounding. The numerical results were gained using a Laplace transform approach.

Chapter 3

Basic Definitions and Equations

This chapter includes several common definitions and rules to help readers better comprehend the analyses in the next chapters.

3.1 Continuum mechanics

A branch of mechanics that deals with the behavior of materials and fluids as continuous substances, rather than discrete particles. It provides a mathematical framework for studying the mechanics of deformable bodies and fluid flows by considering them as continuous media. Continuum mechanics focuses on describing the macroscopic behavior of materials under the influence of forces, including their deformation, motion, stress and strain. It involves concepts such as stress, strain, conservation laws, constitutive equations and equations of motion, which enable the analysis and prediction of the mechanical behavior of solids and fluids on a macroscopic scale. Applications of continuum mechanics can be found in various fields, including engineering, physics, materials science and geophysics. [63]

There are two types of continuum mechanics:

3.1.1 Solid mechanics

A branch of continuum mechanics that focuses on the analysis of the behavior of solid materials under the influence of external forces. It deals with the analysis of the mechanical properties, deformation, and response of solid objects to various types of loads. Solid mechanics involves the study of stress, strain, elasticity, plasticity, fracture mechanics and the mechanical behavior of materials. [63]

3.1.2 Fluid mechanics

An important branch of engineering and physics that involves the behavior of fluids, including liquids, plasmas and gases. It comprises study of fluid motion, forces acting on fluids, and the physical properties of fluids such as density, pressure and viscosity. Fluid mechanics is essential for understanding and analyzing the flow of fluids in various applications, ranging from everyday phenomena like water flow in pipes to complex processes such as aerodynamics and ocean currents. Applications of fluid mechanics can be found in a wide range of fields, including aerospace engineering, civil engineering (for analyzing water flow in rivers and pipes), chemical engineering, environmental engineering and meteorology. It is fundamental for designing efficient systems, such as pumps, turbines and heat exchangers, as well as for understanding natural phenomena like weather patterns and ocean currents. [63]

Fluid mechanics can be divided in to three categories:

3.1.2.1 Fluid statics

The well-known branch in fluid mechanics that is associated with fluids at rest, rather than in motion. It is also known as hydrostatics and pressures while remaining stationary. Another important concept in fluid statics is the hydrostatic equation, which relates the pressure of a fluid at a certain depth to the weight of the fluid above that depth. This equation is consequent from the law of conservation of mass and can be used to calculate the pressure at any given depth in a fluid. Fluid statics has many practical applications, such as in the design of dams, water tanks, and other structures that hold or transport fluids. It is also used in medical applications, such as measuring blood pressure and monitoring intravenous fluid infusion rates. [63]

3.1.2.2 Fluid kinematics

A significant branch of fluid mechanics concerning the fluid’s motion irrespective of the forces responsible for motion. It is concerned with describing and analyzing the characteristics of fluid flow, such as velocity, deformation and acceleration. One of the key

concepts in fluid kinematics is the motion of a fluid particle. A fluid particle is a small volume of fluid that moves with the fluid flow. By tracking the motion of fluid particles, insights into the characteristics of the fluid flow can be gained, such as its velocity and acceleration. Fluid kinematics is also related with describing the geometry of fluid flow including the shape and size of fluid elements as they move through a flow field. This is important for analyzing the behavior of fluids in different utilities such as in the design of hydraulic systems or the study of ocean currents. [63]

3.1.2.3 Fluid dynamics

Fluid dynamics relates fluids in motion with the forces acting on them. It is the analysis of fluids (liquids, gases, and plasmas) in motion. It is a sub-discipline of fluid mechanics, a branch of physics dealing with the behavior of fluids either at rest or in motion as well. It is an important field of study with applications in countless fields, including aerospace engineering, mechanical engineering, chemical engineering, environmental engineering, geophysics and meteorology, among others. The study of fluid dynamics involves understanding the physical properties of fluids, such as viscosity, density and pressure and how they behave in response to external forces such as gravity or fluid flow. Key concepts in fluid dynamics include Bernoulli's principle, Navier-Stokes equations, Reynolds number, turbulence and boundary layers. Applications of fluid dynamics range from the design of aircraft and spacecraft to the study of ocean currents and weather patterns. Some common examples of fluid dynamics in action include the flow of blood through the human body, the flow of water through pipes and channels and the behavior of fluids in engines and turbines. [64]

3.2 Fluid

"Fluid" typically refers to a material that can flow and can attain the shape of its vessel. It is referred to be a state of matter, distinct from solids and gases. Fluids can include liquids, such as water, oil or milk, as well as gases, such as air or helium. Fluids possess unique properties, including the ability to exert pressure evenly in all directions, known as hydrostatic pressure. They also exhibit viscosity, which refers to their resistance to flow. Viscosity can vary among different fluids, with some being more "thick" or resistant to flow (high viscosity) and others being more "thin" or easily flowing (low viscosity).

Fluid dynamics is the observation that how fluids act and interrelate with forces, such as when they flow through pipes or around objects. This field of study encompasses various phenomena, including turbulence, Bernoulli's principle and the conservation of mass, momentum and energy. Fluids have numerous applications in everyday life and various industries, including transportation, engineering, medicine and meteorology. They play a crucial role in hydraulic systems, cooling mechanisms, blood circulation, weather patterns and many other processes. Liquids are a typical type of fluid that has possess fixed volume while they have no permanent shape. They are almost incompressible and can flow easily, conforming to the form of the container. Examples of liquids comprise of oil, water and blood. Gases are another type of fluid that possess neither a certain shape nor a certain volume. They are extremely compressible and can broaden to fill up their vessel. Examples of gases comprise of helium, air and carbon dioxide. Fluids exhibit a variety of interesting behaviors, including viscosity, surface tension and fluid flow. These properties are vital in numerous areas of science and also engineering, comprising fluid dynamics, thermodynamics and materials science. [62]

3.3 Field

A field is a measurable characteristic that is assigned to a specific value at every point in space and time. Fields are used to describe various types of physical phenomena, such as the electric and magnetic fields, the gravitational field and the temperature field. Fields are often represented using mathematical equations that describe how the field varies with respect to position and time. For example, the electric field can be described by Coulomb's law, which relates the electric field strength to the charge and distance between two objects. Fields are important in many areas of physics, including electromagnetism, quantum mechanics and general relativity. They are also used in engineering and technology, such as in the design of electrical circuits, antennas and sensors. In addition to the physical fields, there are also abstract fields in mathematics, such as vector fields, scalar fields and tensor fields. These mathematical fields can be used to model and analyze physical phenomena in various fields of science and engineering. [62]

There are three types of fields:

3.3.1 Scalar field

A scalar field is a type of field in physics that associates a scalar value with each point in space and time. A scalar quantity is a physical quantity that only has magnitude, such as temperature, pressure or mass. In the context of a scalar field, these scalar values can vary throughout space and time, creating a continuous distribution of the scalar quantity. This allows for the representation and analysis of scalar quantities that change smoothly and continuously across different points in a given region. A scalar field can be represented statistically using a scalar-valued function that depends on the spatial coordinates of the points in the field. For example, the temperature in a room can be described as a scalar field, with the temperature at each point in space given by a scalar value. Scalar fields are also used in the study of particle physics and cosmology. In particle physics, the Higgs field is a scalar field that is responsible for giving mass to elementary particles. In cosmology, scalar fields are used to describe the inflationary period of the early universe, where a scalar field caused a rapid expansion of space. [62]

3.3.2 Vector field

A vector field is a concept in physics that assigns a vector quantity to each point in space and time. Unlike scalar fields, which have only magnitude, vector fields have both magnitude and direction. At every point in the field, there is a unique vector associated with it. The vectors in a vector field can represent physical quantities such as velocity, force or electric field strength. Vector fields are used to describe and analyze various phenomena in physics, including fluid flow, electromagnetic fields and gravitational fields. They provide a way to understand how these quantities change and interact throughout space and time. By examining the behavior of vector fields, scientists and engineers can gain insights into the underlying dynamics and properties of the systems they represent. A vector field associates a vector to each point in a subset of space. A vector field can be represented mathematically using a vector-valued function that depends on the spatial coordinates of the points in the field. For example, the wind velocity at each point in the atmosphere can be designated as a vector field, with the wind speed and direction given by a vector value. Vector fields are used in many areas of physics, such as in the study of fluid dynamics, electromagnetism and gravitational fields. [62]

3.3.3 Tensor field

A tensor field is a mathematical concept that assigns a tensor to every point within a given space, e.g. Cauchy stress tensor. A tensor is a mathematical object that generalizes the concept of a vector to multiple dimensions and it can represent various types of physical quantities, such as stress, strain or curvature. Tensor fields can be represented mathematically using a tensor-valued function that depends on the spatial coordinates of the points in the field. Tensor fields are important in many areas of mathematics and physics because they provide a powerful framework for representing and analyzing complex physical phenomena that involve multiple dimensions and varying magnitudes and directions. [63]

3.4 Stress

Stress, in the context of physics and mechanics, refers to the internal forces or pressure exerted within a material or object. It is a measure of the internal resistance to deformation or change in shape. Stress can be caused by external forces applied to an object or by internal forces within the material itself. Stress is typically described in terms of its magnitude and direction. The direction of stress indicates the orientation of the internal forces within the material. There are different types of stress, including tensile stress, compressive stress and shear stress. Stress is an important concept in fields such as engineering, materials science and structural analysis. The idea of managing stress within materials and structures is crucial for designing safe and reliable systems. In mathematics, stress is given by

$$Stress(\sigma) = \frac{Force(F)}{Area(A)}, \tag{3.1}$$

where σ, F and A is the stress applied, force applied and area of the force application. The SI units of stress are N/m^2. [63]

The types of stress are:

3.4.1 Tensile stress

Tensile stress is the term used to describe the external force applied to a material per unit area, leading to the elongation or stretching of the material. [63]

3.4.2 Compressive stress

Compressive stress refers to the force exerted on a material that causes it to deform, resulting in a reduction in the material's volume. [63]

3.5 Strain

Strain is a measurement of the extent to which a body deforms in the direction of an applied force, expressed as the ratio of the deformation to the original dimensions of the body.

$$Strain(\epsilon) = \frac{Change\ in\ length(\delta l)}{Original\ length(L)}, \tag{3.2}$$

where ϵ, δl & L is the strain due to the stress applied, change in length and original length of the material. [63]

The types of strain are as follows:

3.5.1 Tensile strain

Tensile strain is the term used to describe the elongation or deformation of a solid body when subjected to a tensile force or stress. Essentially, tensile strain occurs when a body undergoes an increase in length as external forces attempt to stretch it. [63]

3.5.2 Compressive strain

Compressive strain refers to the deformation or change in shape of a solid caused by the application of compressive stress. Simply, compressive strain occurs when a body experiences a reduction in length as equal and opposite forces attempt to compress or squeeze it. [63]

3.6 Viscosity

Viscosity is a resistance of a fluid (liquid or gas) to a change in shape or movement of neighboring particles relative to one another. The two ways of describing viscosity are as follows. [65]

3.6.1 Dynamic viscosity (μ)

The dynamic viscosity of a fluid is the measure of its resistance to flow when an external force is applied.

$$\mu = \frac{\text{shear stress}}{\text{velocity gradient}}. \tag{3.3}$$

The SI unit designated for dynamic viscosity is $\frac{Ns}{m^2}$ or can be expressed as $\frac{kg}{ms}$. [65]

3.6.2 Kinematic viscosity

The kinematic viscosity is defined as the absolute viscosity of a liquid divided by its density at the same temperature.

$$\upsilon = \frac{\mu}{\rho}. \tag{3.4}$$

The SI unit labelled for dynamic viscosity is $\frac{m^2}{s}$. [65]

3.7 Newton law of viscosity

The associated statement implies that exerted shear stress exerted on fluid is considered to be directly and proportionally related to the velocity gradient. In other words, as the velocity gradient increases, the shear stress on the fluid also increases in a linear manner. The mathematical formula is stated as

$$\tau \propto \frac{du}{dy}, \tag{3.5}$$

$$\tau = \mu \frac{du}{dy}, \tag{3.6}$$

where τ denotes shear stress applied on the fluid element. [65]

3.8 Newtonian fluid

A Newtonian fluid is a type of fluid that follows Newton's law of viscosity. The Newtonian fluid is assumed as type of fluid in which the relationship between the shear stress with rate of deformation (or shear rate) is linear and proportional. Most common fluids, such as water, air and many oils, can be classified as Newtonian fluids. In these fluids, the viscosity can be described by a single constant called the dynamic viscosity. The behavior of Newtonian fluids is important to understand in many areas of engineering and science, as it is often necessary to model or predict the flow behavior of these fluids in innumerable applications like the behavior of Newtonian fluids is important in the design of pipes, pumps and other fluid-handling equipment. [65]

3.9 Non-Newtonian fluid

This is the fluid which don’t observe the Newton’s law of viscosity. These fluids are the fluids whose viscosity or flow behavior is not described by the classical laws of fluid mechanics developed by Sir Isaac Newton. In other words, the relationship between the shear stress and the rate of deformation of the fluid is not linear, as it is for Newtonian fluids. The conduct of non-Newtonian fluids is additionally complex than that of Newtonian fluids and can differ subjected to elements such as shear rate, temperature and composition. These fluids can reveal

a kind of dissimilar behaviors, such as shear-thinning (where viscosity decreases with increasing shear rate), shear-thickening (where viscosity increases with increasing shear rate) and viscoelastic behavior (where the fluid exhibits both elastic and also viscous properties). Examples of non-Newtonian fluids include suspensions, emulsions, gels and polymers. Non-Newtonian fluids are commonly encountered in a variety of industrial, medical and biological applications, such as in food processing, pharmaceuticals, cosmetics and biomedical engineering. [65]

3.10 Flow

It is described as measure of fluid which passing a particular point per unit time. In fluid mechanics, flow mentions to fluid's movement, through a system or over a body. The study of fluid flow is important in many areas of science and engineering, as it plays a critical role in a wide range of processes and applications. The knowledge of fluid flow can help scientists and engineers to design optimize systems and devices that involve fluid motion, such as pumps, turbines, heat exchangers and aircraft. The study of fluid flow is a complex and fascinating field that has applications in many areas of science and engineering and is essential for understanding and optimizing the behavior of a wide range of systems and devices. [65]

3.10.1 Compressible flow

This type of flow refers to fluid flow in which the fluid density changes significantly as it flows through a system or over a body. In other words, changes in fluid velocity or pressure are accompanied by changes in fluid density due to the compressibility of the fluid. It is important in many fluid systems, particularly those involving high velocities or changes in pressure or temperature. For example, compressible flow might be important in the design of supersonic aircraft or rocket engines, where the flow velocities are very high and the fluid is subjected to large changes in pressure and temperature. Compressible flow is more complex than incompressible flow and it requires more sophisticated mathematical models to accurately predict system behavior. The equations governing compressible flow take into account the effects of fluid density changes and the associated changes in temperature and pressure that occur as a result. [65]

3.10.2 Incompressible flow

This category of flow refers to fluid flow in which the fluid density does not change significantly as it flows through a system or over a body. In other words, the fluid can be treated as having a constant density and changes in fluid velocity or pressure are not accompanied by changes in fluid density. Incompressible flow is a common assumption made in the analysis of fluid systems and it is often used in engineering and science as a starting point for more complex analyses. For example, incompressible flow might be assumed in the design of a pump or a turbine, where the fluid is flowing at low speeds and with small changes in density. Incompressible flow is useful because it simplifies the mathematical equations governing fluid flow, allowing engineers and scientists to make predictions about how fluids will behave in different systems. However, it is important to recognize that many fluids are not truly incompressible and that changes in density can be important in some cases.

In general, incompressible flow is a good approximation for fluid systems that are flowing at low speeds or are subjected to small changes in pressure or temperature. For more dynamic systems or systems that are subjected to large changes in pressure or temperature, compressibility effects may need to be taken into account to accurately predict system behavior. [65]

3.10.3 Steady flow

In this kind of flow, the velocity vector along with the other fluid's features don't alter with time in a fluid. Steady flow refers to fluid flow in which pressure, velocity or other flow features do not change with time or over time. In other words, the fluid is flowing at a constant rate and with uniform characteristics in all regions of the flow and the flow properties remain constant over time. Steady flow is a simplified and idealized model of fluid flow and it is often used in engineering and sciences as a starting point for more complex analyses. For example, steady flow might be assumed in the design of a pipeline or a duct system where the fluid is flowing steadily and without significant changes in velocity or pressure. In general, steady flow is a good approximation for fluid systems that are in equilibrium and are subjected to slowly varying conditions. For more dynamic systems or systems that are subjected to rapid changes

in boundary conditions, unsteady or transient flow models may be necessary to accurately predict system behavior. [65]

$$\frac{\partial V}{\partial t} = 0 \, , \frac{\partial \rho}{\partial t} = 0 \, , \frac{\partial P}{\partial t} = 0. \tag{3.7}$$

3.10.4 Unsteady flow

The velocity vector and other fluid properties change with time in a fluid. Unsteady flow refers to fluid flow in which the velocity, pressure or other flow properties vary with time or over time. In other words, the fluid is not flowing at a constant rate or with uniform characteristics in all regions of the flow and the flow properties are changing over time. Unsteady flow can occur in many different contexts, such as in fluid systems that are subjected to changes in boundary conditions or in natural flows that are affected by changing environmental factors. For example, the flow of water in a river might be unsteady due to changes in the water level or flow rate or the flow of air in a ventilation system might be unsteady due to changes in temperature or humidity. The unsteady flow is important in many areas of engineering and science, as it plays a critical role in the design and optimization of many natural and engineered systems. Sophisticated mathematical and computational models are often used to simulate and analyze unsteady flow, helping engineers and scientists to design more efficient and effective systems. [65]

$$\frac{\partial V}{\partial t} \neq 0 \, , \frac{\partial \rho}{\partial t} \neq 0 \, , \frac{\partial P}{\partial t} \neq 0. \tag{3.8}$$

3.10.5 Uniform flow

The density, velocity and pressure don’t change from one point to the other point in the fluid. This flow refers to fluid flow in which the velocity, pressure or other flow properties are constant throughout the flow domain. In other words, the fluid is flowing at a constant rate and with uniform characteristics in all regions of the flow. Uniform flow can also be used as a baseline for comparing the performance of more complex flows. For example, if a fluid is flowing with non-uniform velocity or pressure, engineers might compare its performance to

that of a hypothetical uniform flow with the same average velocity or pressure. While uniform flow is often an approximation of more complex flows, it can provide valuable insights into the behavior of fluids and the performance of fluid systems. Engineers and scientists use mathematical models and computational simulations to analyze and optimize uniform flow and other types of fluid flows in a wide range of natural and engineered systems. [65]

$$\frac{\partial V}{\partial x} = 0 \, , \frac{\partial \rho}{\partial x} = 0 \, , \frac{\partial P}{\partial x} = 0. \tag{3.9}$$

3.10.6 Non-uniform flow

Non-uniform flow refers to fluid flow in which the velocity, pressure or other flow properties vary spatially or temporally throughout the flow domain. In other words, the fluid is not flowing at a constant rate or with uniform characteristics in all regions of the flow. Non-uniform flow can occur in many different contexts, such as in natural flows like rivers or ocean currents, in industrial processes or in engineering systems like heat exchangers or ventilation systems. It can have significant effects on the behavior of the fluid and the performance of the system in which it is occurring. For example, in a heat exchanger, non-uniform flow can cause inefficient heat transfer, leading to hot spots or cold spots and reducing the overall efficiency of the system. In a river, non-uniform flow can cause erosion or deposition of sediment, affecting the ecology and changing the river's course over time. The non-uniform flow is important in many areas of engineering and science, as it plays a precious role in the design and optimization of many natural and engineered systems. Sophisticated mathematical and computational models are often used to simulate and analyze non-uniform flow, helping engineers and scientists to design more efficient methods. [65]

$$\frac{\partial V}{\partial x} \neq 0 \, , \frac{\partial \rho}{\partial x} \neq 0 \, , \frac{\partial P}{\partial x} \neq 0. \tag{3.10}$$

3.10.7 Laminar flow

A stream lines does not cross each other. Laminar flow refers to the motion of fluid molecules in a smooth and ordered manner, following straight and parallel streamlines. It is

typically observed in narrow pipes with low fluid velocity, high viscosity and is also known as streamline or viscous flow. There are different types of laminar flow, including unidirectional, pulsatile and oscillatory flow. Some examples of this flow are the oil flow via thin tube, the blood's flow via capillaries and also ascending movement of smoke in a straight line from a stick. However, the smoke transitions into turbulent flow after rising to a certain height, as it begins to move irregularly from its original path. [65]

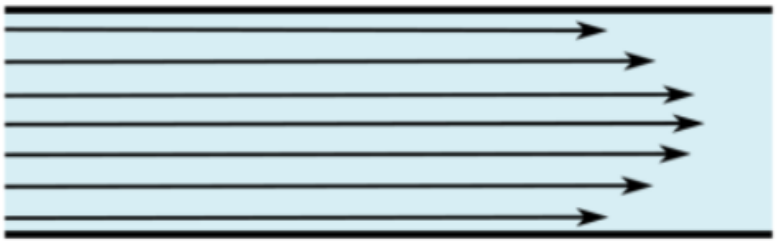

Figure 3.1. Laminar flow

3.10.8 Turbulent flow

This type of flow is characterized by the irregular motion of fluid particles, resulting in the formation of eddies that cause significant energy loss. This type of flow involves constantly changing fluid speeds and directions and is typically observed in large-diameter pipes with high fluid velocities. CFD analysis is a commonly used method for analyzing turbulent flow. CFD or computational fluid dynamics, is a field of fluid mechanics that employs algorithms and numerical analysis to solve problems related to turbulent fluid flows. Most CFD codes are based on the Naiver-Stokes equation or simplified Reynolds-averaged Navier-Stokes equations. The Reynolds number, a non-dimensional parameter is used to determine the type of flow in pipe flow. [65]

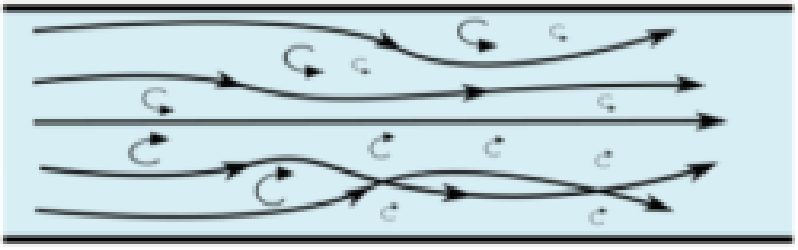

Figure 3.2. Turbulent flow

3.11 Stream line

Stream line is an imaginary line that is drawn in to the fluid where velocity is along the tangent. In fluid dynamics, the information of streamlines can provide valuable insights. The curvature of a streamline is related to the pressure gradient that acts perpendicularly to the streamline. The center of curvature of a streamline is oriented in the direction of decreasing radial pressure. By knowing the density of the fluid, the curvature of the streamline and the local velocity, the radial pressure gradient can be directly calculated. [65]

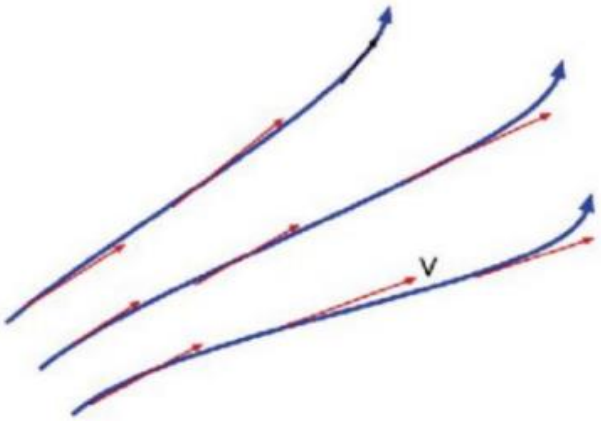

Figure 3.3. Stream lines

3.12 Heat source

A heat source refers to any factor that can cause an increase in temperature within a spacecraft. These sources can originate from outside the spacecraft (external) or within the spacecraft (internal). Examples of external heat sources include sunlight from the Sun, reflected light from planets and moons, heating caused by friction while passing through an atmosphere or gas clouds and released heat from planets. On the other hand, internal heat sources are often generated by a spacecraft's propulsion or electrical systems and can also result from friction when parts move against each other. [65]

3.13 Heat flow mechanism

The significant types of heat flow are mentioned as follows:

3.13.1 Conduction

The transfer of heat due to interaction of electrons or molecules is termed as conduction. It is a method by which heat energy is transferred from one substance to another through collisions between neighboring atoms or molecules. This is one of the three primary ways in which heat can travel. Conduction is most efficient in solids and liquids, where the molecules are closer together than in gases. A practical example of conduction can be observed while cooking on a camp stove. The heat from the stove makes the molecules in the frying pan vibrate faster and collide with their neighbors, thereby increasing the temperature of the pan. The thermal energy is transferred through the rest of the pan through collisions between the molecules. Many pots and pans come with insulated handles because some materials, such as metals are better heat conductors than others, like air and water, which are insulators. [69]

3.13.2 Convection

The transfer of heat by actual movement of molecules from hot place to cold place. It is the transfer of heat energy by the movement of a fluid, such as air or water. It occurs when a fluid is heated, causing it to become less dense and rise, while cooler, denser fluid sinks to take its place. This creates a circular flow of fluid, with warm fluid rising and cool fluid sinking in a continuous cycle. It is a natural process that occurs in many different contexts, from the atmosphere to the oceans to the inside of our own bodies. For example, convection is responsible for the circulation of air in a room when a heater is turned on, or for the movement of ocean currents around the world. It is an important mechanism for transferring heat energy from one place to another and it plays a key role in shaping our planet's climate and weather patterns. It is also important in many industrial processes, such as cooling systems for machinery and in cooking, where heat is transferred by the movement of hot air or liquids. [69]

3.13.3 Mixed convection

The blend of free and forced convection is notified as mixed convection. It is a type of heat transfer that occurs when both natural and also forced convection are present in a fluid flow. In mixed convection, the fluid is driven both by the buoyancy forces resulting from

temperature differences and by external forces, such as fans or pumps. It is often encountered in practical engineering applications, such as in heat exchangers or electronic cooling systems. The characteristics of mixed convection depend on the relative strengths of the buoyancy and forced convection forces, as well as the system's geometry and fluid's properties. In some cases, mixed convection can lead to more efficient heat transfer compared to purely forced or natural convection alone. However, the complexity of mixed convection can also make it difficult to predict and analyze, requiring sophisticated modeling techniques and experimental methods to fully understand its behavior. [69]

3.13.4 Free convection

The motion within a fluid caused due to density variations is referred to as free convection, also known as natural convection. It is considered as a type of heat transference that occurs in a fluid, such as liquids or can be gases, due to density differences caused by temperature variations. It is driven solely by buoyancy forces resulting from these temperature differences, without any external means of driving the fluid flow. In engineering applications, free convection can be important in designing cooling systems and heat exchangers and in predicting the performance of electronic devices or building ventilation systems. The free convection is critical in many areas of sciences, as it plays a fundamental role in the transfer of heat and mass in a wide range of natural and engineered systems. [69]

3.13.5 Forced convection

It is a motion within a fluid caused due to external agent like pump for a liquid. It is a type of heat transfer that happens if a fluid is forced to flow above a surface or through a channel by an external means, such as a fan or a pump. The external force causes the fluid to move, which enhances heat transfer by increasing the rate of fluid flow. In forced convection, the heat transfer rate is considered proportional to the flow velocity of the fluid, which is controlled by the external means. The quicker the fluid flows, the greater the transfer rate. Forced convection is commonly used in many engineering applications, such as in cooling systems for electronics, internal combustion engines and industrial processes. It is also used in heating systems, where heated air or water is forced through ducts or pipes to warm up a space or a fluid. [69]

3.13.6 Radiation

The transfer of heat by infra-red radiation requiring no medium for their transmission is termed to be radiation. Radiation discusses energy released by material as electromagnetic waves or particles. There are many types of radiation, including electromagnetic radiation such as radio waves, microwaves, infrared radiation, visible light, ultraviolet radiation, X-rays and gamma rays, as well as particle radiation such as alpha particles, beta particles and neutrons. Radiation is all around us and we are exposed to various forms of radiation every day. Some radiation is naturally occurring, such as cosmic radiation from outer space and radiation from radioactive elements in the Earth's crust. Other sources of radiation are man-made, such as medical X-rays and nuclear power plants. While radiation can have many beneficial uses, such as in medical diagnosis and treatment, it can also be harmful to human health. Exposure to high levels of radiation can damage living tissues and increase the risk of cancer, radiation sickness and other health problems. Therefore, it is important to limit our exposure to radiation and to take appropriate safety measures when working with or around sources of radiation. [69]

3.14 Thermal conductivity

Thermal conductivity refers to the property of a material that determines its ability to conduct heat. It describes how well a material can transfer thermal energy or heat through conduction. It is a measure of how easily heat can flow through a substance. Materials with high thermal conductivity allow heat to transfer quickly, while materials with low thermal conductivity impede heat transfer. The concept of thermal conductivity of materials is crucial in countless fields, such as engineering, building construction and thermal management. It helps in designing efficient heat transfer systems, selecting appropriate insulation materials and optimizing the performance of devices that involve heat transfer. The mathematical expression for thermal conductivity is

$$k = \frac{QL}{A\Delta T}, \tag{3.11}$$

where k is designated for thermal conductivity, Q response to heat flow per unit time, A is associated with cross sectional area and ΔT symbolizes temperature difference. The SI unit noted for thermal conductivity is $\frac{kgm}{s^3K}$. [69]

3.15 Thermal diffusivity

Thermal diffusivity is a property that characterizes how quickly heat can spread or diffuse through a material. It combines thermal conductivity, density and specific heat capacity to describe the rate at which temperature changes occur within a substance. It quantifies the ability of a material to conduct heat relative to its ability to store heat. Thermal diffusivity plays a significant role in various applications, including heat transfer analysis, material characterization and the design of thermal management systems. It helps in predicting temperature profiles, evaluating heat conduction through different materials and optimizing thermal performance in fields such as engineering, materials science and thermodynamics. Mathematically,

$$\alpha_f = \frac{k}{\rho c_p}, \tag{3.12}$$

where α_f denotes thermal diffusivity, ρ is density and c_p represents specific heat capacity. The SI unit for thermal diffusivity is $\frac{m^2}{s}$. [67]

3.16 Dimensionless numbers

3.16.1 Reynolds number

The phenomena was first investigated in the 1880's by Osbourne Reynolds in an experiment which has become classic in fluid mechanics. Reynold number indicates the important correspondence of the inertial and viscus effect in a fluid motion. In mathematical form,

$$Re = \frac{\text{inertial force}}{\text{viscus force}}, \tag{3.13}$$

i.e.,

$$Re = \frac{\rho v^2 / L}{\mu v / L} = \frac{vL}{v}, \tag{3.14}$$

where ρ is symbolized for density, v for mean velocity, L for characteristic length, μ for dynamic viscosity and υ for kinematic viscosity.

At low Reynolds number, the viscous effect governs resulting the fluid motion to be laminar while at enhanced number, the inertial effect directs turbulent flow. Reynolds number establishes an important criteria of kinematic and dynamic similarity in heat transfer. [65]

3.16.2 Prandtl number

Prandtl number is the ratio of kinematic viscosity to thermal diffusivity of the fluid. In terms of mathematical formula,

$$\text{Prandtl number} = \frac{\text{kinematic viscosity}}{\text{thermal diffusivity}}, \tag{3.15}$$

i.e.,

$$\text{Pr} = \frac{\upsilon}{\alpha_f} = \frac{{}^{\mu}/_{\rho}}{{}^{k}/_{\rho c_p}} = \frac{\mu c_p}{k}, \tag{3.16}$$

where υ is noted for kinematic viscosity, α_f for thermal diffusivity, k for thermal conductivity and c_p for specific heat.

It can be observed that when the Prandtl number Pr is much lesser than 1, then thermal diffusivity plays a prevailing part. Conversely, when the Prandtl number is much superior to 1, then the momentum diffusivity takes precedence. The Prandtl number has a significant impact on the associated thickness of boundary layers. When the Prandtl number is higher, indicating larger values of kinematic viscosity, the momentum boundary layer is thicker compared to the thermal boundary layer. [68]

3.16.3 Grashof number

It is named after Franz Grashof, and is a dimensionless quantity that compares the influence of buoyancy to the effect of viscosity on a fluid within the velocity boundary layer.

In natural convection, it plays a parallel role as Reynolds number's role in forced convection. Thus

$$\text{Grashof number} = \frac{\text{bouyant force}}{\text{viscus force}}, \tag{3.17}$$

i.e.,

$$Gr = \frac{g\beta(T_{wall}-T_{\infty})L^3}{\upsilon^2}, \tag{3.18}$$

where g is denoted to be the acceleration due to Earth's gravity, β to be coefficient of thermal expansion, T_{wall} to be wall temperature T_{∞} to be , bulk temperature, υ to be kinematic viscosity and L to be vertical length. [68]

3.16.4 Eckert number

It is a dimensionless number used in fluid dynamics to describe the ratio of kinetic energy to enthalpy (flow energy) difference of a fluid. The Eckert number is often used to characterize the behavior of compressible fluids, such as those found in supersonic flow. In these situations, the Eckert number can be used to determine the effects of heat transfer on the fluid flow. The formula for this number is:

$$Ec = \frac{u^2}{c_p \Delta T}, \tag{3.19}$$

where u is represented for velocity of considered fluid, c_p for specific heat capacity at constant pressure, T for fluid's temperature of the fluid

A low value of Eckert number designates that the thermal energy is better than kinetic energy, while a high value of Eckert number notifies that the kinetic energy is much superior to the thermal energy. [70]

3.16.5 Skin friction coefficient

The skin friction coefficient refers to the form of friction generated when a fluid and a solid surface are moving in relation to each other. The expression for skin friction is

$$C_f = \frac{\tau_w}{\frac{1}{2}\rho u^2}, \tag{3.20}$$

where τ_w is symbolized for shear stress, ρ for density u for velocity. [70]

3.16.6 Nusselt number

The Nusselt number is a dimensionless quantity that quantifies the proportion of heat transferred through convection compared to heat transferred solely through conduction. Relationships describing convective heat transfer are commonly expressed in terms of the Nusselt number, which depends on the Reynolds number and the Prandtl number. Therefore,

$$\left.\begin{aligned} Nu_L &= \frac{\text{Convection heat transfer}}{\text{Conduction heat transfer}} \\ Nu_L &= \frac{h(T_w - T_\infty)}{k(T_w - T_\infty)/L} = \frac{hL}{k} \end{aligned}\right\}, \tag{3.21}$$

where *L* is denoted to be characteristic length, k to be thermal conductivity, *h* to be heat transfer coefficient. [70]

Chapter 4

The Hybrid Nanofluid Flow via an Exponentially Stretching Sheet in the Existence of an Uneven Heat Sink/Source and Thermal Radiation

4.1 Introduction

In this chapter, an analysis is conducted on a laminar, two-dimensional, incompressible, viscous and Newtonian fluid flowing over the exponentially shrinking surface. The study takes into account the influencing effects of uneven heat generation/absorption and also the thermal radiation. By means of seemly similarity transformations, the nonlinear ordinary differential equations are assimilated from the principal partial differential equations. The numerical method, bvp4c is employed using MATLAB software to solve these complicated equations. The study scrutinizes the effects of numerous parameters on the considered flow and also heat transfer consequences graphically. In addition to this, the fallouts for skin friction coefficient and also Nusselt number at the wall are explored for the considered fluid. The obtained results are matched with earlier works to verify their accuracy and they are found to be in good agreement. This chapter provides a detailed review of the research paper Rehman *et al.* [80].

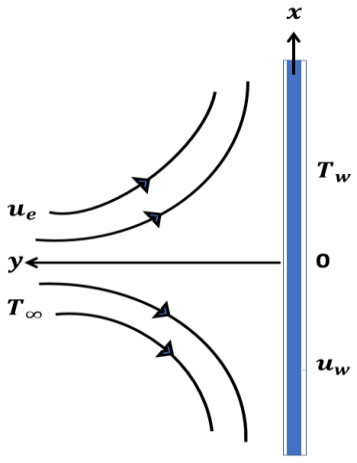

Figure 4.1. Flow configuration model

4.2 Mathematical formulation

An incompressible, steady, laminar and viscous liquid towards a surface which is stretched exponentially is considered. Thermal radiation and the presence of an uneven heat sink/source are taken into account during the flow inquiry. The Cartesian coordinate i.e., *x*, *y* system has been appraised. The following is a description of the boundary layer flow's prescribed velocity pattern:

$$\mathbf{V} = [u(x,y), v(x,y), 0]. \tag{4.1}$$

The continuity, momentum and energy equations are as follows:

$$\boldsymbol{\nabla}.\mathbf{V} = 0, \tag{4.2}$$

$$\rho \frac{D\boldsymbol{V}}{Dt} = \boldsymbol{\nabla}.\boldsymbol{\tau} + \mathbf{b}, \tag{4.3}$$

$$\rho c_p \frac{DT}{Dt} = -\text{div}\,\mathbf{q} - \frac{\partial q_r}{\partial y} + q''', \tag{4.4}$$

where

$$\mathbf{q} = -k\text{grad}T. \tag{4.5}$$

The Cauchy stress tensor for the incompressible viscous fluid is:

$$\boldsymbol{\tau} = -\,\text{p}\mathbf{I} + \mu\mathbf{A}_1, \tag{4.6}$$

in which ρ, $\mathbf{V}$, T, $\boldsymbol{q}$, c_p,$\boldsymbol{\tau}$, q''', q_r, k, $\mathbf{I}$, and $\mathbf{A_1}$ is denoted to be density, velocity field, fluid's temperature, heat flux, specific heat at constant pressure, stress tensor, non-uniform heat source/sink, radiation heat flux, thermal conductivity, unit tensor and first Rivilin-Erickson tensor which is given by:

$$\mathbf{A_1} = \mathbf{L} + \mathbf{L}^{\text{T}}. \tag{4.7}$$

Through

$$\mathbf{L} = \text{grad } \mathbf{V} = \begin{bmatrix} \frac{\partial u}{\partial x} & \frac{\partial u}{\partial y} & 0 \\ \frac{\partial v}{\partial x} & \frac{\partial v}{\partial y} & 0 \\ 0 & 0 & 0 \end{bmatrix} \quad \text{and} \quad \mathbf{L}^{\mathrm{T}} = (\text{grad } \mathbf{V})^{\mathrm{T}} = \begin{bmatrix} \frac{\partial u}{\partial x} & \frac{\partial v}{\partial x} & 0 \\ \frac{\partial u}{\partial y} & \frac{\partial v}{\partial y} & 0 \\ 0 & 0 & 0 \end{bmatrix}. \tag{4.8}$$

Thus

$$[\nabla . \boldsymbol{\tau}]_{\mathrm{x}} = -\frac{\partial p}{\partial x} + \mu(2\frac{\partial^2 u}{\partial x^2} + \frac{\partial^2 u}{\partial y^2} + \frac{\partial^2 v}{\partial x \partial y}), \tag{4.9}$$

$$[\nabla . \boldsymbol{\tau}]_{\mathrm{y}} = -\frac{\partial p}{\partial y} + \mu(\frac{\partial^2 v}{\partial x^2} + \frac{\partial^2 u}{\partial x \partial y} + 2\frac{\partial^2 v}{\partial y^2}). \tag{4.10}$$

Further

$$\text{div } \mathbf{q} = -k\left(\frac{\partial^2 T}{\partial x^2} + \frac{\partial^2 T}{\partial y^2}\right). \tag{4.11}$$

The heat flow arising from radiation can be represented as follows using the Roseland approximation

$$q_r = -\frac{4\sigma}{3k^*}\frac{\partial T^4}{\partial y}. \tag{4.12}$$

The Stefan-Boltzmann constant is represented through σ, while the absorption coefficient is represented by the symbol k^*. Using Taylor's series, the temperature is expanded as T^4 around the reference temperature T_∞ to give the following expression:

$$T^4 = 4T_\infty{}^3 T - 3T_\infty{}^4. \tag{4.13}$$

Differentiating Eq. (4.13) with respect to y,

$$\frac{\partial T^4}{\partial y} = 4T_\infty{}^3 \frac{\partial T}{\partial y}, \tag{4.14}$$

And

$$q_r = -\frac{16\sigma T_\infty{}^3}{3k^*}\frac{\partial T}{\partial y}. \tag{4.15}$$

The boundary layer approximations (i.e., x = O(1); u = O(1); y = O(δ) and v = O(δ)), and the equations (4.6) – (4.11) and (4.15) results in the following equations.

$$\frac{\partial u}{\partial x}+\frac{\partial v}{\partial y}=0, \tag{4.16}$$

$$u\frac{\partial u}{\partial x}+v\frac{\partial u}{\partial y}=u_e\frac{\partial u_e}{\partial x}+\vartheta_{hnf}\frac{\partial^2 u}{\partial y^2}+\frac{(\rho\beta)_{hnf}}{\rho_{hnf}}(T-T_\infty)g, \tag{4.17}$$

$$u\frac{\partial T}{\partial x}+v\frac{\partial T}{\partial y}=\frac{k_{hnf}}{\left(\rho c_p\right)_{hnf}}\frac{\partial^2 T}{\partial y^2}-\frac{1}{\left(\rho c_p\right)_{hnf}}\frac{\partial q_r}{\partial y}+\frac{q'''}{\left(\rho c_p\right)_{hnf}}. \tag{4.18}$$

The boundary conditions for the flow are

$$\left.\begin{array}{llll} v=0, & u=u_w, & T=T_w & \text{at} \quad y=0 \\ u\to u_e, & T\to T_\infty & \text{as} & y\to\infty \end{array}\right\}. \tag{4.19}$$

The characteristics and references of q''' (the non uniform heat source or can also be sink) are given in [75]

$$q'''=\frac{k_{hnf}u_w}{2Lv_f}[\varsigma_1(T_w-T_\infty)f'+\varsigma_2(T-T_\infty)]. \tag{4.20}$$

The values of ς_1 & $\varsigma_2$determine whether heat is being generated or absorbed inside a space. When ς_1 and $\varsigma_2>0$, heat is being generated and ς_1 and $\varsigma_2<0$, heat is being absorbed. ς_1 and ς_2 are the heat source or sink in terms of space and temperature respectively.

Substituting Eq. (4.20) in Eq. (4.18),

$$u\frac{\partial T}{\partial x}+v\frac{\partial T}{\partial y}=\frac{1}{(\rho c_p)_{hnf}}\left(k_{hnf}+\frac{16\sigma {T_\infty}^3}{3k^*}\right)\frac{\partial^2 T}{\partial y^2}+\frac{k_{hnf}u_w}{2Lv_f(\rho c_p)_{hnf}}\left[\begin{array}{l}\varsigma_1(T_w-T_\infty)f' \\ +\varsigma_2(T-T_\infty)\end{array}\right]. \tag{4.21}$$

The expression includes several variables and terms that describe the behavior of a surface under certain conditions. The term β refers to the volumetric thermal expansion coefficient. The function $u_w=v_0e^{Nx/L}$represents the velocity of a surface that is being stretched, with $v_0>0$ is exponentially assisting surface, $v_0=0$ is static sheet and $v_0<0$ is exponentially opposing surface. The function $u_e=u_0e^{Nx/L}$ represents the velocity (free stream) with u_0 is a source speed. The surface temperature is given by the function $T_w=T_\infty+T_0e^{2Nx/L}$, which depends on the ambient temperature T_∞, a reference length L, and an initial temperature T_0.

The fit transformations are

$$\left.\begin{array}{c}\eta=y\sqrt{\frac{u_0}{2v_fL}}e^{\frac{Nx}{2L}}, \quad \psi=\sqrt{2u_0v_fL}\,f(\eta)e^{\frac{Nx}{2L}}, \quad \theta(\eta)=\frac{T-T_\infty}{T_w-T_\infty}, \\ u=u_0e^{\frac{Nx}{L}}f'(\eta), \quad v=-N\sqrt{\frac{u_0v_f}{2L}}e^{\frac{Nx}{2L}}[f(\eta)+\eta f'(\eta)],\end{array}\right\}. \tag{4.22}$$

The governing Eq.(4.16) is satisfied and Eqs. (4.17, 4.19, 4.21) are transformed when the similarity variables are included, as well as when data from Tables 4.1 and 4.2 are used.

$$\frac{\frac{\mu_{hnf}}{\mu_f}}{\frac{\rho_{hnf}}{\rho_f}} f'''(\eta) + Nf(\eta)f''(\eta) - 2N\left(f'(\eta)\right)^2 + 2N + 2\frac{\frac{(\rho\beta)_{hnf}}{(\rho\beta)_f}}{\frac{\rho_{hnf}}{\rho_f}}\lambda\,\theta(\eta) = 0, \tag{4.23}$$

$$\frac{1}{\Pr}\frac{1}{\frac{(\rho c_p)_{hnf}}{(\rho c_p)_f}}\left(\frac{k_{hnf}}{k_f} + \frac{4}{3}R\right)\theta''(\eta) + \frac{\varepsilon}{\Pr}\frac{\frac{k_{hnf}}{k_f}}{\frac{(\rho c_p)_{hnf}}{(\rho c_p)_f}}[\varsigma_1 f' + \varsigma_2\theta(\eta)] + Nf(\eta)\theta'(\eta)$$
$$- 4N\theta(\eta)f'(\eta) = 0. \tag{4.24}$$

The refurbished boundary restrictions:

$$\left.\begin{aligned} f(0) = 0, \quad f'(0) = \varepsilon, \quad \theta(0) = 1, \\ f'(\infty) = 1, \quad \theta(\infty) = 0. \end{aligned}\right\}. \tag{4.25}$$

Here, $\Pr = \frac{(\mu c_p)_f}{k_f}$ is signified as Prandtl number, $R = \frac{4\sigma T^3{}_\infty}{k^* k_f}$ is denoted as thermal radiation parameter, $\varepsilon = \frac{v_0}{u_0}$ is the velocity ratio parameter, $\lambda = \frac{g\beta_f T_0 L}{{u_0}^2} = \frac{Gr_x}{{Re_x}^2}$ is the assisting and opposing parameter, ${Re_x}^2 = \frac{u_0 L e^{\frac{Nx}{L}}}{\nu_f}$ is symbolized as Reynolds number and $Gr_x = \frac{g\beta_f T_0 L^3 e^{\frac{2Nx}{L}}}{{\nu_f}^2}$ is noted as local Grashof number.

The following expression provides the skin friction coefficient and also Nusselt number: ([75], [79], [84]).

$$(2Re_x)^{-\frac{1}{2}} C_{fx} = \frac{\mu_{hnf}}{\mu_f} f''(0), \tag{4.26}$$

$$\left(\frac{Re_x}{2}\right)^{-\frac{1}{2}} Nu_x = -\left(\frac{k_{hnf}}{k_f} + \frac{4}{3}R\right)\theta'(0). \tag{4.27}$$

4.3 Numerical simulation

By employing the similarity variable η and incorporating the data from Tables 4.1 and 4.2, the nonlinear ODEs Eq. (4.23) and Eq. (4.24) are obtained. Subsequently, these ODEs are numerically solved using the bvp4c-solver, a computational tool provided by the MATLAB software program. The boundary conditions Eq. (4.25) are also solved alongside the ODEs. Shampine *et al.* [72] formed the bvp4c tool, which utilizes a 3-stage Lobatto IIIa computational method. To utilize this method, operators are obliged to supply a set of initial estimates that encompass the precise value of the border layer thickening parameter η_∞ . Assuming that the boundary conditions are met asymptotically and there are no errors in the MATLAB program, the desired results can be obtained with the prescribed level of accuracy. Additionally, users may need to engage in a process of trial and error to determine the appropriate initial estimates in order to achieve the desired results. Yahaya *et al.* [71] & Waini *et al.* [73] have both published papers that discuss the use of the bvp4c method for solving time-independent fluid flow problems. In order to solve Eqs. (4.24) and (4.25) subject to the conditions (4.26), it is necessary to simplify the given equations.

$$\left.\begin{gathered} f = y(1),\ f' = y(2),\quad f'' = y(3),\quad f''' = y(4), \\ y(4) = \frac{\frac{\rho_{hnf}}{\rho_f}}{\frac{\mu_{hnf}}{\mu_f}}\left(-y(1)y(3) + 2y(2)y(2) - 2 - 2\lambda\frac{\frac{(\rho\beta)_{hnf}}{(\rho\beta)_f}}{\frac{\rho_{hnf}}{\rho_f}}y(5)\right) \end{gathered}\right\}, \tag{4.28}$$

$$\left.\begin{gathered} \theta = y(5),\ \theta' = y(6),\quad \theta'' = y(7), \\ y(7) = \mathrm{Pr}\frac{\frac{(\rho c_p)_{hnf}}{(\rho c_p)_f}}{\left(\frac{k_{hnf}}{k_f} + \frac{4}{3}R\right)}\left(-y(1)y(6) + 4y(5)y(2) - \frac{\epsilon}{\mathrm{Pr}}\frac{\frac{k_{hnf}}{k_f}}{\frac{(\rho c_p)_{hnf}}{(\rho c_p)_f}}(y(2)\varsigma_1 + y(5)\varsigma_2)\right) \end{gathered}\right\}, \tag{4.29}$$

and the boundary conditions are

$$y_a(2) - \epsilon, \quad y_a(1), \quad y_a(5) - 1, \quad y_b(2) - 1, \quad y_b(5). \tag{4.30}$$

4.4 Result and discussion

The extensive computational calculations have been performed to generate detailed graphical outcomes related to the problem. The system of ODEs, specifically Eq. (4.24) and (4.25), subjected to the boundary conditions defined in Eq. (4.26), is investigated by the use of bvp4c package available in the software MATLAB. The values of the problem parameters including the fractional sizes of nano-molecules of Al_2O_3 (ϕ_1) and Cu (ϕ_2), as well as the well-known Prandtl number (Pr), the opposing & assisting parameter (λ), velocity ratio parameter (ε), parameters related to the temperature ς_1, radiation parameter R and space-dependent heat source/sinks ς_2 are considered for numerical analysis. Table 4.1 and 4.2 are presented to show the thermo-physical features of the nanoparticles and the fluids, which are needed to execute the study. Table 4.3 to Table 4.6 show an excellent agreement of the obtained values for the present study and the already found values in the literature. Table 4.5 contains a summary of all the parametric values used in the study. The impacts of specific factors on $f'(\eta)$ and $\theta(\eta)$ are illustrated in figure 4.2-4.13. The flow profiles eventually converge to the free-stream equations Eq. (4.24) and Eq. (4.25) asymptotically.

The figure 4.2 displays that changing impact of volume fraction coefficient for Al_2O_3 nanoparticles ϕ_1 in terms of velocity profile $f'(\eta)$ for the assisting and opposing flows, i.e., $\lambda = 1, -1$ and the result indicates that the velocity and momentum boundary layer thickness increases as ϕ_1 reduces for $\lambda = 1$ and opposite trend appear for $\lambda = -1$. Figure 4.3 show the velocity sketch for different volume fraction coefficient's ϕ_2 values and it is obvious that $f'(\eta)$ increase on changing values of ϕ_2 for $\lambda = 1$ and also for $\lambda = -1$ and momentum layer thickness upturns as ϕ_2 increases for both cases. The impact of the radiation parameter R on $f'(\eta)$ is visible in figure 4.4 for both assisting and opposing cases. It is perceived that the $f'(\eta)$ rises with growing values of R for $\lambda = 1$, indicating a rise in momentum border layer thickness. On the contrary, for $\lambda = -1$, the $f'(\eta)$ decreases with growing values of R implying a reduction in momentum border layer thickness. Figure 4.5 illustrates the impact of the velocity ratio parameter ϵ on $f'(\eta)$ for $\lambda = 1$ and $\lambda = -1$ flows. The observation indicates that $f'(\eta)$ rises with growing values of ϵ, indicating an upsurge in momentum border layer width for $\lambda = 1$ and $\lambda = -1$. Figure 4.6 exemplifies the profile of $f'(\eta)$ for different values of Prandtl number Pr. The velocity $f'(\eta)$ rises with growing values of Pr for $\lambda = -1$, but opposite inclination appear for $\lambda = 1$. Consequently, the momentum layer width rises for the value $\lambda = -1$ and

declines for the value $\lambda = 1$. Figure 4.7 depicts how the variation in values of ς_1 alter the velocity profile. It has been noted that boost in the parameter ς_1 displays to grow the profile $f'(\eta)$ when $\lambda = 1$, while it tends to decline the profile $f'(\eta)$ when $\lambda = -1$. This consequences the growth and reduction in the thickness of the momentum boundary for $\lambda = 1$ and $\lambda = -1$. Figure 4.8 depict the variation in the value of ς_2 and its impact for velocity. The boost in the parameter ς_2 results to grow the velocity $f'(\eta)$ when $\lambda = 1$, while it shows a decline for velocity $f'(\eta)$ when $\lambda = -1$. Figure 4.9 is sketched to find impact of volume fraction coefficient ϕ_1 on temperature profile for both the flows. It is perceived that the $\theta(\eta)$ rises with growing values of ϕ_1 for $\lambda = 1$ and $\lambda = -1$, indicating a rise in thermal boundary layer thickness. Figure 4.10 demonstrates the impact of volume fraction coefficient ϕ_2 on velocity profile for $\lambda = 1$ and $\lambda = -1$ flows. The profile $\theta(\eta)$ rises with growing values of ϕ_2 for $\lambda = 1$ and $\lambda = -1$, and thus the thermal boundary layer thickness also augments. Figure 4.11 shows the temperature profile $\theta(\eta)$ in terms of enhancing values of R and it is noted that with the increasing values of radiation parameter R, the temperature profile amplifies for both assisting $\lambda = 1$ and opposing $\lambda = -1$ flows. Figure 4.12 is indicated for the temperature profile $\theta(\eta)$ and the profile increases with increasing values of ϵ for both assisting $\lambda = 1$ and opposing $\lambda = -1$ flows. Figure 4.13 explain the temperature profile $\theta(\eta)$ for different values of the Prandtl number Pr and the temperature profile $\theta(\eta)$ decreases for both cases of $\lambda = -1$ and $\lambda = 1$, indicating that thickness of heat boundary layer also condenses. Figure 4.14 depicts the variation in thermal profile for various value of ς_1 and the figure clarifies that the upturn in the parameter ς_1 leads to a augmentation in profile $\theta(\eta)$ when $\lambda = 1$ and also for $\lambda = -1$. Figure 4.15 describes the variation in ς_2 and the resulting temperature profile and it has been apparent that an intensification in the parameter ς_2 clues towards a surge in the profile $\theta(\eta)$ when $\lambda = 1$ and $\lambda = -1$.

The plots shown in Figure 4.16 illustrate the impact of parameter λ and ϕ_2 on the drag force represented by $f''(0)$. The observations indicate that $f''(0)$ rises as ϕ_2 and λ rise for both assisting and opposing flows. Figure 4.17 displays the variation of ε and ϕ_2 for the drag force, $f''(0)$. The result reveals that $f''(0)$ decreases as ϕ_2 and ε are tended to increase for the considered cases. Figure 4.18 is depicted for the impact of the radiation parameter R and $\phi_2$on the drag force factor $f''(0)$, for assisting $\lambda = 1$ and opposing $\lambda = -1$ flows. It is observed that increasing the value of size ϕ_2 led to an increase in the skin friction coefficient $f''(0)$ for assisting and opposing flows. However, the effect of R was different for the two types of

considered flows. The impact of the ς_1 and ϕ_2 on the skin friction factor is illustrated in figure 4.19 for both assisting $\lambda = 1$ and opposing $\lambda = -1$ flows and the sketch predicts that the skin friction coefficient $f''(0)$ is increased with the growing ϕ_2 values regardless of whether the flow is assisting or opposing. However, the impact of $\varsigma_1$is different. In the case of an opposing flow, $f''(0)$ is slightly reducing with the increasing value of ς_1, while in the case of an assisting flow, it amplifies. Figure 4.20 elucidates the impact of temperature reliant heat generating (sinking) coefficient ς_2, along with the parameter ϕ_2 on the skin friction factor for assisting note by $\lambda = 1$ and opposing noted by $\lambda = -1$ flows. The skin friction coefficient $f''(0)$ increased with increasing value of ϕ_2 and ς_2 in both assisting and opposing cases. Figure 4.21 clarifies the impact of λ and ϕ_2 on the Nusselt value $\theta'(0)$ and the Nusselt number sketch decreases as ϕ_2 increases, but it increases as λ increases. Figure 4.22 spectacles the effects of ε and ϕ_2 on Nusselt number $\theta'(0)$ and the Nusselt number decreases as ϕ_2 increases but increases as ε increases. Figure 4.23 depicts the impact of the radiation parameter R and the parameter ϕ_2 on Nusselt value $\theta'(0)$ has an enhancing effect for assisting ($\lambda = -1$) flow. However, it has a reducing impact for the growing value of R for both types of flows. The impact of the space-dependent heat source coefficient ς_1 and the parameter ϕ_2 on Nusselt number is illustrated in Figure 4.24 for both assisting $\lambda = 1$ and opposing $\lambda = -1$ flows. It is observed that the Nusselt number lessened with aggregated values of ς_1 and volume fraction ϕ_2 for both assisting and opposing flows. Figure 4.25 explains the impact of temperature reliant heat generating (sinking) coefficient ς_2 and the parameter ϕ_2 on the Nusselt number for assisting ($\lambda = 1$) and also opposing ($\lambda = -1$) flows. The Nusselt number shows a reduction with increasing values of both the parameters ς_2 and ϕ_2 for assisting and opposing flows.

Table 4.1: Thermo-physical appearances of nanoparticles and water.
Waini *et al.* [73], Devi, & Devi [74], Polu & Reddy [75].

Thermo-physical appearances	Base fluid	Nanoparticles	
	H_2O	Al_2O_3	Cu
$\rho(kg/m^3)$	997.1	3970	8933
$c_{p(J/kgK)}$	4179	765	385
$k(W/mK)$	0.613	40	400
$\beta \times 10^{-5}$	21	0.85	1.67
Prandtl Number	6.20	-	-

Table 4.2: Thermo-physical phases of nano-fluid and hybrid nano-fluid.
Yahaya *et al.* [71], Waini *et al.*[76], Waini *et al.* [77].

Thermo-physical phases	Nano-fluid	Hybrid nano-fluid
Density	$\rho_{nf} = (1-\phi_1)\rho_f + \phi_1\rho_{n1}$	$\rho_{hnf} = (1-\phi_2)\rho_{nf} + \phi_2\rho_{n2}$
Dynamic viscosity	$\mu_{nf} = \frac{\mu_f}{(1-\phi_1)^{2.5}}$	$\mu_{hnf} = \frac{\mu_{nf}}{(1-\phi_1)^{2.5}(1-\phi_2)^{2.5}}$
Thermal expansion	$(\rho\beta)_{nf} = (1-\phi_1)(\rho\beta)_f + \phi_1(\rho\beta)_{n1}$	$(\rho\beta)_{hnf} = (1-\phi_2)(\rho\beta)_{nf} + \phi_2(\rho\beta)_{n2}$
Heat capacity	$(\rho c_p)_{nf} = (1-\phi_1)(\rho c_p)_f + \phi_1(\rho c_p)_{n1}$	$(\rho c_p)_{hnf} = (1-\phi_2)(\rho c_p)_{nf} + \phi_2(\rho c_p)_{n2}$
Thermal conductivity	$\frac{k_{nf}}{k_f} = \frac{k_{n1}+2k_f-2\phi_1(k_f-k_{n1})}{k_{n1}+2k_f+\phi_1(k_f-k_{n1})}$	$\frac{k_{hnf}}{k_{nf}} = \frac{k_{n2}+2k_{nf}-2\phi_2(k_{nf}-k_{n2})}{k_{n2}+2k_{nf}+\phi_2(k_{nf}-k_{n2})}$

Table 4.3: Comparative values of $f''(0)$ for different ϵ when $\phi_2 = \lambda = R = \varsigma_1 = \varsigma_2 = 0$, Pr = 6.2.

ϵ	ϕ_1	Values of $f''(0)$			
		Bachok *et al*. [78]	Waini *et al*. [79]	Rehman *et al*. [80]	Present Values
-0.5	0	2.1182	2.1182	2.1182	2.118169
0	0	1.6872	1.6872	1.6872	1.687218
0.5	0	0.9604	0.9604	0.9604	0.960416

Table 4.4: Comparative values of $\theta'(0)$ for various amounts of ϵ when $\phi_2 = \lambda = R = \varsigma_1 = \varsigma_2 = 0$, Pr = 6.2.

ϵ	ϕ_1	Values of $\theta'(0)$		
		Waini *et al*. [79]	Rehman *et al*. [80]	Present Values
-0.5	0	0.0588	0.05687	0.058787
0	0	2.5066	2.5066	2.506625
0.5	0	4.0816	4.0816	4.081572

Table 4.5: Comparative values of $f''(0)$ & $\theta'(0)$ for different ϕ_2 and λ at Pr = 6.2, $\lambda = R = \varsigma_1 = \varsigma_2 = 0$.

		$Cu/water\ (\phi_1 = 0)$					
ϕ_2	λ	Waini *et al.* [79]	Rehman *et al.* [80]	Present Values	Waini *et al.* [79]	Rehman *et al.* [80]	Present Values
		$f"(0)$	$f"(0)$	$f"(0)$	$\theta'(0)$	$\theta'(0)$	$\theta'(0)$
0	0	1.6872	1.6872	1.687218	2.5066	2.5066	2.506625
0.02	0	1.8630	1.8630	1.863005	2.6390	2.5246	2.638967
0.04	0	2.0387	2.0387	2.038680	2.7677	2.5357	2.767735
0.04	-1	1.6229	1.6002	1.622894	2.6330	2.4050	2.632998
0.04	-0.5	1.8345	1.8235	1.834463	2.7031	2.4732	2.703140
0.04	1	2.4291	2.4291	2.429107	2.8838	2.6474	2.883847

Table 4.6: Comparative values of $f''(0)$ & $\theta'(0)$ for different ϕ_2 and λ at Pr = 6.2, $\lambda = R = \varsigma_1 = \varsigma_2 = 0$.

		$Cu - Al_2O_3/water\ (\phi_1 = 0.1)$					
ϕ_2	λ	Waini *et al.* [79]	Rehman *et al.* [80]	Present Values	Waini *et al.* [79]	Rehman *et al.* [80]	Present Values
		$f"(0)$	$f"(0)$	$f"(0)$	$\theta'(0)$	$\theta'(0)$	$\theta'(0)$
0	0	2.1930	2.1930	2.192963	2.9655	2.9655	2.965516
0.02	0	2.3781	2.3781	2.378071	3.1050	3.1050	3.104963
0.04	0	2.5657	2.5657	2.565729	3.2426	3.2426	3.242618
0.04	-1	2.1500	2.1500	2.149957	3.1183	3.1183	3.118294
0.04	-0.5	2.3607	2.3607	2.360691	3.1825	3.1825	3.182453
0.04	1	2.9613	2.9613	2.961257	3.3531	3.3531	3.353054

Table 4.7: Parametric values involved in the present analysis.

Parametric Symbols	Values	References
Pr	5.0, 6.2, 7.0	Waini *et al.* [76], Waini *et al.* [77]
ϕ_1	0, 0.1	Waini *et al.* [79]
ϕ_2	0, 0.02, 0.04	Waini *et al.* [79]
λ	-8 to 6	Waini *et al.* [79]
R	0, 1, 2	Waini *et al.* [78]
ς_1	-0.5, 0, 0.5	Waini *et al.* [79], Polu and Reddy [75] and Waini *et al.* [73]
ς_2	-0.5, 0, 0.5	Waini *et al.* [79], Polu and Reddy [75] and Waini *et al.* [73]
ϵ	-0.5, 0.5, 1	Waini *et al.* [79]

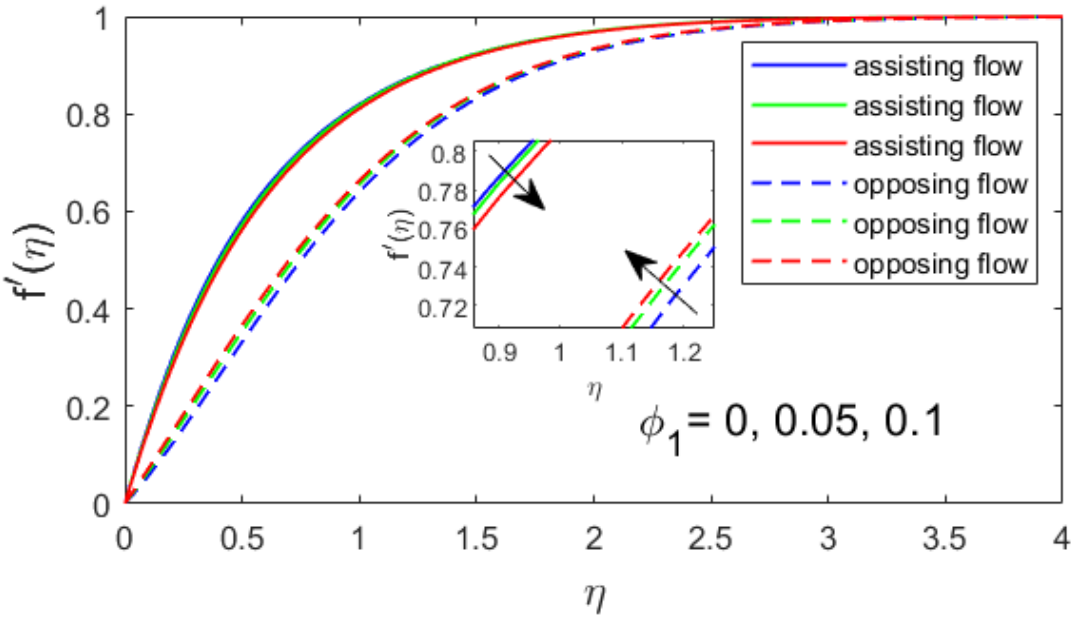

Figure 4.2. Conduct of ϕ_1 in terms of $f'(\eta)$.

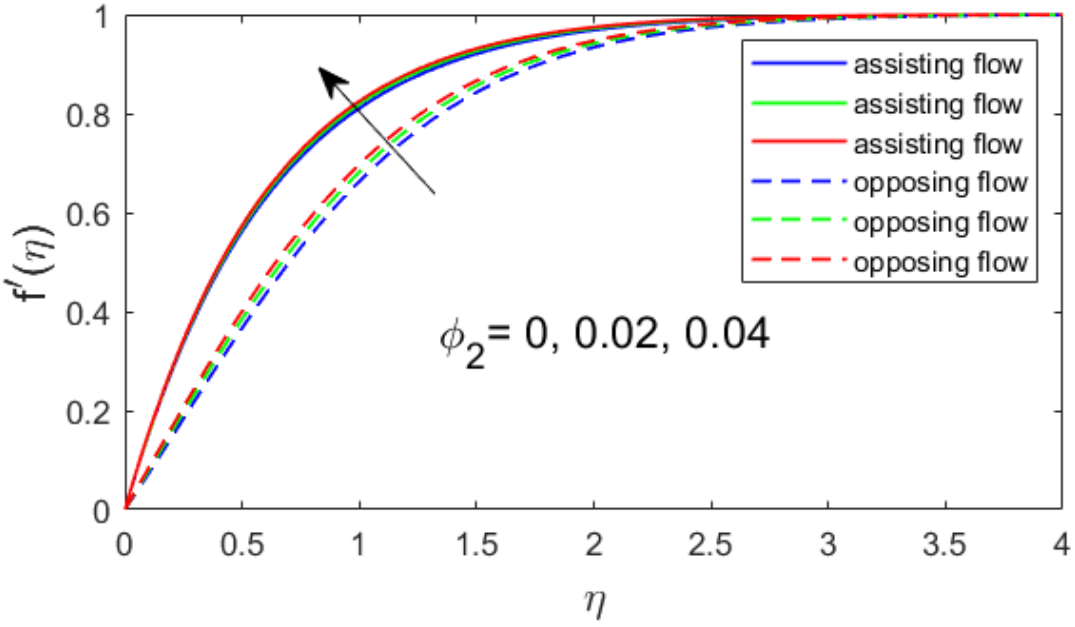

Figure 4.3. Conduct of ϕ_2 in terms of $f'(\eta)$.

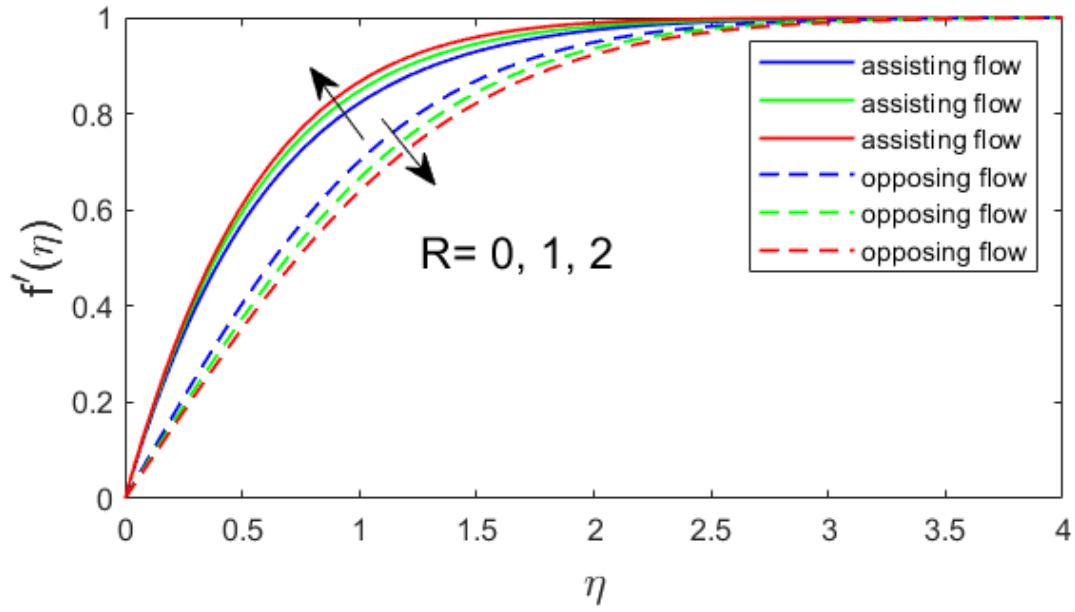

Figure 4.4. Conduct of R in term of $f'(\eta)$.

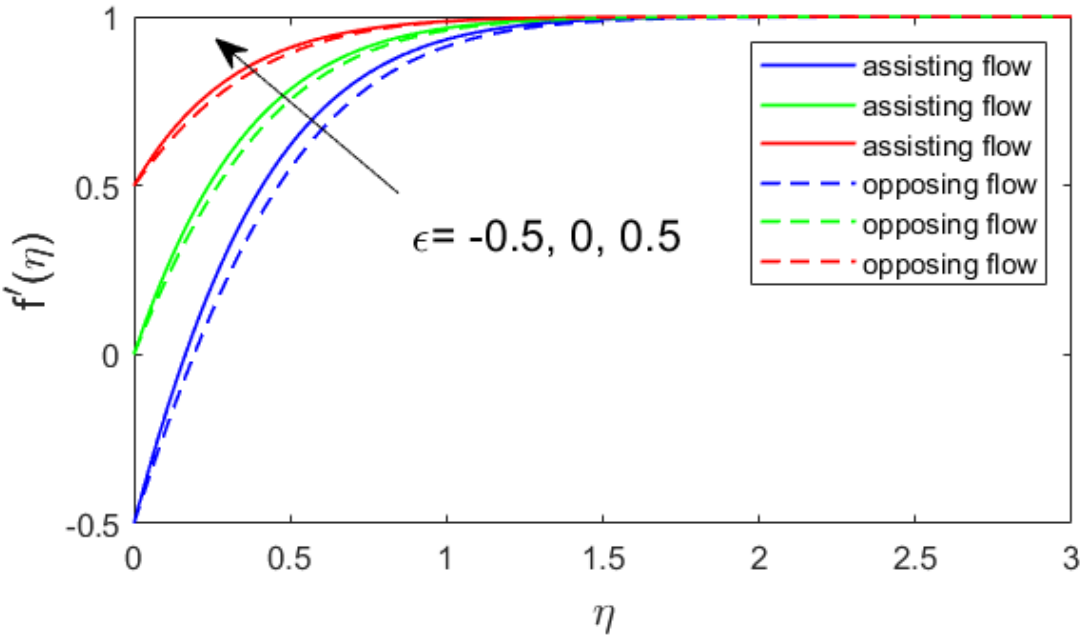

Figure 4.5. Conduct of ε in term of $f'(\eta)$.

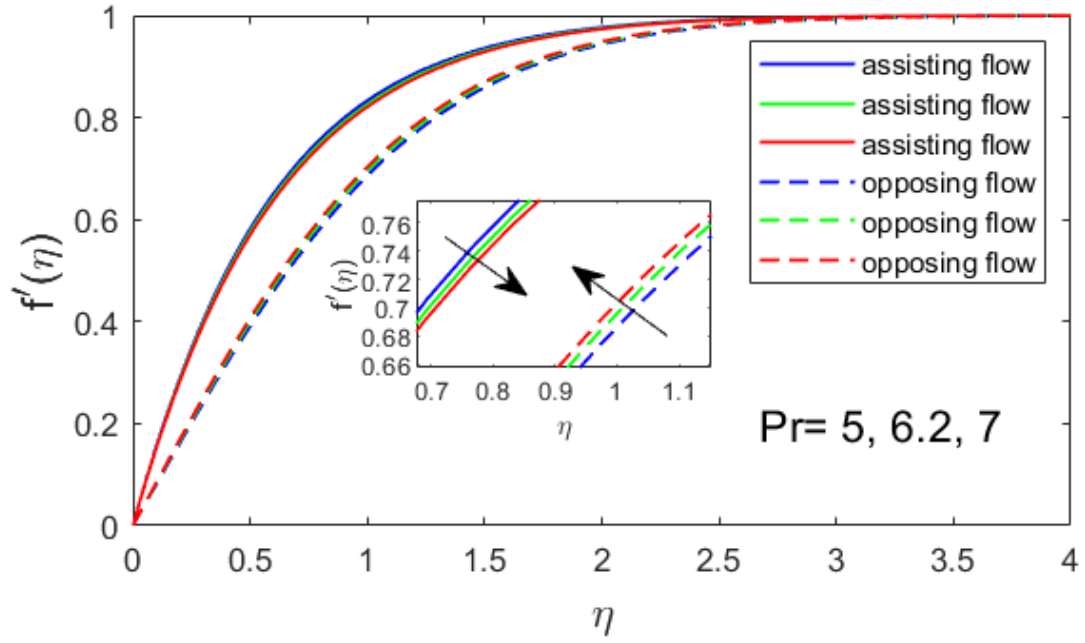

Figure 4.6. Conduct of Pr in terms of $f'(\eta)$.

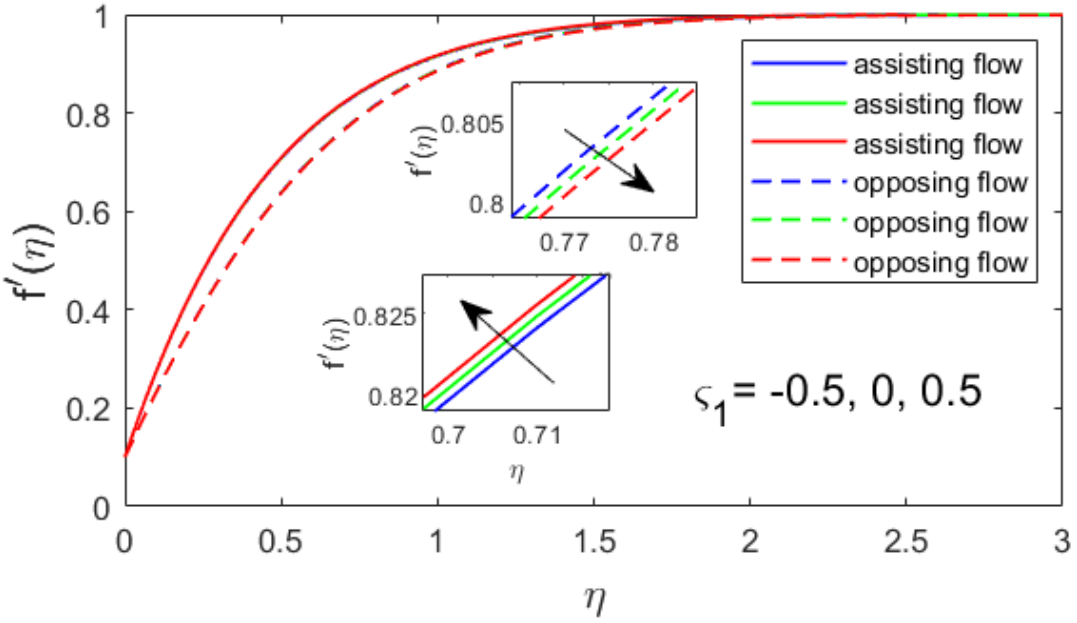

Figure 4.7. Conduct of ς_1 in term of $f'(\eta)$.

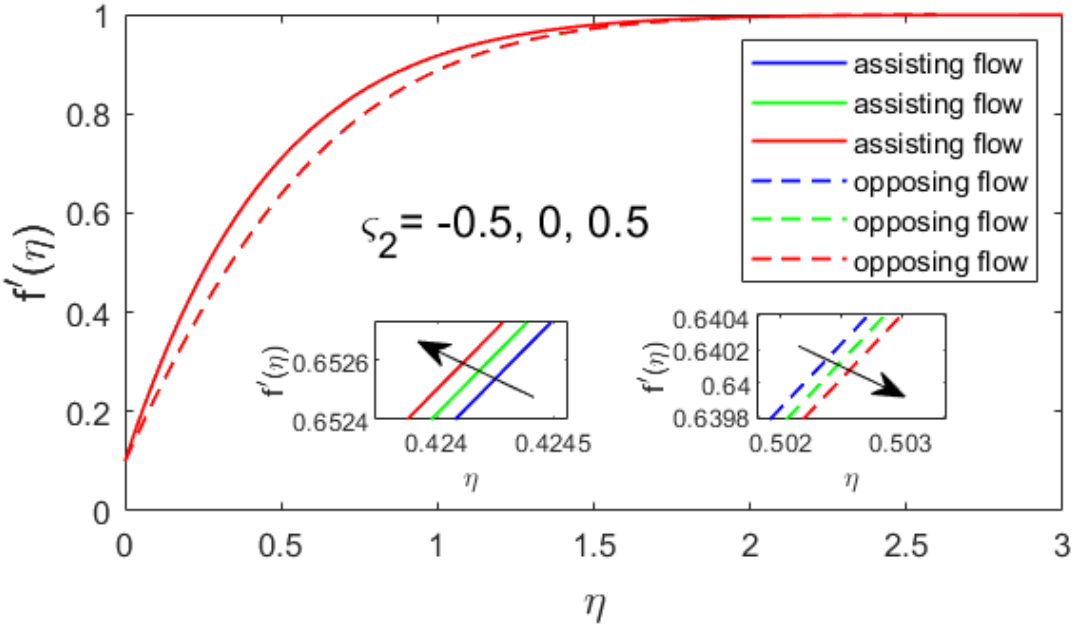

Figure 4.8. Conduct of ς_2 in term of $f'(\eta)$.

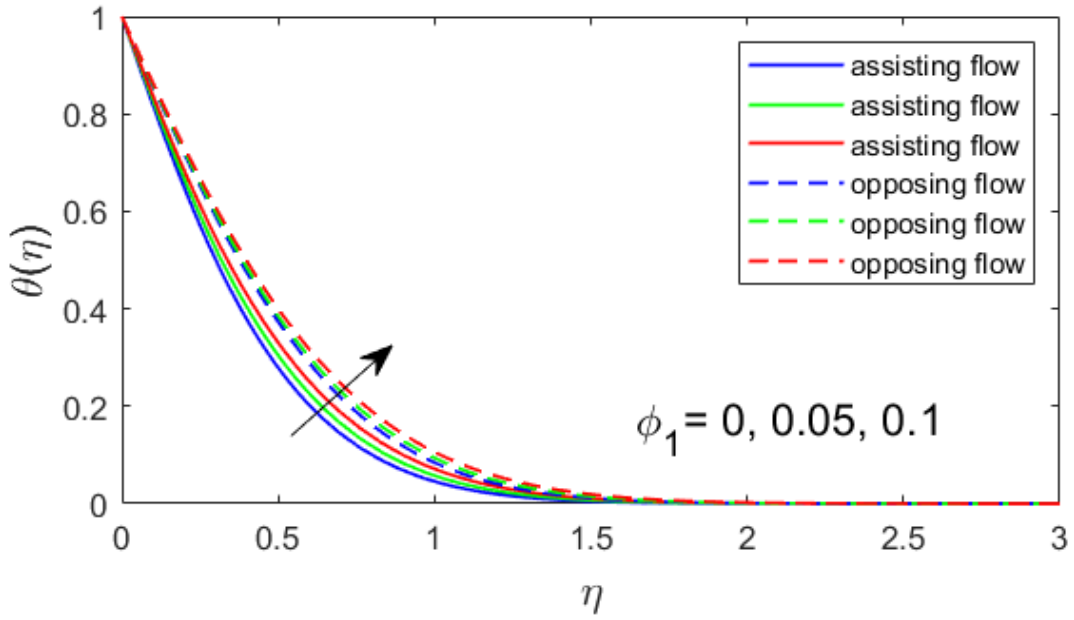

Figure 4.9. Conduct of ϕ_1 in term of $\theta(\eta)$.

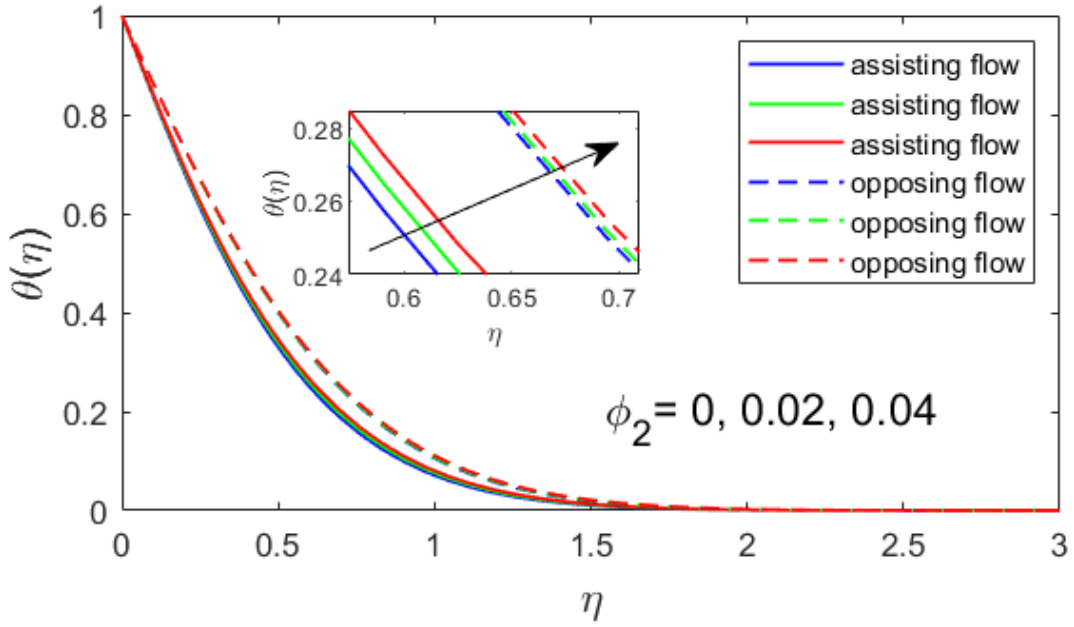

Figure 4.10. Conduct of ϕ_2 in term of $\theta(\eta)$.

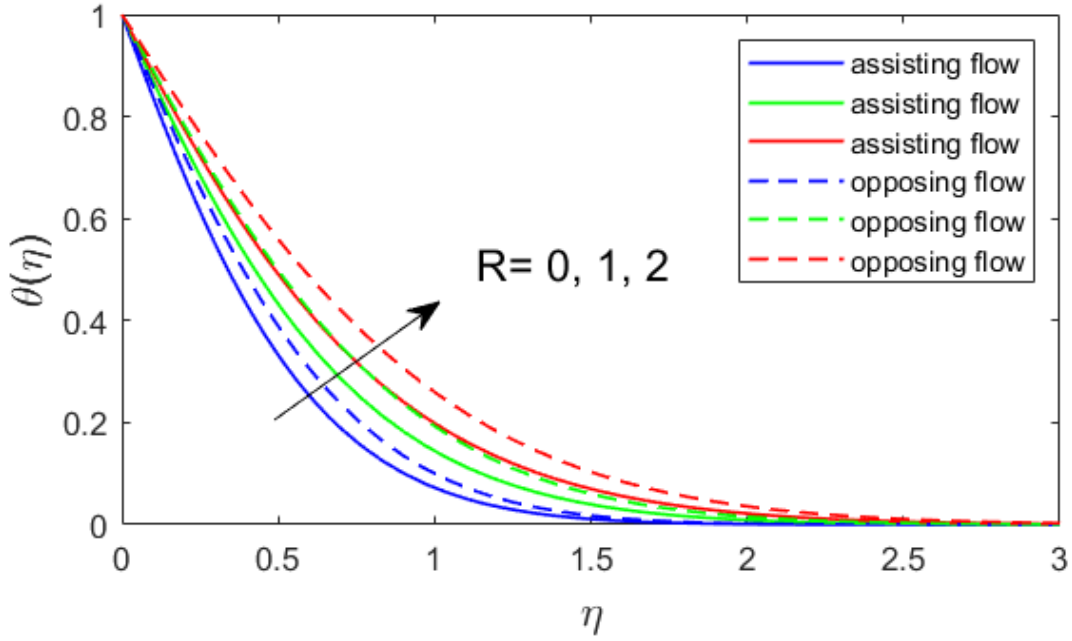

Figure 4.11. Conduct of R in terms of $\theta(\eta)$.

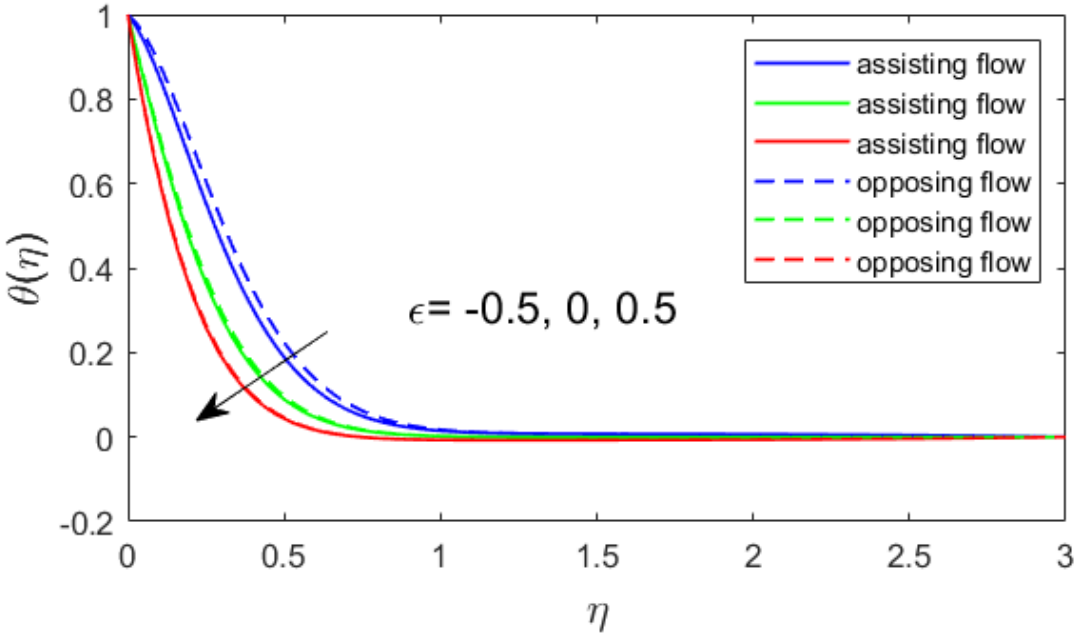

Figure 4.12. Conduct of ϵ in term of $\theta(\eta)$.

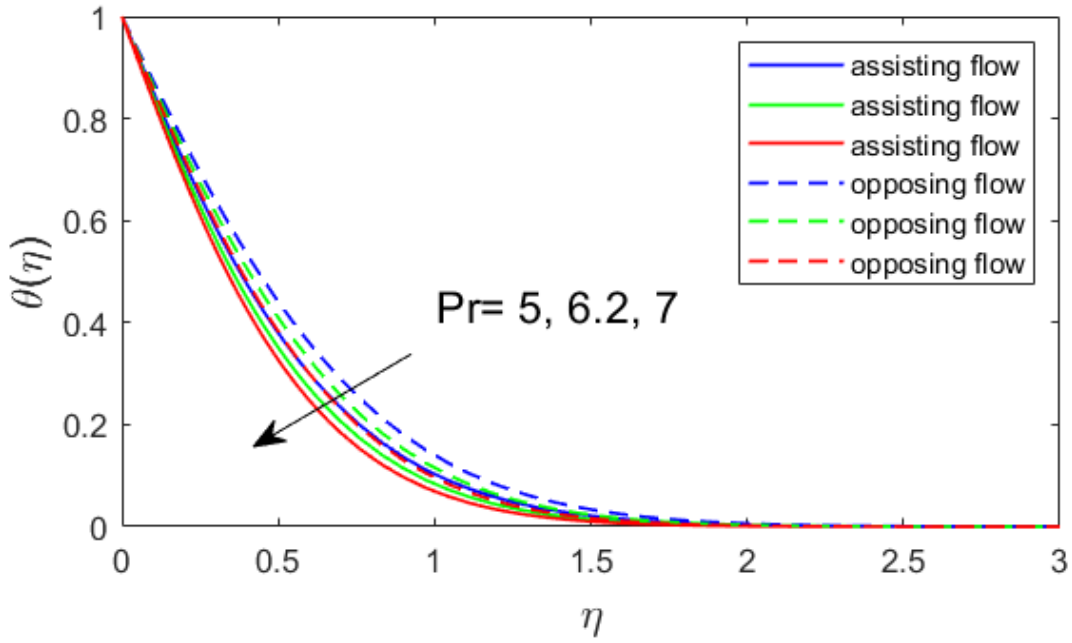

Figure 4.13. Conduct of Pr in terms of $\theta(\eta)$.

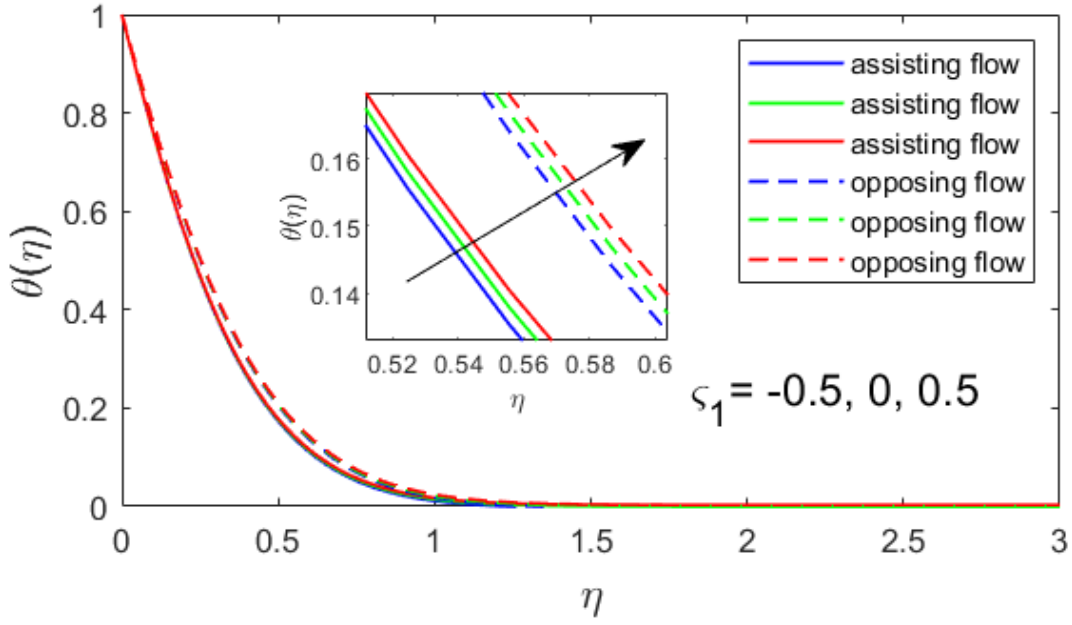

Figure 4.14. Conduct of ς_1 in terms of $\theta(\eta)$.

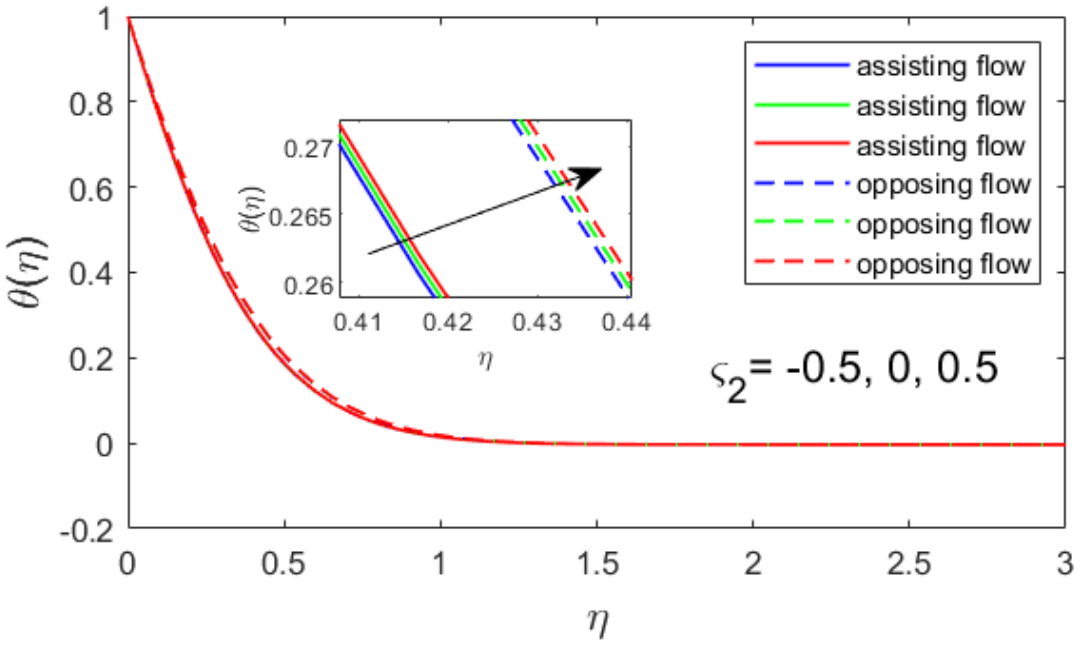

Figure 4.15. Conduct of ς_2 in terms of $\theta(\eta)$.

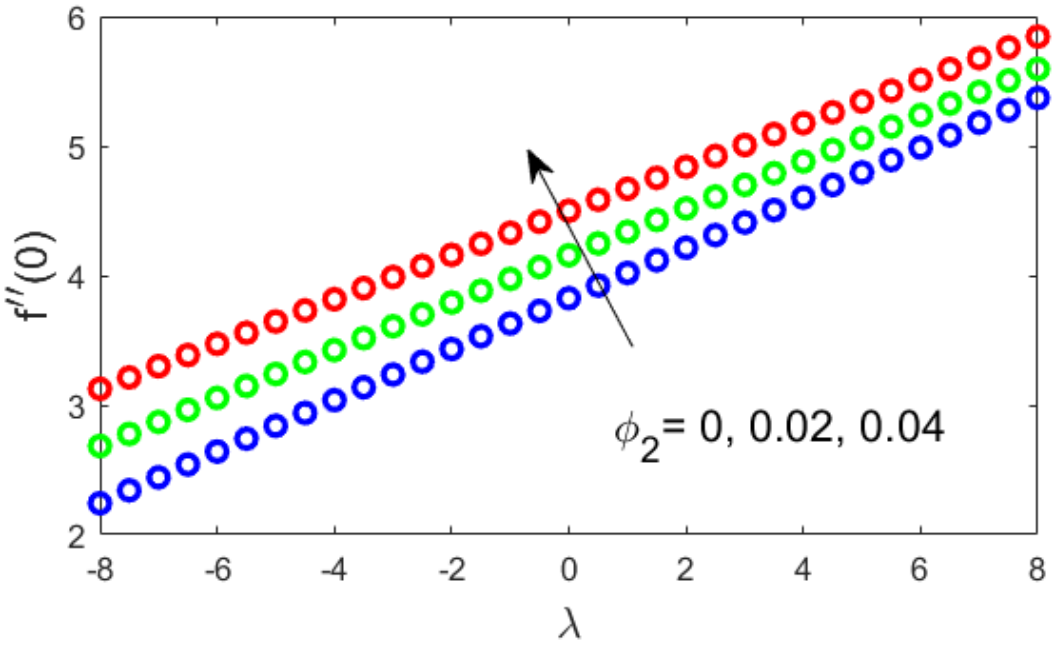

Figure 4.16. Conduct of λ and ϕ_2 in terms of $f''(0)$.

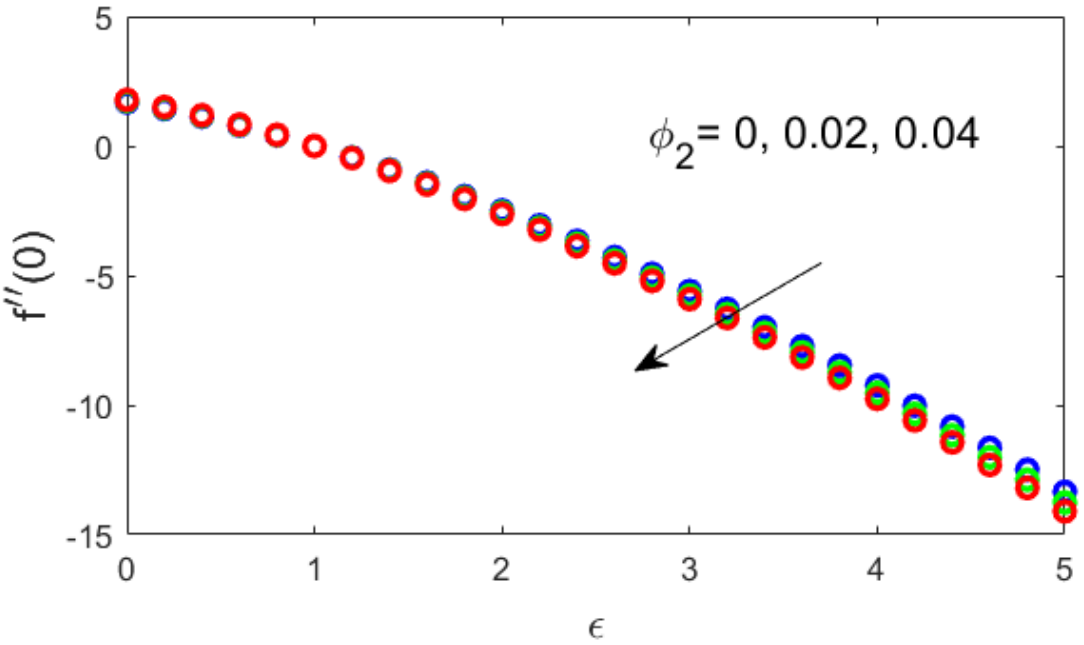

Figure 4.17. Conduct of ϵ and ϕ_2 in terms of $f''(0)$.

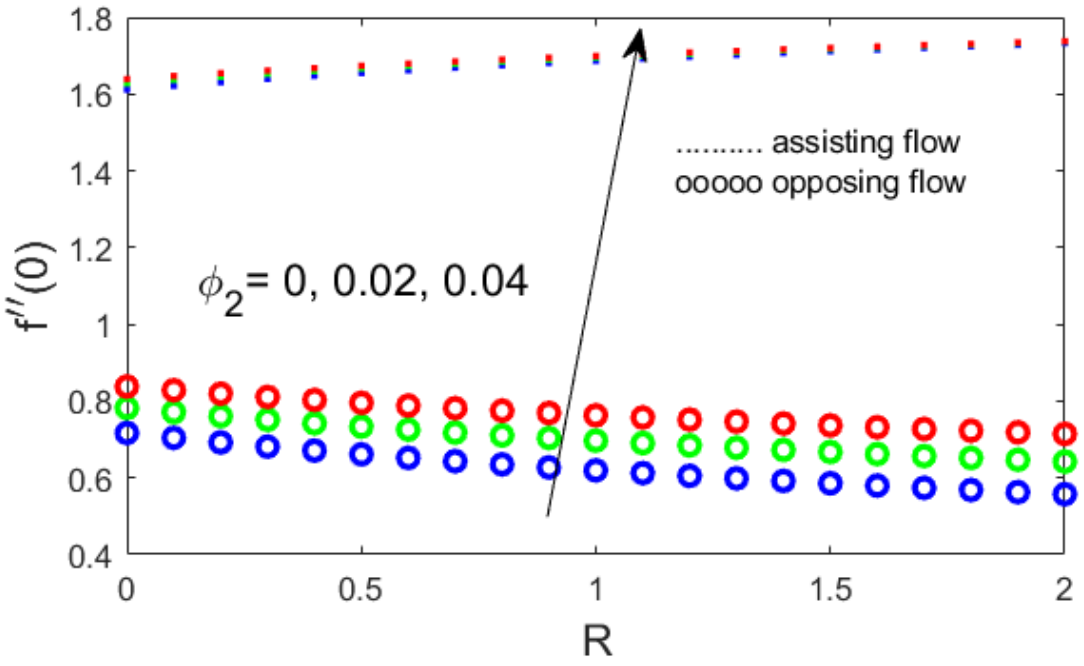

Figure 4.18. Conduct of R and ϕ_2 in terms of $f''(0)$.

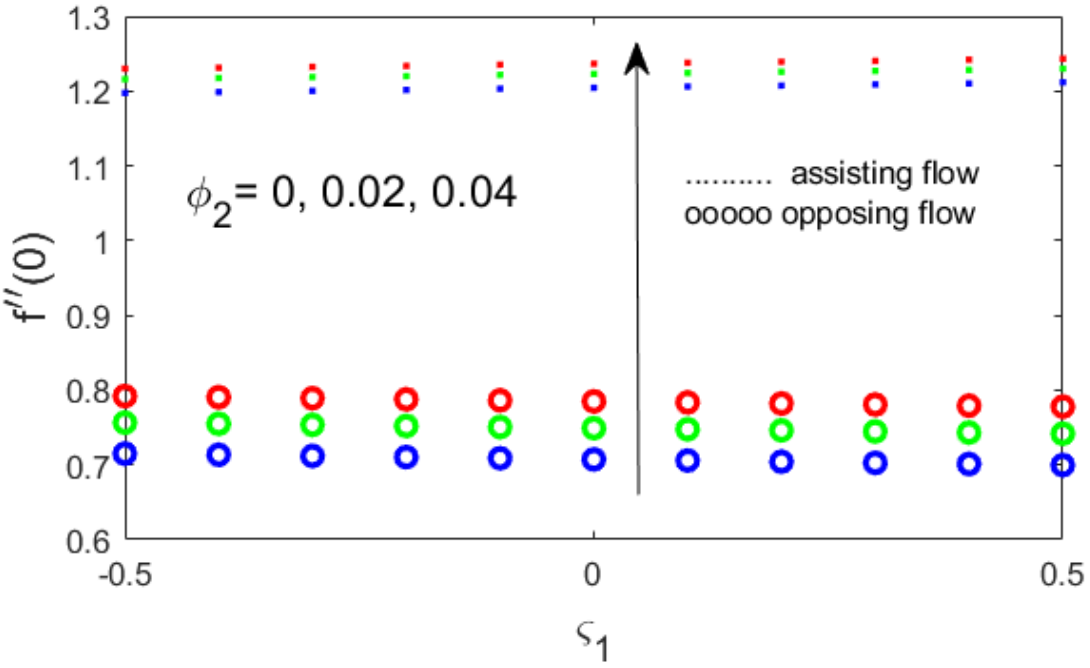

Figure 4.19. Conduct of ς_1 and ϕ_2 in terms of $f''(0)$.

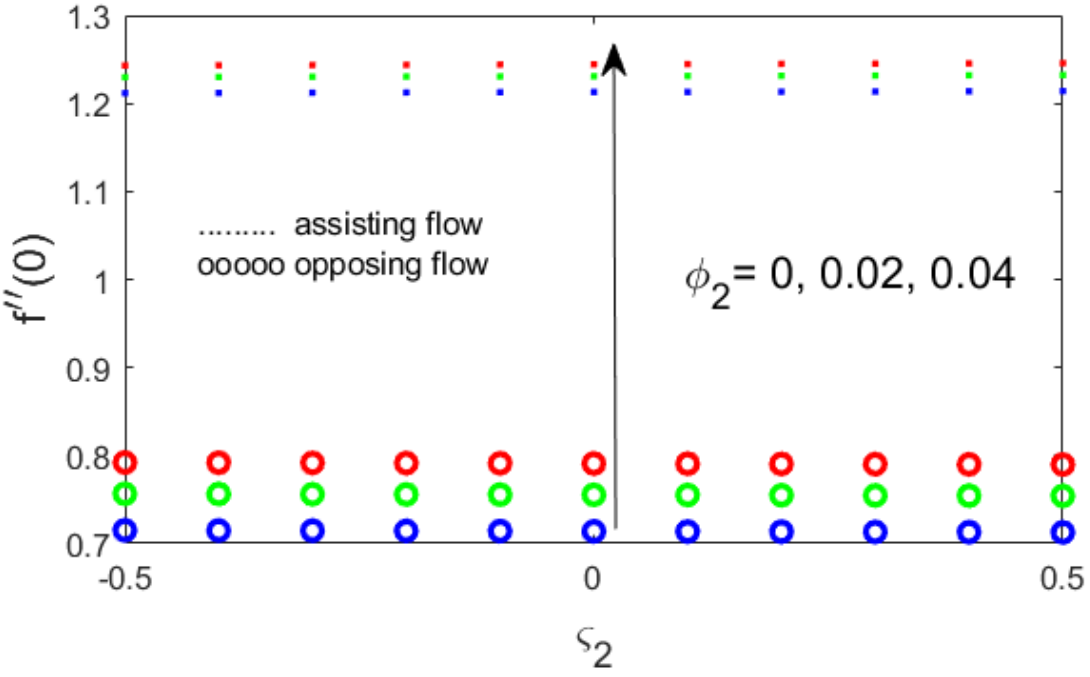

Figure 4.20. Conduct of ς_2 and ϕ_2 in terms of $f''(0)$.

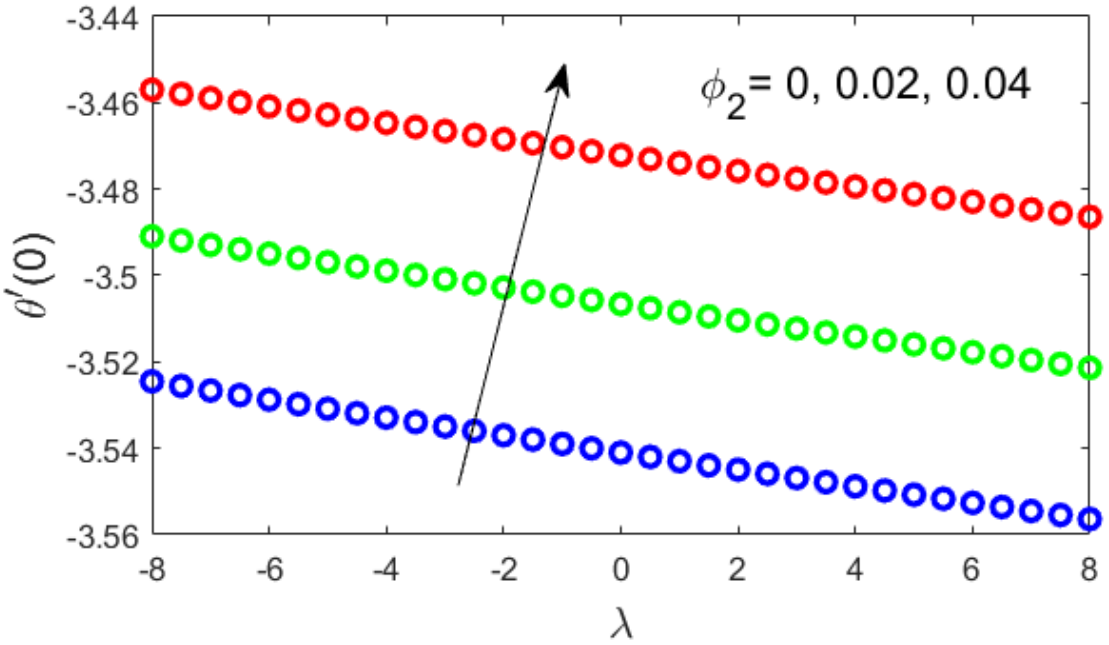

Figure 4.21. Conduct of λ and ϕ_2 in terms of $\theta'(0)$.

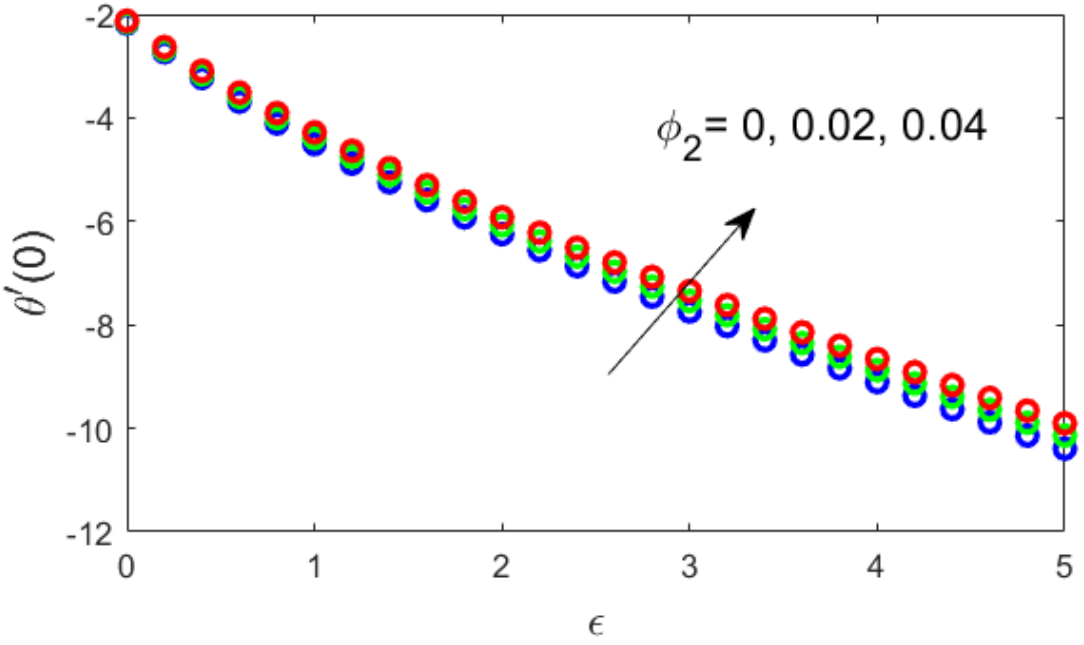

Figure 4.22. Conduct of ϵ and ϕ_2 in terms of $\theta'(0)$.

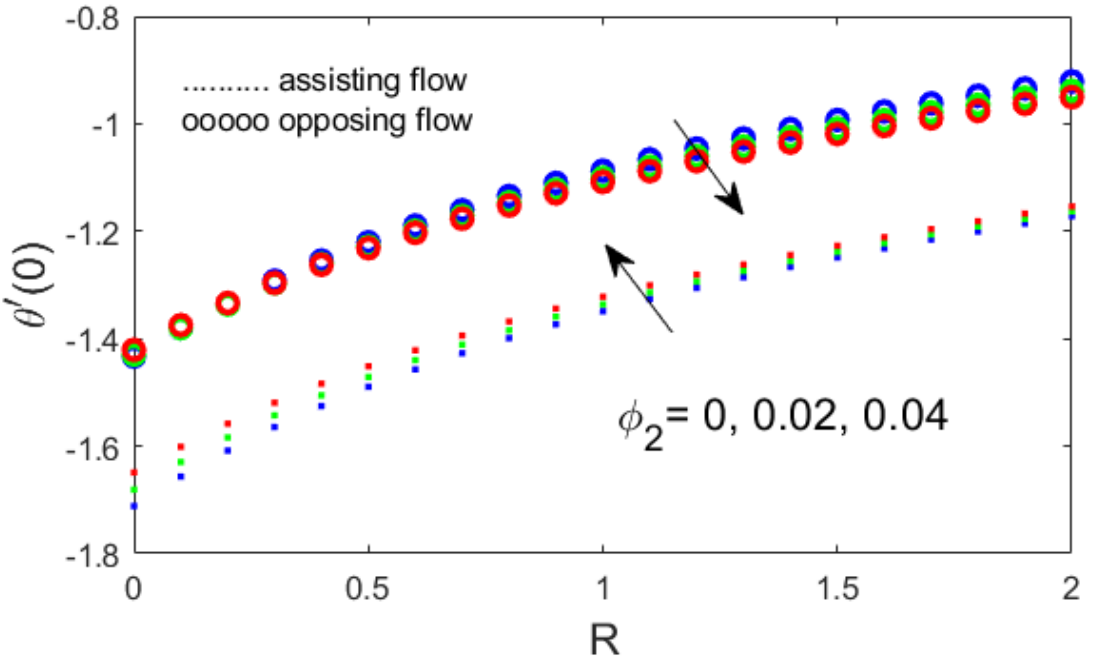

Figure 4.23. Conduct of R and ϕ_2 in terms of $\theta'(0)$.

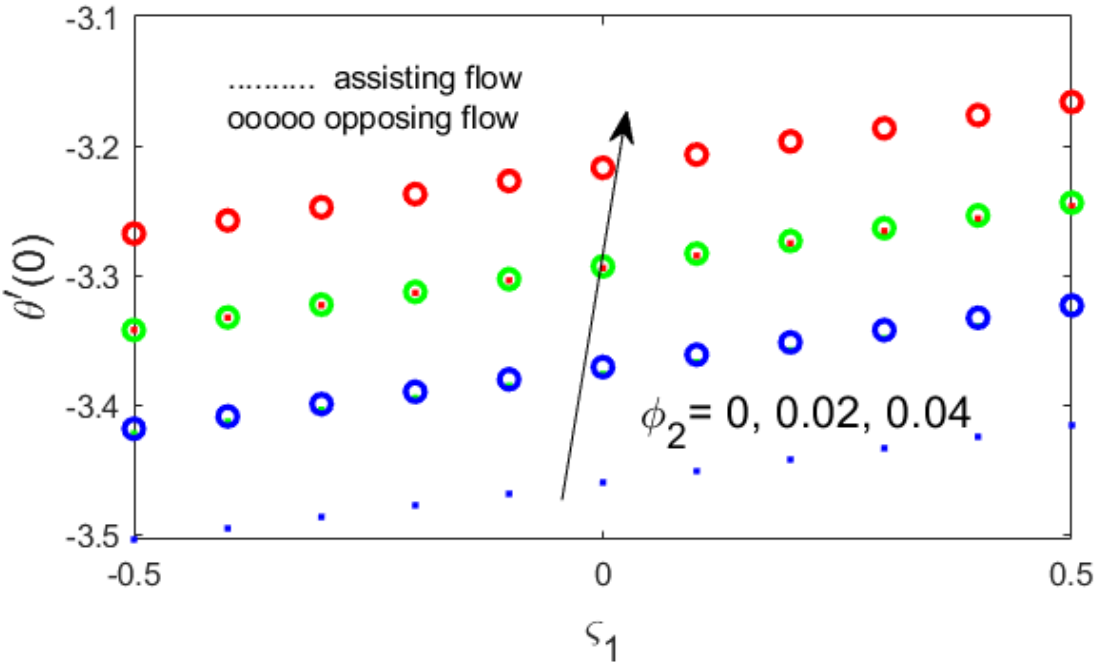

Figure 4.24. Conduct of ς_1 and ϕ_2 in terms of $\theta'(0)$.

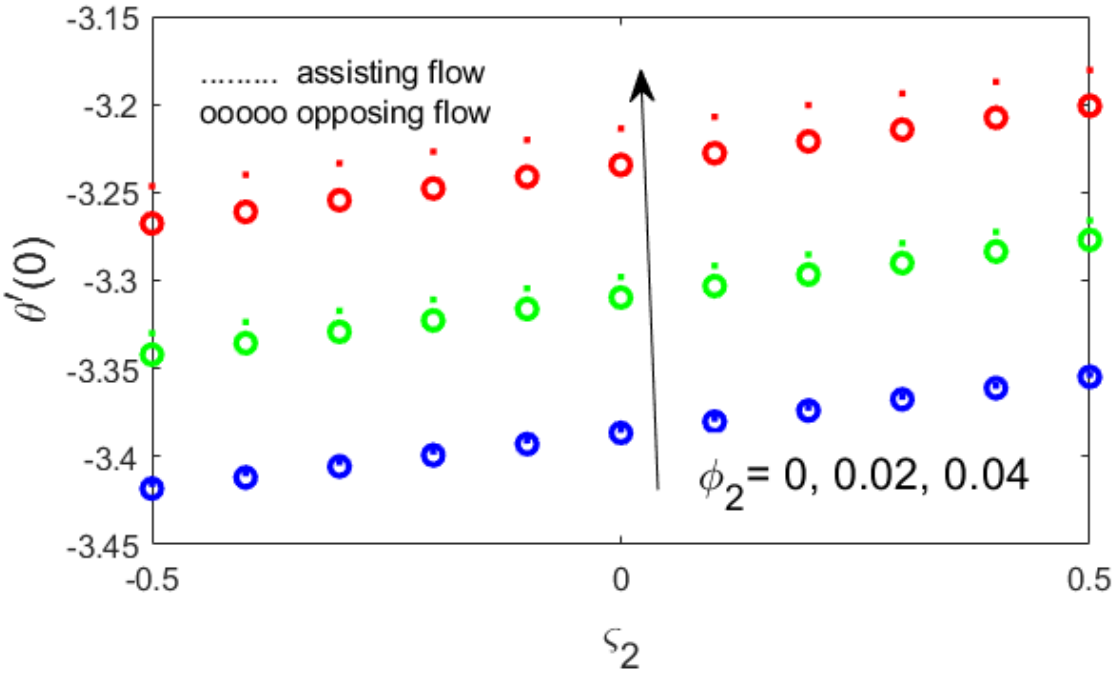

Figure 4.25. Conduct of ς_2 and ϕ_2 in terms of $\theta'(0)$.

Chapter 5

The Analysis of Magnetohydrodynamic Flow for a Hybrid Nanofluid Flowing across a Stretching Surface with Convective Boundary Conditions

5.1 Introduction

This study examines the characteristics of a steady flow for a two-dimensional, laminar, viscous, incompressible hybrid nanofluid moving over a surface. The surface exhibits stretching behavior described by an exponential function and the flow is influenced by various effects, including magneto hydrodynamics (MHD), permeability and convective boundary conditions. The assumed model is obtainable as the form of a system of partial differential equations. This complex system of PDEs is a modified into system of ODEs via using transformations. A numerical method is utilized for attaining major results from the study. These results are presented graphically as velocity and temperature profiles. The impact of different parameter are also obtained for friction drag and Nusselt number. The existing study is authenticated through a comparison study with the published literature.

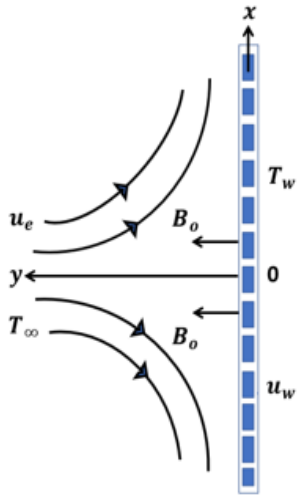

Figure 5.1 Flow configuration model

5.2 Mathematical formulation

The investigation involves a steady flow of hybrid nanoliquid towards a sheet which is permeable and is stretched exponentially. The flow enquiry is supported through consideration of thermal radiation, magnetic field, heat source/sink and convective boundary conditions. A perpendicular magnetic field associated with strength B_0 is assumed for the flow. The surface stretches in the *x* direction with a surface velocity denoted as $u_w = v_0 e^{Nx/L}$ and $u_e(x) = u_0 e^{Nx/L}$ characterizes free stream velocity. The surface temperature is $T_w(x) = T_\infty + T_0 e^{2Nx/L}$ where T_∞ denotes the ambient temperature and T_0 corresponds to the initial temperature.

The velocity pattern of the boundary layer flow is specified as follows:

$$\mathbf{V} = [u(x,y), v(x,y), 0]. \tag{5.1}$$

The continuity, momentum and energy equations are as follows:

$$\nabla.\mathbf{V} = 0, \tag{5.2}$$

$$\rho \frac{D\boldsymbol{V}}{Dt} = \nabla.\boldsymbol{\tau} + \mathbf{J} \times \mathbf{B}, \tag{5.3}$$

$$\rho c_p \frac{DT}{Dt} = -\text{div}\,\mathbf{q} - \frac{\partial q_r}{\partial y} + q''', \tag{5.4}$$

With

$$\boldsymbol{\tau} = -\,\text{p}\mathbf{I} + \mu\mathbf{A}_1, \quad \mathbf{q} = -\boldsymbol{k}\text{grad}T, \tag{5.5}$$

in which ρ, $\mathbf{V}$, c_p, T, $\mathbf{q}$, $\boldsymbol{\tau}$, q''', k, q_r, $\mathbf{I}$, A_1, $\mathbf{J}$ and $\mathbf{B}$ is designated as density, as velocity field, the specific heat (at constant pressure), as fluid's temperature, as heat flux, as stress tensor, as heat source/sink, as thermal conductivity, as radiation heat flux, as unit tensor and as first Rivilin-Erickson tensor, as electric current density, as total magnetic field. Thus

$$\mathbf{A_1} = \mathbf{L} + \mathbf{L}^{\text{T}}, \tag{5.6}$$

$$\mathbf{L} = \text{grad}\,\mathbf{V} = \begin{bmatrix} \frac{\partial u}{\partial x} & \frac{\partial u}{\partial y} & 0 \\ \frac{\partial v}{\partial x} & \frac{\partial v}{\partial y} & 0 \\ 0 & 0 & 0 \end{bmatrix} \quad \text{and} \quad \mathbf{L}^{\text{T}} = (\text{grad}\,\mathbf{V})^{\text{T}} = \begin{bmatrix} \frac{\partial u}{\partial x} & \frac{\partial v}{\partial x} & 0 \\ \frac{\partial u}{\partial y} & \frac{\partial v}{\partial y} & 0 \\ 0 & 0 & 0 \end{bmatrix}. \tag{5.7}$$

$$\boldsymbol{A}_1 = \begin{bmatrix} 2\frac{\partial u}{\partial x} & \frac{\partial u}{\partial y} + \frac{\partial v}{\partial x} & 0 \\ \frac{\partial v}{\partial x} + \frac{\partial u}{\partial y} & 2\frac{\partial v}{\partial y} & 0 \\ 0 & 0 & 0 \end{bmatrix}. \tag{5.8}$$

The electromagnetic force is expressed as [85]

$$\mathbf{J} \times \mathbf{B} = \sigma(\mathbf{E} + \mathbf{V} \times \mathbf{B}) \times \mathbf{B}, \tag{5.9}$$

$$\mathbf{B} = [0, B_0, 0]. \tag{5.10}$$

So

$$\mathbf{J} \times \mathbf{B} = -\sigma \boldsymbol{B}_0{}^2 \boldsymbol{V}, \tag{5.11}$$

where B_0 is denoted for applied magnetic field (in the *y*-direction), σ for electrical conductivity and *E* for electric field which is neglected. Further

$$\text{div } \mathbf{q} = -k\left(\frac{\partial^2 T}{\partial x^2} + \frac{\partial^2 T}{\partial y^2}\right). \tag{5.12}$$

With the help of Roseland approximation,

$$q_r = -\frac{4\sigma}{3k^*}\frac{\partial T^4}{\partial y}, \tag{5.13}$$

where σ stands for the Stefan-Boltzman constant and k^* represents the absorption coefficient while

$$T^4 = 4T_\infty{}^3 T - 3T_\infty{}^4. \tag{5.14}$$

Differentiation of Eq. (5.14) gives

$$\frac{\partial T^4}{\partial y} = 4T_\infty{}^3 \frac{\partial T}{\partial y}. \tag{5.15}$$

Using Eq. (5.15) in Eq. (5.13) results in the following expression

$$q_r = -\frac{16\sigma T_\infty{}^3}{3k^*}\frac{\partial T}{\partial y}. \tag{5.16}$$

The non uniform heat source (or can be sink) is identified by [75] as

$$q''' = \frac{k_{hnf} u_w}{2L\nu_f}[\varsigma_1(T_w - T_\infty)f' + \varsigma_2(T - T_\infty)], \tag{5.17}$$

where $\varsigma_1 < 0$ (space dependent) and ς_2 (space dependent) > 0 respond to generation of heat while ς_1 and $\varsigma_2 < 0$ is associated with heat absorption.

Substituting the Eqs. (5.6)–(5.12) and (5.16) in the governing equations,

$$\frac{\partial u}{\partial x} + \frac{\partial v}{\partial y} = 0, \tag{5.18}$$

$$u\frac{\partial u}{\partial x}+v\frac{\partial u}{\partial y}=u_e\frac{\partial u_e}{\partial x}+\nu_{hnf}\left(\frac{\partial^2 u}{\partial y^2}\right)+\frac{(\rho\beta)_{hnf}}{\rho_{hnf}}(T-T_\infty)g-\frac{\sigma_{hnf}}{\rho_{hnf}}{\beta_0}^2(u-u_e), \quad (5.19)$$

$$u\frac{\partial T}{\partial x}+v\frac{\partial T}{\partial y}=\frac{1}{(\rho c_p)_{hnf}}\left(k_{hnf}+\frac{16\sigma{T_\infty}^3}{3k^*}\right)\frac{\partial^2 T}{\partial y^2}+\frac{k_{hnf}u_w}{2Lv_f(\rho c_p)_{hnf}}[\varsigma_1(T_w-T_\infty)f'+\varsigma_2(T-T_\infty)]+\frac{\sigma_{hnf}}{(\rho c_p)_{hnf}}{\beta_0}^2(u-u_e)^2. \quad (5.20)$$

The boundary conditions for the flow are

$$\left.\begin{aligned} v=v_w,\quad u=u_w,\quad -k_{hnf}\frac{\partial T}{\partial y}=h_f(T_w-\mathrm{T}) \quad \text{at} \quad \mathrm{y}=0\\ u\to u_e,\quad T\to T_\infty \quad as \quad y\to\infty \end{aligned}\right\}. \quad (5.21)$$

The function $u_w=v_0e^{Nx/L}$represents the velocity corresponding to stretching of sheet, with $v_0>0$ being exponentially assisting surface, $v_0<0$ being exponentially opposing surface. The function $u_e=u_0e^{Nx/L}$ represents the free stream velocity and the surface temperature is given as $T_w=T_\infty+T_0e^{2Nx/L}$, T_∞ is the ambient temperature, L is reference length, T_0 is an initial temperature, $v_w=-N\sqrt{\frac{u_0\nu_f}{2L}}e^{\frac{Nx}{2L}}S$, S is the suction/injection parameter while suction corresponds to $S>0$ and injection corresponds to $S<0$.

The required transformations are expressed as

$$\left.\begin{aligned} \eta=y\sqrt{\frac{u_0}{2\nu_fL}}e^{\frac{Nx}{2L}},\quad \psi=\sqrt{2u_0\upsilon_fL}\,f(\eta)e^{\frac{Nx}{2L}},\quad \theta(\eta)=\frac{T-T_\infty}{T_w-T_\infty},\\ u=u_0e^{\frac{Nx}{L}}f'(\eta),\quad v=-N\sqrt{\frac{u_0\nu_f}{2L}}e^{\frac{Nx}{2L}}[f(\eta)+\eta f'(\eta)], \end{aligned}\right\}. \quad (5.22)$$

The continuity Eq. (5.18) is satisfied via the transformations and Eqs (5.19), (5.20) and (5.21) after employing the transformations become

$$\left.\begin{aligned} \frac{\frac{\mu_{hnf}}{\mu_f}}{\frac{\rho_{hnf}}{\rho_f}}f'''(\eta)+Nf(\eta)f''(\eta)-2N\left(f'(\eta)\right)^2+2N+2\frac{\frac{(\rho\beta)_{hnf}}{(\rho\beta)_f}}{\frac{\rho_{hnf}}{\rho_f}}\lambda\,\theta(\eta)\\ -\frac{\frac{\sigma_{hnf}}{\sigma_f}}{\frac{\rho_{hnf}}{\rho_f}}M(f'(\eta)-1)=0, \end{aligned}\right\}, \quad (5.23)$$

$$\left.\begin{aligned}&\frac{1}{Pr}\frac{1}{\frac{(\rho c_p)_{hnf}}{(\rho c_p)_f}}\left(\frac{k_{hnf}}{k_f}+\frac{4}{3}R\right)\theta''(\eta)+Nf(\eta)\theta'(\eta)-4N\theta(\eta)f'(\eta)\\&+\frac{\frac{\sigma_{hnf}}{\sigma_f}}{\frac{\rho_{hnf}}{\rho_f}}MEc(f'(\eta)-1)^2+\frac{\epsilon}{Pr}\frac{\frac{k_{hnf}}{k_f}}{\frac{(\rho c_p)_{hnf}}{(\rho c_p)_f}}[\xi_1 f'(\eta)+\xi_2\theta(\eta)]=0,\end{aligned}\right\}. \tag{5.24}$$

The needed boundary restrictions are

$$\left.\begin{aligned}&f(0)=S, \qquad f'(0)=\epsilon, \qquad \theta'(0)=-\frac{k_f}{k_{hnf}}Bi(1-\theta(0)),\\&\qquad\qquad f'(\infty)=1, \qquad \theta(\infty)=0.\end{aligned}\right\}. \tag{5.25}$$

Here, $\Pr=\frac{(\mu c_p)_f}{k_f}$ is denoted for Prandtl number, $R=\frac{4\sigma T^3{}_\infty}{k^* k_f}$ for thermal radiation parameter, $\varepsilon=\frac{v_0}{u_0}$ for velocity ratio parameter, $\lambda=\frac{g\beta_f T_0 L}{{u_0}^2}=\frac{Gr_x}{{Re_x}^2}$ for assisting and opposing parameter, ${Re_x}^2=\frac{u_0 L e^{\frac{Nx}{L}}}{{\nu_f}}$ for local Reynolds number, $Gr_x=\frac{g\beta_f T_0 L^3 e^{\frac{2Nx}{L}}}{{\nu_f}^2}$ for local Grashof number, $M=\frac{2L\sigma_f {\beta_0}^2}{\rho_f u_e}$ for magnetic parameter, $Ec=\frac{{u_e}^2}{(T_w-T_\infty)(C_p)_f}$ for Eckert number, $Bi=\frac{h_f}{k_f}\sqrt{\frac{2\nu_f L}{u_e}}e^{-\frac{Nx}{2L}}$ for Biot number.

The skin friction coefficient and thus the Nusselt number are illustrated through the following mathematical expressions. [75], [79], [84]

$$(2Re_x)^{-\frac{1}{2}}C_{fx}=\frac{\mu_{hnf}}{\mu_f}f''(0), \tag{5.26}$$

$$\left(\frac{Re_x}{2}\right)^{-\frac{1}{2}}Nu_x=-\left(\frac{k_{hnf}}{k_f}+\frac{4}{3}R\right)\theta'(0). \tag{5.27}$$

5.3 Numerical simulations

The Bvp4c technique by means of MATLAB software is adopted to find solutions for the less difficult system of ODEs but these differential equations are in general higher order differential equations and initially a scheme is devised to revise these higher order ODEs as a

system of first order ODEs. This serves the purpose to initiate this numerical technique. In order to solve the system of ODEs, the model equations are simplified as.

$$\left.\begin{array}{c} f = y(1),\ f' = y(2),\ f'' = y(3),\ f''' = y(4) \\ y(4) = \dfrac{\frac{\rho_{hnf}}{\rho_f}}{\frac{\mu_{hnf}}{\mu_f}} \left(\begin{array}{c} 2Ny(2)y(2) - Ny(1)y(3) - 2N - 2\lambda \dfrac{\frac{(\rho\beta)_{hnf}}{(\rho\beta)_f}}{\frac{\rho_{hnf}}{\rho_f}} y(5) \\ + \dfrac{\frac{\sigma_{hnf}}{\sigma_f}}{\frac{\rho_{hnf}}{\rho_f}} M(y(2) - 1) \end{array} \right) \end{array}\right\}, \tag{5.28}$$

$$\left.\begin{array}{c} \theta = y(5),\ \theta' = y(6),\ \theta'' = y(7) \\ y(7) = \Pr \dfrac{\frac{(\rho c_p)_{hnf}}{(\rho c_p)_f}}{\left(\frac{k_{hnf}}{k_f} + \frac{4}{3}R\right)} \left(\begin{array}{c} 4Ny(5)y(2) - Ny(1)y(6) - \dfrac{\epsilon}{\Pr} \dfrac{\frac{k_{hnf}}{k_f}}{\frac{(\rho c_p)_{hnf}}{(\rho c_p)_f}} (y(2)\varsigma_1 + y(5)\varsigma_2) \\ - \dfrac{\frac{\sigma_{hnf}}{\sigma_f}}{\frac{(\rho c_p)_{hnf}}{(\rho c_p)_f}} MEc(y(2)y(2) - 2y(2) + 1) \end{array} \right) \end{array}\right\}. \tag{5.29}$$

Along with the conditions

$$y_a(1) - S,\quad y_a(2) - \epsilon,\quad y_b(2) - 1,\quad y_b(5),\qquad y_a(6) + \frac{k_f}{k_{hnf}} Bi\big(1 - y_a(5)\big). \tag{5.30}$$

5.4 Result and discussion

The velocity derivative $f'(\eta)$ and the temperature distribution $\theta(\eta)$ are affected by the different parameters as shown in Figures 5.2-5.23. Equations (5.28) and (5.29) that reflect the free-stream conditions and equation (5.30) that specifies the boundary condition gradually match up with the flow patterns.

Tables 5.1 and Table 5.2 are illustrated to mention the thermo-physical required properties for the analysis. The comparative study for the skin friction and Nusselt number values are elaborated in Tables 5.3 to Table 5.6. The comparison executed is in decent agreement with the exiting work.

The figures 5.2 exhibit volume fraction coefficient for Al_2O_3 nanoparticles ϕ_1 affecting the velocity profile in both assisting $\lambda = 1$ and opposing flows $\lambda = -1$ for $\phi_2 = 0.04$, $\epsilon = 0$, $R = 0.1$, $\varsigma_1 = -0.5$, $\varsigma_2 = -0.5$, $\Pr = 6.2$, $N = 0.5$, $M = 0.5$, $S = 0.5$, $Ec = 0.3$ and $Bi = 1$. After ϕ_1 increases, the velocity and hence momentum boundary layer thickness decline for both the assisting and opposing flows. Figure 5.3 display how alterations in the volume fraction

coefficient for Cu nanoparticles ϕ_2 affect velocity profiles in both assisting and opposing flows for $\phi_1 = 0.1$, $\epsilon = 0$, $R = 0.1$, $\varsigma_1 = -0.5$, $\varsigma_2 = -0.5$, Pr $= 6.2$, $N = 0.5$, $M = 0.5$, $S = 0.5$, $Ec = 0.3$ and $Bi = 1$. The increase in ϕ_2 is associated with increased velocity and momentum boundary layer thickness accordingly for both the considered cases. Figure 5.4 depict the influence of changes in the radiation parameter *R* on the velocity profile $f'(\eta)$ for both assisting $(\lambda = 1)$ and opposing $(\lambda = -1)$ fluid flows, assuming $\phi_1 = 0.1$, $\phi_2 = 0.04$, $\epsilon = 0$, $\varsigma_1 = -0.5$, $\varsigma_2 = -0.5$, Pr $= 6.2$, $N = 0.6$, $M = 0.5$, $S = 0.5$, $Ec = 0.3$ and $Bi = 1$. The results indicate that when $\lambda = 1$, an increase in R leads to an amplified velocity profile $f'(\eta)$ and subsequently an increased momentum layer thickness. Conversely for $\lambda = -1$, the momentum layer thickness cuts down as *R* increases. Figure 5.5 demonstrate the impact of the velocity ratio parameter ϵ on the velocity profile $f'(\eta)$ for both assisting $(\lambda = 1)$ and opposing $(\lambda = -1)$ fluid flows. The tentative values involve $\phi_1 = 0.1$, $\phi_2 = 0.04$, $R = 0.1$, $\varsigma_1 = 0$, $\varsigma_2 = -0.5$, Pr $= 6.2$, $N = 0.5$, $M = 0.5$, $S = 0.5$, $Ec = 0.3$ and $Bi = 1$. The results indicate that an proliferation in ϵ leads to an rise in the velocity profile $f'(\eta)$ and the thickness of the momentum boundary layer for both $\lambda = 1$ and $\lambda = -1$. Figure 5.6 display the velocity profile $f'(\eta)$ for Prandtl numbers Pr with given values, $\phi_1 = 0.1$, $\phi_2 = 0.04$, $\epsilon = 0$, $R = 0.1$, $\varsigma_1 = -0.5$, $\varsigma_2 = -0.5$, $N = 0.5$, $M = 0.5$, $S = 0.5$, $Ec = 0.3$ and $Bi = 1$. The results indicate that when $\lambda = -1$, the growth in Pr leads to an augmentation in $f'(\eta)$ and a corresponding increase in the thickness of the momentum boundary layer. On the other hand, for $\lambda = 1$, $f'(\eta)$ decreases and the momentum layer thickness also decreases as Pr increases. Figure 5.7 demonstrate the influence of the parameter ς_1 on the velocity profile $f'(\eta)$, assuming $\phi_1 = 0.1$, $\phi_2 = 0.04$, $\epsilon = 0.2$, $R = 0.1$, $\varsigma_1 = -0.5$, $\varsigma_2 = -0.5$, Pr $= 6.2$, $N = 0.5$, $M = 0.5$, $S = 0.5$, $Ec = 0.3$ and $Bi = 1$. The results indicate that an increase in ς_1 leads to an augmentation in $f'(\eta)$ and the thickness of the momentum layer for $\lambda = 1$. However for $\lambda = -1$, $f'(\eta)$ decreases and the momentum boundary layer thickness falls out as $\varsigma_1$increases. Figure 5.8 present the impact of the magnetic parameter *M* on the velocity profile $f'(\eta)$ for both assisting $\lambda = 1$ and opposing $\lambda = -1$ fluid flows. The experimental values encompass $\phi_1 = 0.1$, $\phi_2 = 0.04$, $\epsilon = 0$, $R = 0.1$, $\varsigma_1 = -0.5$, $\varsigma_2 = -0.5$, Pr $= 6.2$, $N = 0.3$, $S = 0.5$, $Ec = 0.1$ and $Bi = 1$. The upshots specify that an escalation in M points towards an augmentation in the velocity profile $f'(\eta)$ and the thickness of the momentum layer for both $\lambda = 1$ and $\lambda = -1$. Figure 5.9 depict the impact of the suction/injunction parameter *S* on the velocity profile $f'(\eta)$ for both assisting $\lambda = 1$ and opposing $\lambda = -1$ fluid flows. The experimental values consist of $\phi_1 = 0.1$, $\phi_2 = 0.04$, $\epsilon = 0$, $R = 0.1$, $\varsigma_1 = -0.5$, $\varsigma_2 = -0.5$, Pr $= 6.2$, $N = 0.5$, $M = 0.5$, $Ec = 0.3$ and $Bi = 1$. The

results indicate that an increase in S leads to an enhancement in the velocity profile $f'(\eta)$ and the thickness of the momentum layer for both $\lambda = 1$ and also for $\lambda = -1$. Figures 5.10 demonstrate the control of the Eckert number parameter Ec on the velocity profile $f'(\eta)$, assuming $\phi_1 = 0.1$, $\phi_2 = 0.04$, $\epsilon = 0$, $R = 0.1$, $\varsigma_1 = -0.5$, $\varsigma_2 = -0.5$, $\mathrm{Pr} = 6.2$, $N = 0.5$, $M = 0.5$, $S = 0.5$ and $Bi = 1$.The results indicate that an increase in Ec leads to an amplification in $f'(\eta)$ and the thickness of the momentum boundary layer for $\lambda = 1$. Conversely for $\lambda = -1$, $f'(\eta)$ decreases and the momentum boundary layer thickness decreases as Ec increases. Figure 5.11 show the outcome of varying parameter *Bi* on the velocity profile $f'(\eta)$. The experimental considered values are $\phi_1 = 0.1$, $\phi_2 = 0.04$, $\epsilon = 0$, $R = 0.1$, $\varsigma_1 = -0.5$, $\varsigma_2 = -0.5$, $\mathrm{Pr} = 6.2$, $N = 0.5$, $M = 0.5$, $S = 0.5$ and $Ec = 0.3$. The results indicate that for $\lambda = 1$, an increase in Bi leads to an augmentation in $f'(\eta)$ and the thickness of the momentum boundary layer. However for $\lambda = -1$, $f'(\eta)$ decreases and the momentum boundary layer thickness decreases as Bi increases. An increase in volume fraction coefficient ϕ_1 causes both opposing and aiding flows $\lambda = 1, -1$ flows to have increased temperature profiles, which in turn causes the thickness of the heat boundary layer to grow for both types of flows, as shown in Figure 5.12 for $\phi_2 = 0.04$, $\epsilon = 0$, $R = 0.1$, $\varsigma_1 = -0.5$, $\varsigma_2 = -0.5$, $\mathrm{Pr} = 6.2$, $N = 0.5$, $M = 0.5$, $S = 0.5$, $Ec = 0.3$ and $Bi = 1$. Figure 5.13 examines how a rise in volume fraction coefficient ϕ_2 causes both opposing and aiding $\lambda = -1$ and $\lambda = 1$ flows to have higher temperature profiles, which in turn causes the thickness of the heat boundary layer to rise for both kinds of fluids for $\phi_1 = 0.1$, $\epsilon = 0$, $R = 0.1$, $\varsigma_1 = -0.5$, $\varsigma_2 = -0.5$, $\mathrm{Pr} = 6.2$, $N = 0.5$, $M = 0.5$, $S = 0.5$, $Ec = 0.3$ and $Bi = 1$. Figure 5.14 inspects that an increase in R causes an elevation in the temperature profile $\theta(\eta)$ for both assisting ($\lambda = 1$) and opposing ($\lambda = -1$) fluid flows assuming $\phi_1 = 0.1$, $\phi_2 = 0.04$, $\epsilon = 0$, $\varsigma_1 = -0.5$, $\varsigma_2 = -0.5$, $\mathrm{Pr} = 6.2$, $N = 0.6$, $M = 0.5$, $S = 0.5$, $Ec = 0.3$ and $Bi = 1$. This finding aligns with the physical observation that higher *R* values correspond to an increase in the thickness of the heat boundary layer. Figure 5.15 reviews that an increase in ϵ results in a decrease in the temperature profile $\theta(\eta)$ for both $\lambda = 1$ and $\lambda = -1$, with $\phi_1 = 0.1$, $\phi_2 = 0.04$, $R = 0.1$, $\varsigma_1 = 0$, $\varsigma_2 = -0.5$, $\mathrm{Pr} = 6.2$, $N = 0.5$, $M = 0.5$, $S = 0.5$, $Ec = 0.3$ and $Bi = 1$. Figure 5.16 is sketched to assess the results for both $\lambda = 1$ and $\lambda = -1$, and an increase in Pr results in a shrinkage in temperature profile $\theta(\eta)$ and a reduction in the thickness of the heat boundary layer as well for $\phi_1 = 0.1$, $\phi_2 = 0.04$, $\epsilon = 0$, $R = 0.1$, $\varsigma_1 = -0.5$, $\varsigma_2 = -0.5$, $\mathrm{Pr} = 6.2$, $N = 0.5$, $M = 0.5$, $S = 0.5$, $Ec = 0.3$ and $Bi = 1$. Figure 5.17 explores that an increase in ς_2 results in an elevation of the temperature profile $\theta(\eta)$ for both $\lambda = 1$ and $\lambda = -1$. The values consist of $\phi_1 = 0.1$, $\phi_2 =$

0.04, $\epsilon = 0.4$, $R = 0.1$, $\varsigma_1 = 0$, $\mathrm{Pr} = 6.2$, $N = 0.5$, $M = 0.5$, $S = 0.5$, $Ec = 0.3$ and $Bi = 1$. Figure 5.18 investigates that an increase in *M* causes a decrease in the temperature profile $\theta(\eta)$ for both $\lambda = 1$ and $\lambda = -1$ involving $\phi_1 = 0.1$, $\phi_2 = 0.04$, $\epsilon = 0$, $R = 0.1$, $\varsigma_1 = -0.5$, $\varsigma_2 = -0.5$, $\mathrm{Pr} = 6.2$, $N = 0.5$, $M = 0.5$, $S = 0.5$, $Ec = 0.3$ and $Bi = 1$. Figure 5.19 illuminates that an increase in *S* also causes a reduction in the temperature profile $\theta(\eta)$ for both $\lambda = 1$ and $\lambda = -1$, while covering $\phi_1 = 0.1$, $\phi_2 = 0.04$, $\epsilon = 0$, $R = 0.1$, $\varsigma_1 = -0.5$, $\varsigma_2 = -0.5$, $\mathrm{Pr} = 6.2$, $N = 0.5$, $M = 0.5$, $S = 0.5$, $Ec = 0.3$ and $Bi = 1$. Figure 5.20 is plotted to confirm that an increase in *Ec* results in an elevation of the temperature profile $\theta(\eta)$ for both $\lambda = 1$ and $\lambda = -1$, while $\phi_1 = 0.1$, $\phi_2 = 0.04$, $\epsilon = 0$, $R = 0.1$, $\varsigma_1 = -0.5$, $\varsigma_2 = -0.5$, $\mathrm{Pr} = 6.2$, $N = 0.5$, $M = 0.5$, $S = 0.5$, $Ec = 0.3$ and $Bi = 1$. Figure 5.21 depicts the *Bi* values effect on the temperature profile and an increase in *Bi* corresponds the temperature profile $\theta(\eta)$ for both $\lambda = 1$ and $\lambda = -1$ in different ways. An amplified profile is depicted for assisting case while for the opposing flow, the reverse is seen for $\phi_1 = 0.1$, $\phi_2 = 0.04$, $\epsilon = 0$, $R = 0.1$, $\varsigma_1 = -0.5$, $\varsigma_2 = -0.5$, $\mathrm{Pr} = 6.2$, $N = 0.5$, $M = 0.5$, $S = 0.5$, $Ec = 0.3$ and $Bi = 1$.

The research investigates the impact of λ and also ϕ_2 on the drag force coefficient $f"(0)$ and the findings are presented in Figure 5.22, based on experimental values set as $\phi_1 = 0.1$, $\epsilon = 0.1$, $R = 0.1$, $\varsigma_1 = -0.5$, $\varsigma_2 = -0.5$, $\mathrm{Pr} = 6.2$, $N = 0.5$, $M = 0.1$, $S = 0.5$, $Ec = 0.3$ and $Bi = 1$. It is observed that the drag force $f"(0)$ increases as both λ and ϕ_2 values increase. In Figure 5.23, the impact of ϵ and ϕ_2 on the drag force coefficients $f"(0)$ is examined. The parametric value are $\phi_1 = 0.1$, $R = 0.1$, $\varsigma_1 = -0.5$, $\varsigma_2 = -0.5$, $\mathrm{Pr} = 6.2$, $N = 0.5$, $M = 0.1$, $S = 0.5$, $Ec = 0.3$ and $Bi = 1$. It is suggested that as the values of ϕ_2 and ϵ increase, the drag force coefficients decrease for ϵ and increase for ϕ_2. Figure 5.24 display the outcomes obtained by varying the values R and ϕ_2. Specifically, the effects of the parameters while keeping $\phi_1 = 0.1$, $\epsilon = 0.1$, $\varsigma_1 = -0.5$, $\varsigma_2 = -0.5$, $\mathrm{Pr} = 6.2$, $N = 0.5$, $M = 0.5$, $S = 0.5$, $Ec = 0.2$ and $Bi = 1$ are seen. The results indicate that as ϕ_2 increases, there is an observed increase in the skin friction coefficient for both assisting and opposing flow. Figure 5.25 depict the influence of the skin friction factor with respect to the coefficient ς_1 associated with the spatially dependent heat source or sink. This analysis considers both assisting flows $\lambda = 1$ and opposing flows $\lambda = -1$, while maintaining the parameters $\phi_1 = 0.1$, $\epsilon = 0$, $R = 0.1$, $\varsigma_2 = -0.5$, $\mathrm{Pr} = 6.2$, $N = 0.5$, $M = 0.5$, $S = 0.5$, $Ec = 0.3$ and $Bi = 1$. As ϕ_2 increases the skin friction coefficient $f"(0)$ shows an increase for both aiding and opposing flows. Furthermore, increase in ς_1 shows that the skin friction coefficient $f"(0)$ rise for assisting flow but the opposite trend for opposing flow. Figures 5.26 show the results obtained by varying the values of M and ϕ_2. For $\phi_1 = 0.1$,

$\epsilon = 0.1$, $R = 0.1$, $\varsigma_1 = -0.5$, $\varsigma_2 = -0.5$, $\mathrm{Pr} = 6.2$, $N = 0.5$, $S = 0.5$, $Ec = 0.1$ and $Bi = 1$, the findings indicate that the drag force coefficient increases with increasing values of ϕ_2 and M for both assisting and opposing flow conditions. Figures 5.27 display the results obtained by varying S and ϕ_2 when $\phi_1 = 0.1$, $\epsilon = 0$, $R = 0.1$, $\varsigma_1 = -0.5$, $\varsigma_2 = -0.5$, $\mathrm{Pr} = 6.2$, $N = 0.5$, $M = 0.5$, $Ec = 0.3$ and $Bi = 1$. The outcomes indicate that the drag force coefficient increases with increasing values of ϕ_2 and S for both flow conditions. Figures 5.28 demonstrate the results obtained by varying the values of Ec and ϕ_2 parameters. With the values $\phi_1 = 0.1$, $\epsilon = 0.1$, $R = 0.1$, $\varsigma_1 = -0.5$, $\varsigma_2 = -0.5$, $\mathrm{Pr} = 6.2$, $N = 0.5$, $M = 0.1$, $S = 0.5$ and $Bi = 1$, it is vibrant that the drag force coefficient grows with aggregated values of ϕ_2 for both assisting and opposing flow conditions and with the raised values of Ec, the skin friction increase for assisting flow and opposite trend is observed for opposing flow. Figures 5.29 sightsee the results obtained by varying the values of Bi and ϕ_2 parameters with $\phi_1 = 0.1$, $\epsilon = 0.1$, $R = 0.1$, $\varsigma_1 = -0.5$, $\varsigma_2 = -0.5$, $\mathrm{Pr} = 6.2$, $N = 0.5$, $M = 0.1$, $S = 0.5$ and $Bi = 1$. The drag force coefficient increases with increasing values of ϕ_2 for both assisting and opposing flow conditions and with the larger value of Bi the skin friction increase for assisting flow and declines for opposing flow. Figure 5.30 discover the impact of λ and ϕ_2 on the Nusselt value $\theta'(0)$. The values are set as $\phi_1 = 0.1$, $\epsilon = 0.1$, $R = 0.1$, $\varsigma_1 = -0.5$, $\varsigma_2 = -0.5$, $\mathrm{Pr} = 6.2$, $N = 0.5$, $M = 0.1$, $S = 0.5$, $Ec = 0.3$ and $Bi = 1$.It is observed that the Nusselt value $\theta'(0)$ decreases with an increase in ϕ_2 and λ is associated with the opposite phenomenon. In Figure 5.31, it is observed that the Nusselt number decreases with an increase in ϕ_2 and ϵ. The suggested values are $\phi_1 = 0.1$, $R = 0.1$, $\varsigma_1 = -0.5$, $\varsigma_2 = -0.5$, $\mathrm{Pr} = 6.2$, $N = 0.5$, $M = 0.1$, $S = 0.5$, $Ec = 0.3$ and $Bi = 1$. Figure 5.32 demonstrate the outcomes obtained by varying the values R and ϕ_2, while $\phi_1 = 0.1$, $\epsilon = 0.1$, $\varsigma_1 = -0.5$, $\varsigma_2 = -0.5$, $\mathrm{Pr} = 6.2$, $N = 0.5$, $M = 0.5$, $S = 0.5$, $Ec = 0.2$ and $Bi = 1$.When ϕ_2 and R are increased under both flow conditions, the Nusselt value $\theta'(0)$ decreases. Figure 5.33 display the findings obtained by varying the values of ς_2 and $\phi_1 = 0.1$, $\epsilon = 0.1$, $R = 0.1$, $\varsigma_1 = -0.5$, $\mathrm{Pr} = 6.2$, $N = 0.5$, $M = 0.5$, $S = 0.5$, $Ec = 0.3$ and $Bi = 1$.The results indicate that as ϕ_2 increases, there is an observed decrease in the Nusselt number for both assisting and opposing flow conditions. Figure 5.34 show the results obtained by varying the values of M and ϕ_2 for $\phi_1 = 0.1$, $\epsilon = 0.1$, $R = 0.1$, $\varsigma_1 = -0.5$, $\varsigma_2 = -0.5$, $\mathrm{Pr} = 6.2$, $N = 0.5$, $S = 0.5$, $Ec = 0.1$ and $Bi = 1$. The findings indicate that the Nusselt number $\theta'(0)$ decreases with increasing values of ϕ_2 for both assisting and opposing flow conditions and opposite result is gained for M. Figure 5.35 spectacle the results obtained by varying the values of S and ϕ_2 and $\phi_1 = 0.1$, $\epsilon = 0.1$, $R = 0.1$, $\varsigma_1 = -0.5$, $\varsigma_2 = -0.5$, $\mathrm{Pr} = 6.2$, $N = 0.5$, $M = 0.5$, $Ec =$

0.3 and $Bi = 1$. The Nusselt number $\theta'(0)$ decreases with increasing values of ϕ_2 for both assisting and opposing flow conditions. Figures 5.36 reveal the results obtained by changing the values of Ec and ϕ_2 for $\phi_1 = 0.1$, $\epsilon = 0.1$, $R = 0.1$, $\varsigma_1 = -0.5$, $\varsigma_2 = -0.5$, Pr $= 6.2$, $N = 0.5$, $M = 0.5$, $S = 0.5$ and $Bi = 1$. The Nusselt number $\theta'(0)$ decreases with increasing values of ϕ_2 for both assisting and opposing flow conditions. Figures 5.37 present the outcomes due to variable values of Bi and ϕ_2.with $\phi_1 = 0.1$, $\epsilon = 0.1$, $R = 0.1$, $\varsigma_1 = -0.5$, $\varsigma_2 = -0.5$, Pr $=$ 6.2, $N = 0.5$, $M = 0.5$, $S = 0.5$ and $Ec = 0.3$. It is indicated that Nusselt number $\theta'(0)$ increases with increasing values of *Bi* for both assisting and opposing flows.

Table 5.1: Thermo-physical physiognomies of nanoparticles and water.
Waini *et al.* [73], Devi and Devi [74], Polu and Reddy [75], Rehman *et al.* [80].

Thermo-physical characteristics	Base fluid	Nanoparticles	
	H_2O	Al_2O_3	Cu
$\rho(kg/m^3)$	997.1	3970	8933
$c_{p(J/kgK)}$	4179	765	385
$k(W/mK)$	0.613	40	400
$\beta \times 10^{-5}$	21	0.85	1.67
$\sigma(s/m)$	5.5×10^{-6}	36.9×10^{6}	59.6×10^{6}
Prandtl Number	6.20	-	-

Table 5.2: Thermo-physical traits of nano-fluid and hybrid nano-fluid.
Yahaya *et al.* [71], Waini *et al.* [76], Waini [77], Rehman *et al.* [80].

Thermo-physical traits	Nano-fluid	Hybrid Nano-fluid
Density	$\rho_{nf} = (1-\phi_1)\rho_f + \phi_1\rho_{n1}$	$\rho_{hnf} = (1-\phi_2)\rho_{nf} + \phi_2\rho_{n2}$
Dynamic viscosity	$\mu_{nf} = \frac{\mu_f}{(1-\phi_1)^{2.5}}$	$\mu_{hnf} = \frac{\mu_{nf}}{(1-\phi_1)^{2.5}(1-\phi_2)^{2.5}}$
Thermal expansion	$(\rho\beta)_{nf} = (1-\phi_1)(\rho\beta)_f + \phi_1(\rho\beta)_{n1}$	$(\rho\beta)_{hnf} = (1-\phi_2)(\rho\beta)_{nf} + \phi_2(\rho\beta)_{n2}$
Heat capacity	$(\rho c_p)_{nf} = (1-\phi_1)(\rho c_p)_f + \phi_1(\rho c_p)_{n1}$	$(\rho c_p)_{hnf} = (1-\phi_2)(\rho c_p)_{nf} + \phi_2(\rho c_p)_{n2}$
Thermal conductivity	$\frac{k_{nf}}{k_f} = \frac{k_{n1}+2k_f-2\phi_1(k_f-k_{n1})}{k_{n1}+2k_f+\phi_1(k_f-k_{n1})}$	$\frac{k_{hnf}}{k_{nf}} = \frac{k_{n2}+2k_{nf}-2\phi_2(k_{nf}-k_{n2})}{k_{n2}+2k_{nf}+\phi_2(k_{nf}-k_{n2})}$
Electrical conductivity	$\frac{\sigma_{nf}}{\sigma_f} = \frac{\sigma_{n1}+2\sigma_f-2\phi_1(\sigma_f-\sigma_{n1})}{\sigma_{n1}+2\sigma_f+\phi_1(\sigma_f-\sigma_{n1})}$	$\frac{\sigma_{hnf}}{\sigma_{nf}} = \frac{\sigma_{n2}+2\sigma_{nf}-2\phi_2(\sigma_{nf}-\sigma_{n2})}{\sigma_{n2}+2\sigma_{nf}+\phi_2(\sigma_{nf}-\sigma_{n2})}$

Table 5.3: Comparative values of $f''(0)$ for different ϕ_1 and ϵ when $Bi \to \infty$, Pr = 6.2, $\phi_2 = Ec = M = \varsigma_1 = \varsigma_2 = S = R = \lambda = 0$.

ϵ	ϕ_1	Values of $f''(0)$			
		Bachok *et al.* [78]	Waini *et al.* [79]	Rehman *et al.* [80]	Present Values
-0.5	0	2.1182	2.1182	2.1182	2.118169
	0.1	2.7531	2.7531		2.753091
	0.2	3.5372	3.5372		3.537175
0	0	1.6872	1.6872	1.6872	1.687218
	0.1	2.1929	2.1930		2.192963
	0.2	2.8174	2.8175		2.817522
0.5	0	0.9604	0.9604	0.9604	0.960416
	0.1	1.2483	1.2483		1.248301
	0.2	1.6039	1.6038		1.603819

Table 5.4: Comparative values of $\theta'(0)$ for different ϕ_1 and ϵ when $Bi \to \infty$, Pr = 6.2, ϕ_2 = Ec = M = ς_1 = ς_2 = S = R = $\lambda = 0$.

ϵ	ϕ_1	Values of $\theta'(0)$		
		Waini *et al.* [79]	Rehman *et al.* [80]	Present Values
-0.5	0	0.0588	0.05687	0.058787
	0.1	0.4439		0.443804
	0.2	0.7636		0.763593
0	0	2.5066	2.5066	2.506625
	0.1	2.9655		2.965516
	0.2	3.4292		3.429219
0.5	0	4.0816	4.0816	4.081573
	0.1	4.6637		4.663649
	0.2	5.2726		5.272613

Table 5.5: Comparative Values of $f''(0)$ & $\theta'(0)$ for different ϕ_2, ϵ and λ at $Bi \to \infty$, Pr = 6.2, Ec = M = ς_1 = ς_2 = S = R = 0.

ϕ_2	λ	ϵ	$Cu/water$ $(\phi_1 = 0)$					
			Waini *et al.*[79]	Rehman *et al.*[80]	Present Values	Waini *et al.*[79]	Rehman *et al.*[80]	Present Values
			$f"(0)$	$f"(0)$	$f"(0)$	$\theta'(0)$	$\theta'(0)$	$\theta'(0)$
0	0	0	1.6872	1.6872	1.6872	2.5066	2.5066	2.5066
0.02	0	0	1.8630	1.8630	1.8630	2.6390	2.5246	2.6390
0.04	0	0	2.0387	2.0387	2.0387	2.7677	2.5357	2.7677
0.04	-1	0	1.6229	1.6002	1.6229	2.6330	2.4050	2.6330
0.04	-0.5	0	1.8345	1.8235	1.8345	2.7031	2.4732	2.7031
0.04	1	0	2.4291	2.4291	2.4291	2.8838	2.6474	2.8838
0.04	-1	-0.5	1.8484		1.8484	-0.1818		-0.1818
0.04	-1	0.5	0.8452		0.8452	4.2931		4.2931
0.04	-1	1	-0.2616		-0.2616	5.5633		5.5633

Table 5.6: Comparative Values of $f''(0)$ & $\theta'(0)$ for different ϕ_2, ϵ and λ at $Bi \to \infty$, Pr = 6.2, $Ec = M = \varsigma_1 = \varsigma_2 = S = R = 0$.

			$Cu/water\ (\phi_1 = 0.1)$					
ϕ_2	λ	ϵ	Waini *et al.*[79]	Rehman *et al.*[80]	Present Values	Waini *et al.*[79]	Rehman *et al.*[80]	Present Values
			$f"(0)$	$f"(0)$	$f"(0)$	$\theta'(0)$	$\theta'(0)$	$\theta'(0)$
0	0	0	2.1930	2.1930	2.1930	2.9655	2.9655	2.9655
0.02	0	0	2.3781	2.3781	2.3781	3.1050	3.1050	3.1050
0.04	0	0	2.5657	2.5657	2.5657	3.2426	3.2426	3.2426
0.04	-1	0	2.1500	2.1500	2.1500	3.1183	3.1183	3.1183
0.04	-0.5	0	2.3607	2.3607	2.3607	3.1825	3.1825	3.1825
0.04	1	0	2.9613	2.9613	2.9613	3.3531	3.3531	3.3531
0.04	-1	-0.5	2.5678		2.5678	0.3209		0.3209
0.04	-1	0.5	1.1384		1.1384	4.9085		4.9085
0.04	-1	1	-0.2698		-0.2698	6.3035		6.3035

Table 5.7: Parametric values were used in the present analysis.

Parameters	Symbols	Values	References
Prandtl number	Pr	5, 6.2, 7	Waini *et al.* [76], Waini *et al*. [77]
Volume friction coefficient	ϕ_1	0, 0.1	Waini *et al*. [79]
Volume friction coefficient	ϕ_2	0, 0.02, 0.04	Waini *et al.* [79]
Assisting and opposing parameter	λ	-8 to 6	Waini *et al.* [79]
Radiation parameter	R	0, 1, 2	Waini *et al.* [77]
Space dependent coefficient	ς_1	-0.5, 0, 0.5	Waini *et al.* [73], Reddy and Reddy [75] and Waini *et al.* [79]
Temperature dependent coefficient	ς_2	-0.5, 0, 0.5	Waini *et al.* [73], Reddy and Reddy [75] and Waini *et al.* [79]
Velocity ratio parameter	ϵ	-0.5, 0.5, 1	Waini *et al.* [79]
Magnetic parameter	M	[0,0.5]	Sarfraz *et al.* [82] and Wahid *et al.* [60]
Suction/ blower parameter	S	$[-5,5]$	Wahid *et al.* [60]
Eckert number	Ec	[0.1,0.3]	Ahmad *et al.* [83]
Biot number	Bi	[1,10]	Alarifi *et al.* [81], Sarfraz *et al.* [82] and Wahid *et al.* [60]

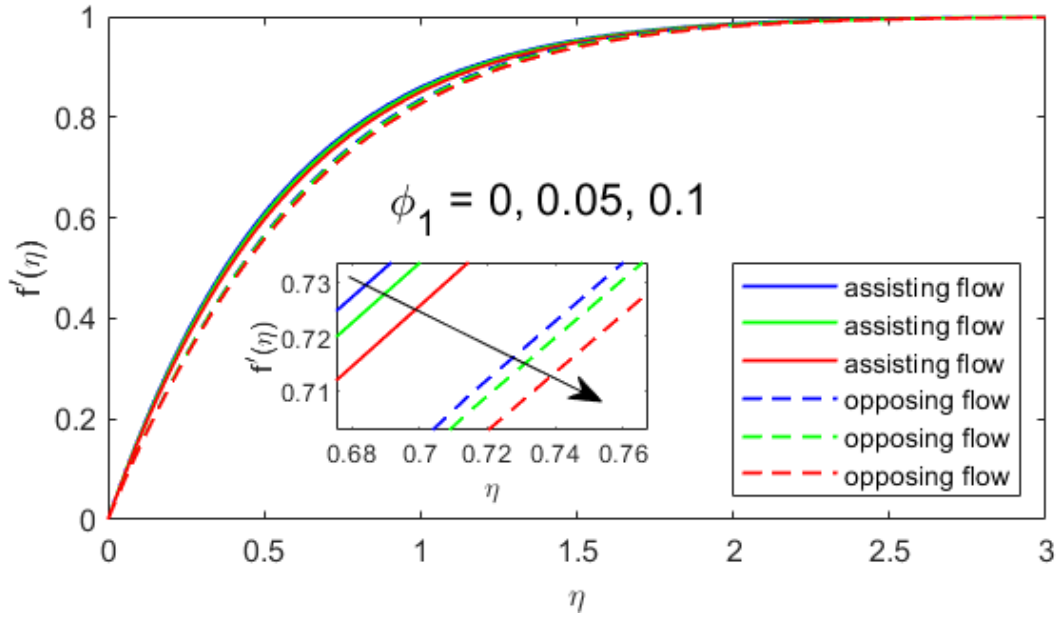

Figure 5.2. Conduct of ϕ_1 in terms of $f'(\eta)$.

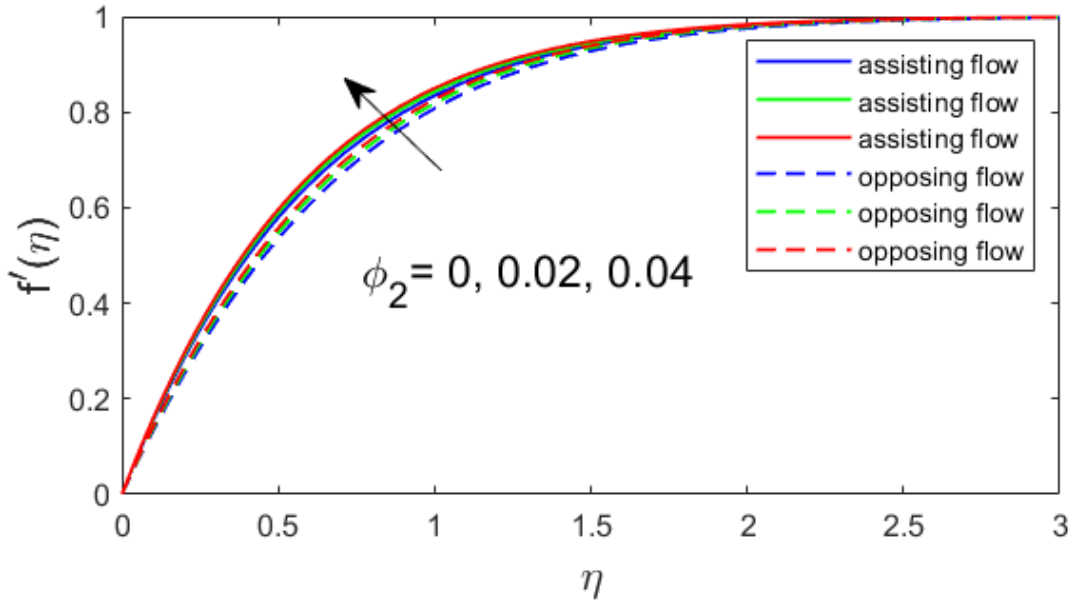

Figure 5.3. Conduct of ϕ_2 in terms of $f'(\eta)$.

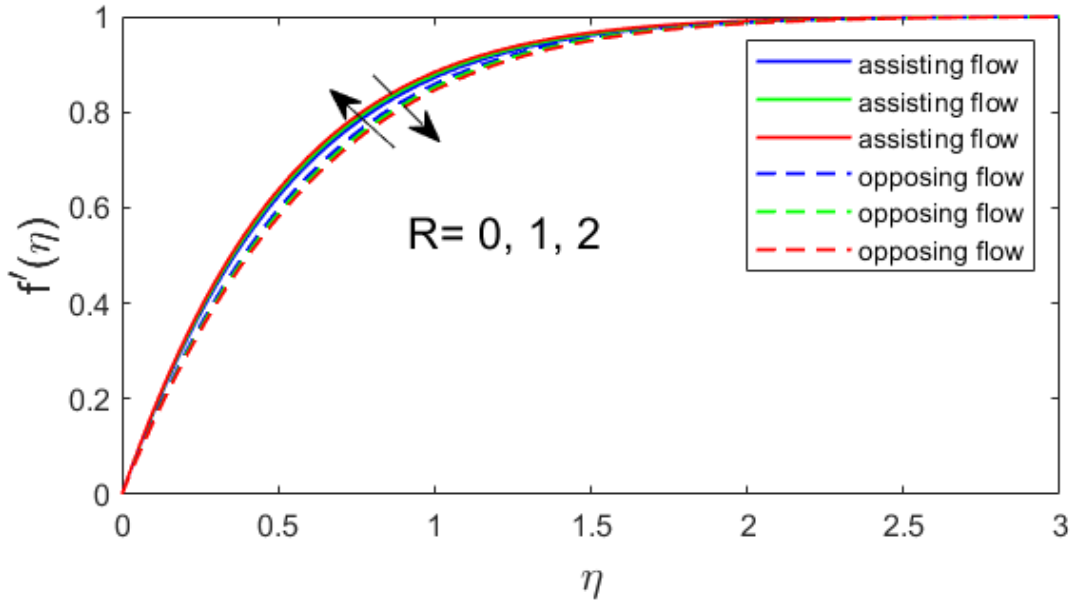

Figure 5.4. Conduct of R in terms of $f'(\eta)$.

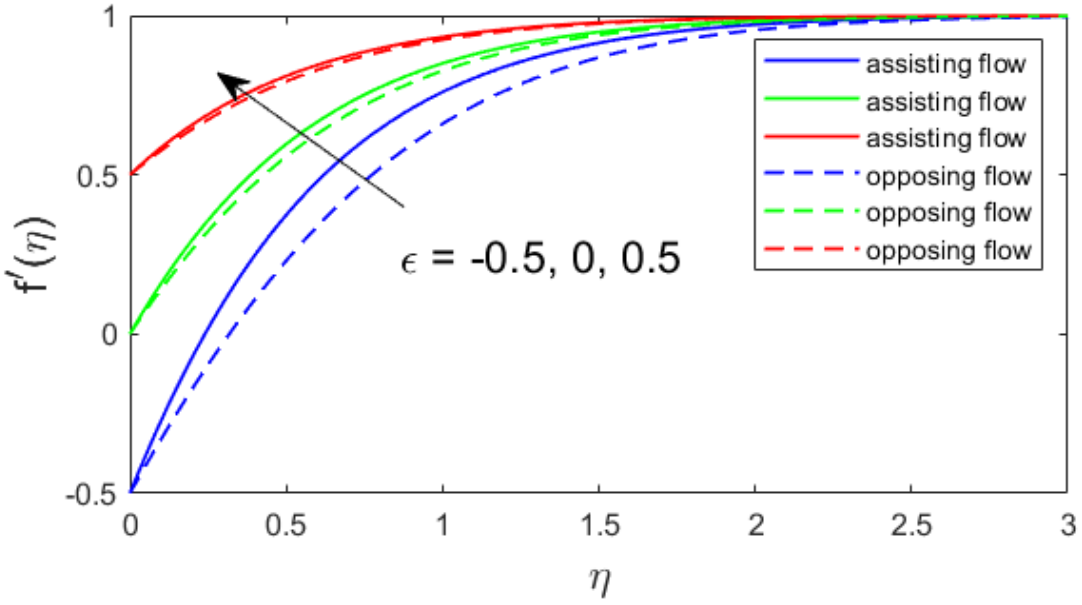

Figure 5.5. Conduct of ϵ in terms of $f'(\eta)$.

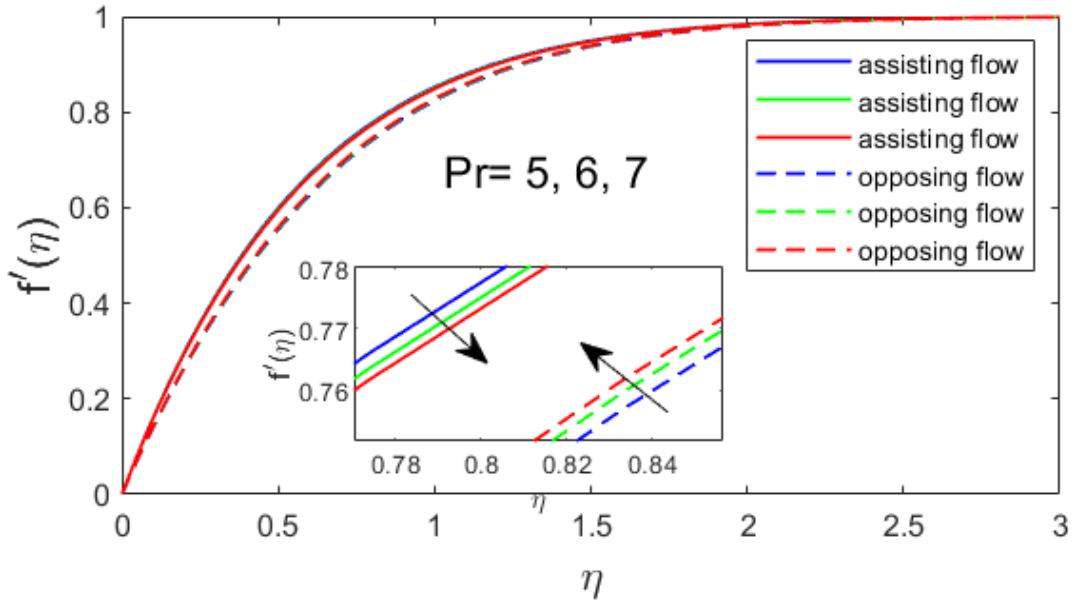

Figure 5.6. Behavior of Pr in terms of $f'(\eta)$.

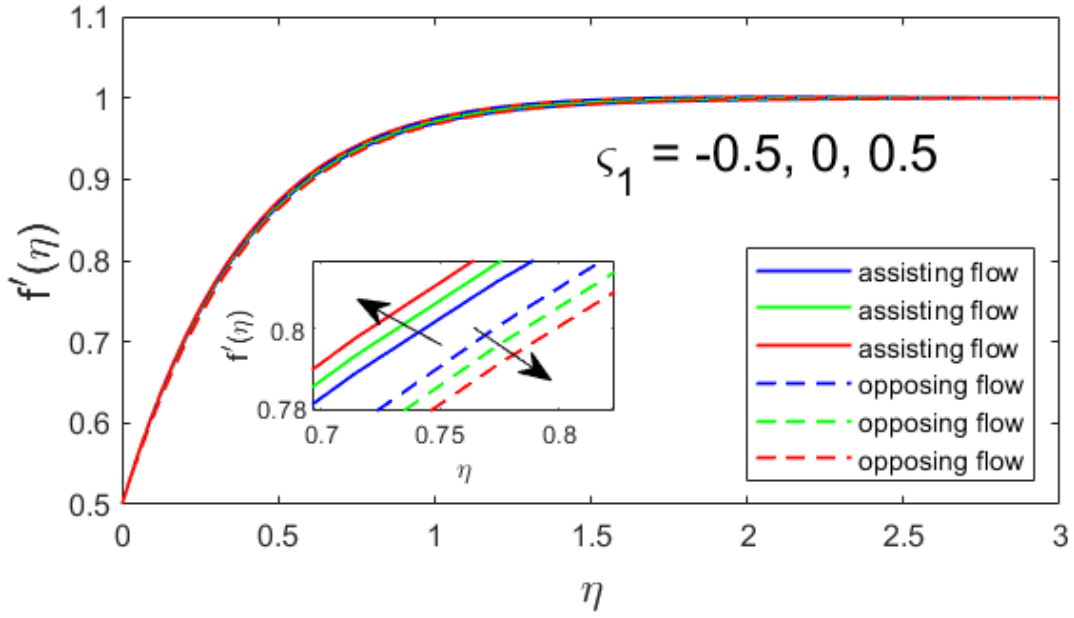

Figure 5.7. Conduct of ς_1 in terms of $f'(\eta)$.

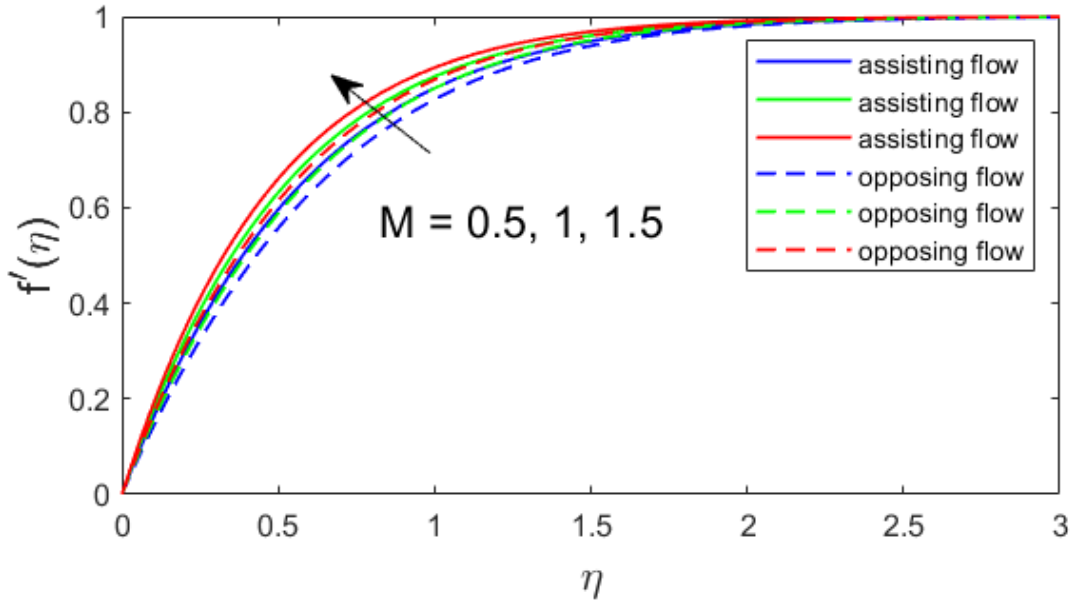

Figure 5.8. Conduct of M in terms of $f'(\eta)$.

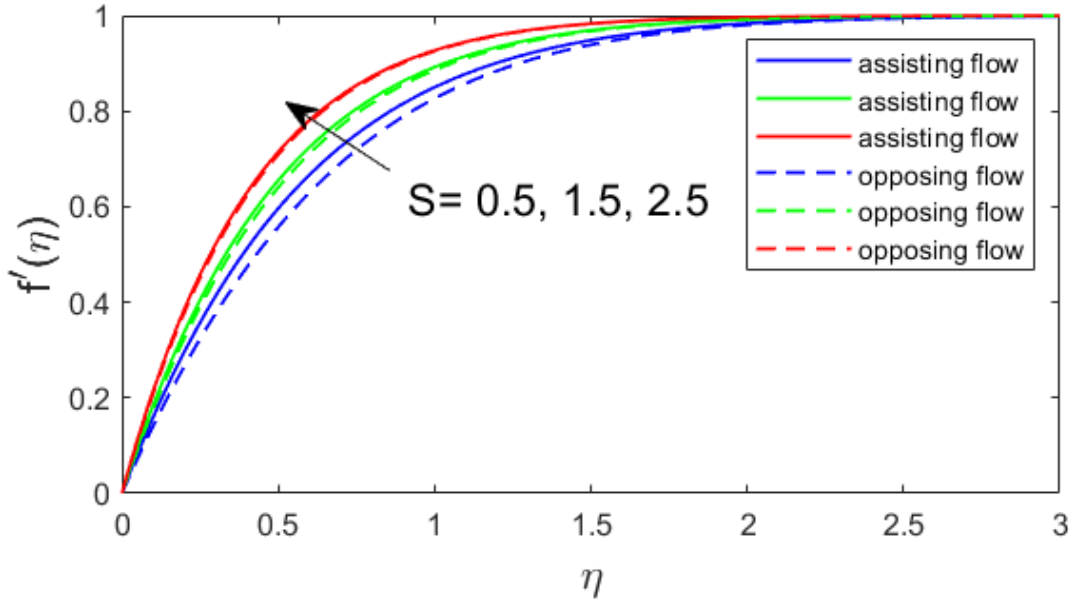

Figure 5.9. Conduct of S in terms of $f'(\eta)$.

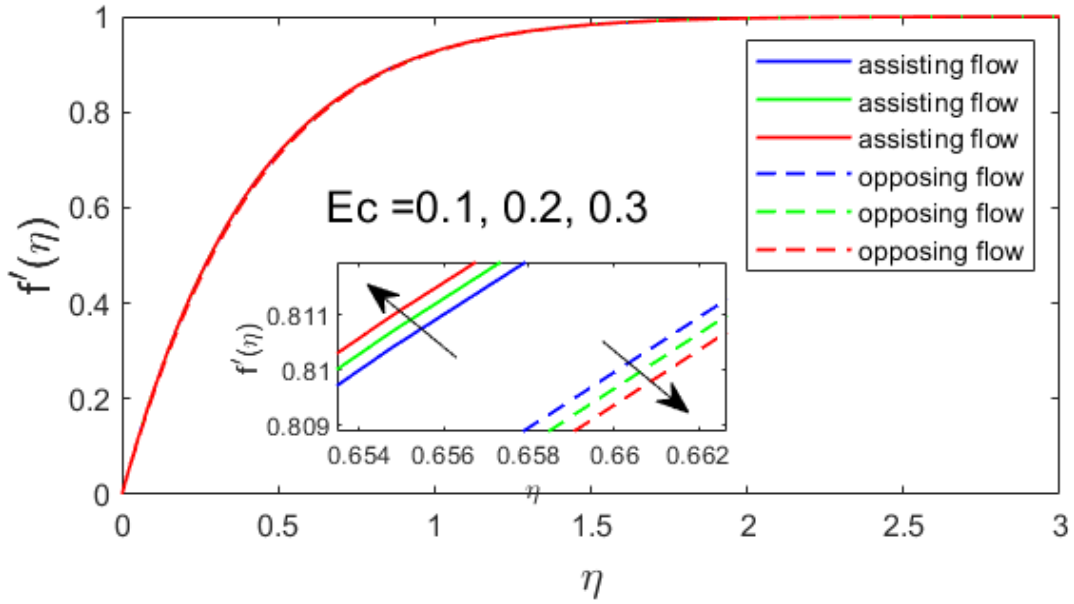

Figure 5.10. Conduct of Ec in terms of $f'(\eta)$.

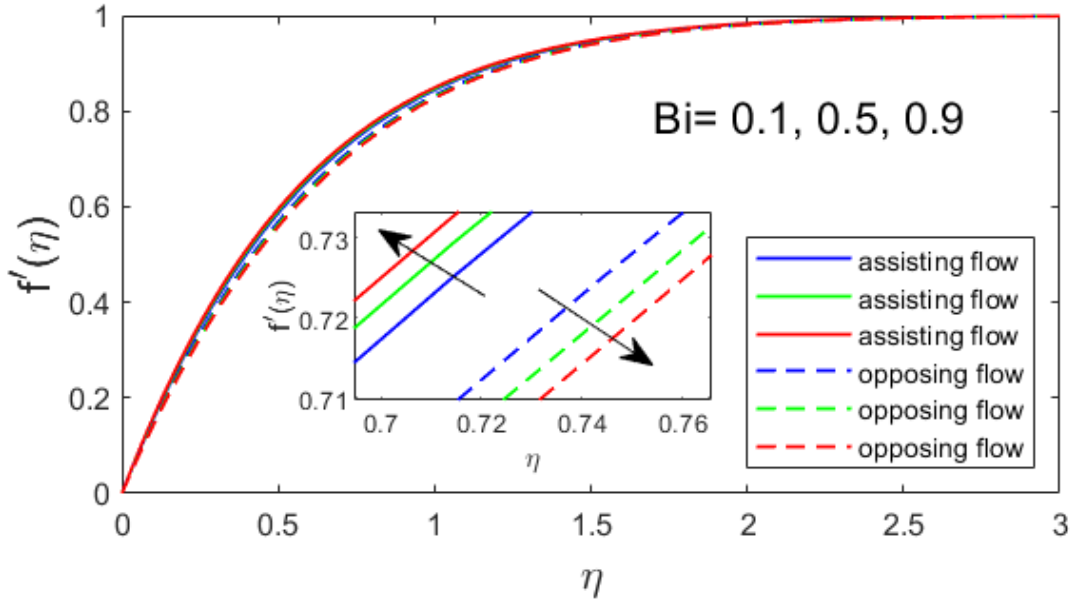

Figure 5.11. Conduct of Bi in terms of $f'(\eta)$.

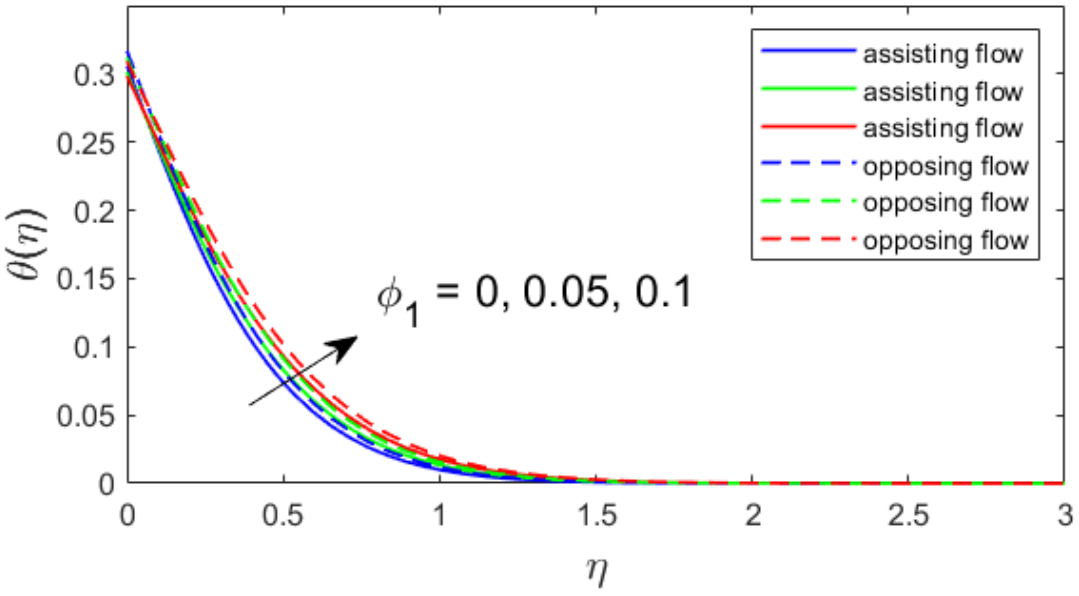

Figure 5.12. Conduct of ϕ_1 in terms of $\theta(\eta)$.

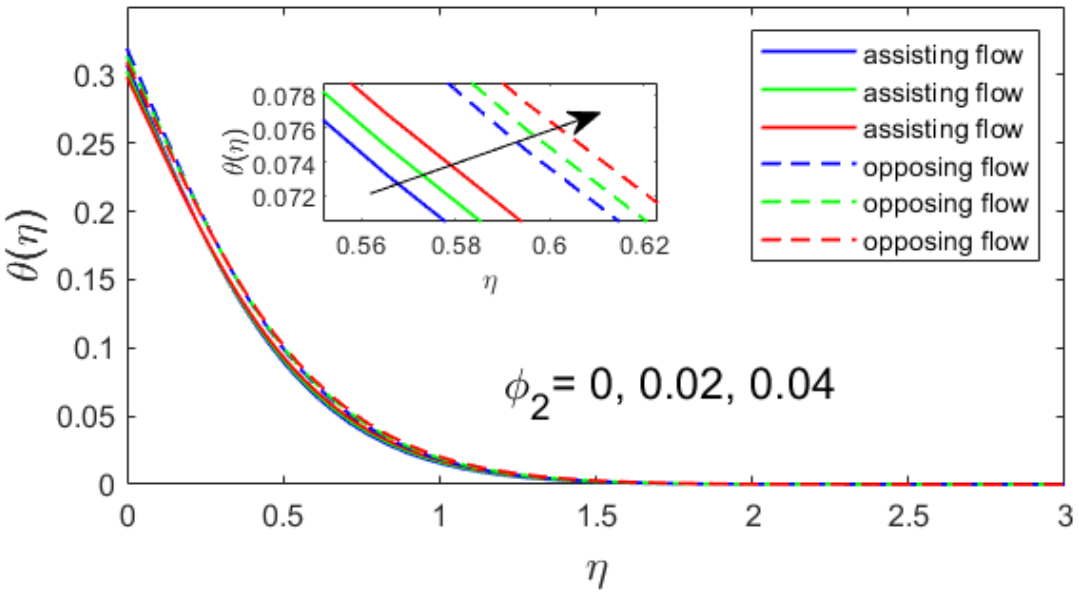

Figure 5.13. Conduct of ϕ_2 in terms of $\theta(\eta)$.

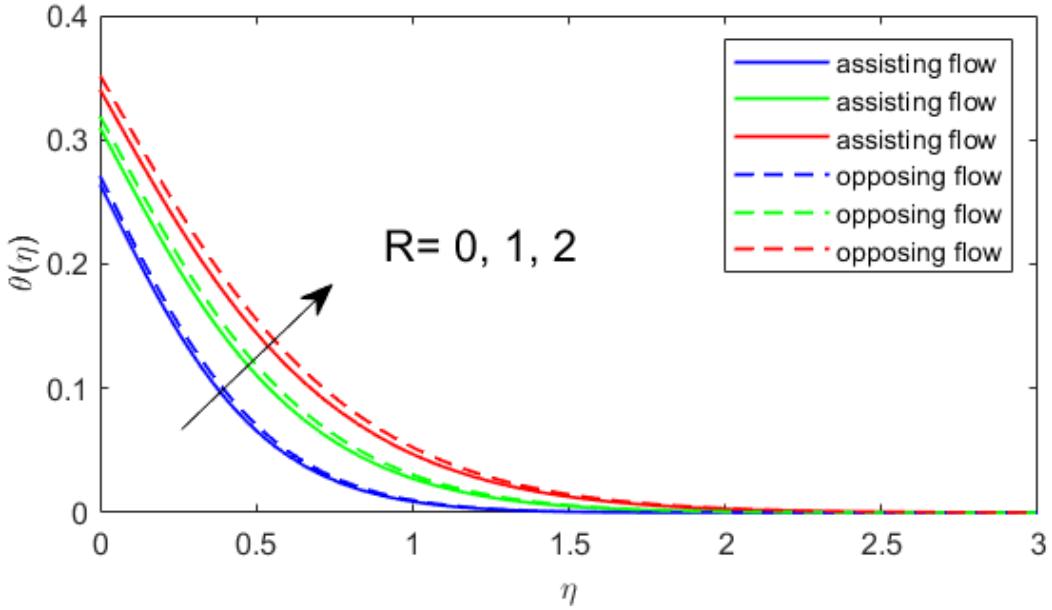

Figure 5.14. Conduct of R in terms of $\theta(\eta)$.

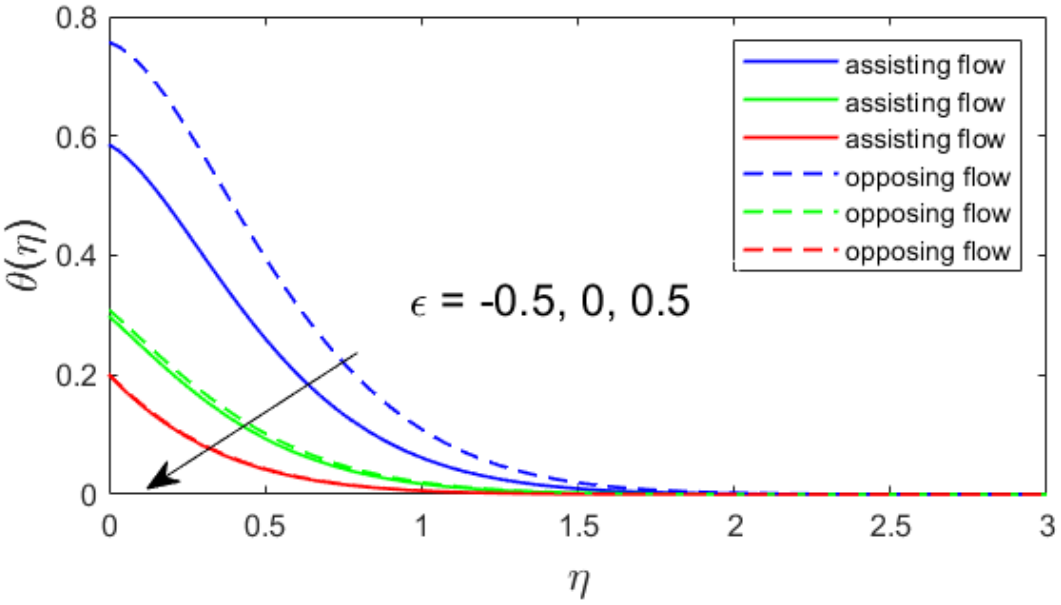

Figure 5.15. Conduct of ε in terms of $\theta(\eta)$.

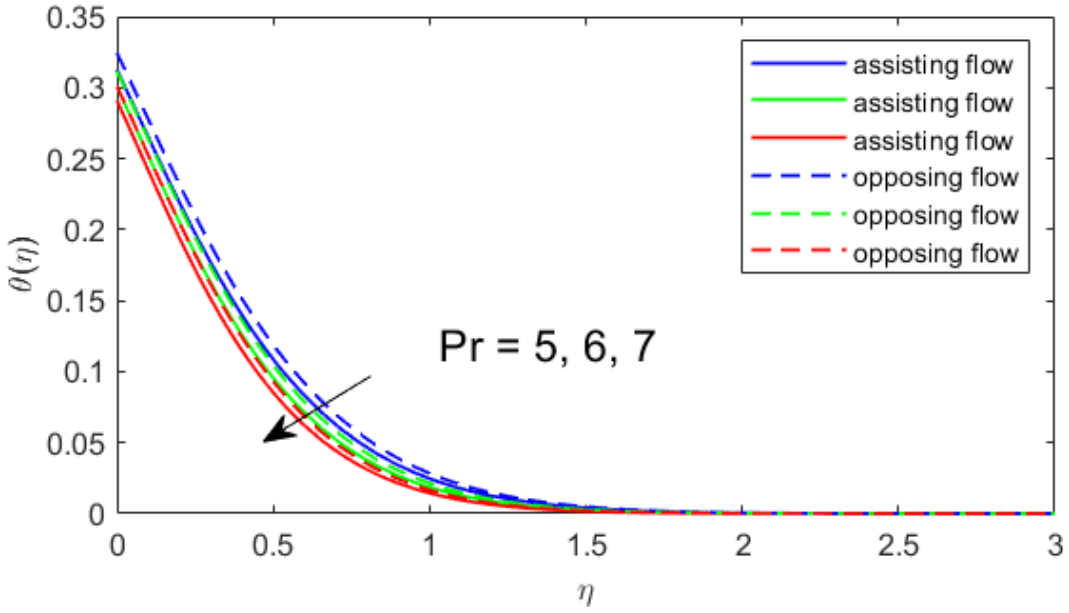

Figure 5.16. Conduct of Pr in terms of $\theta(\eta)$.

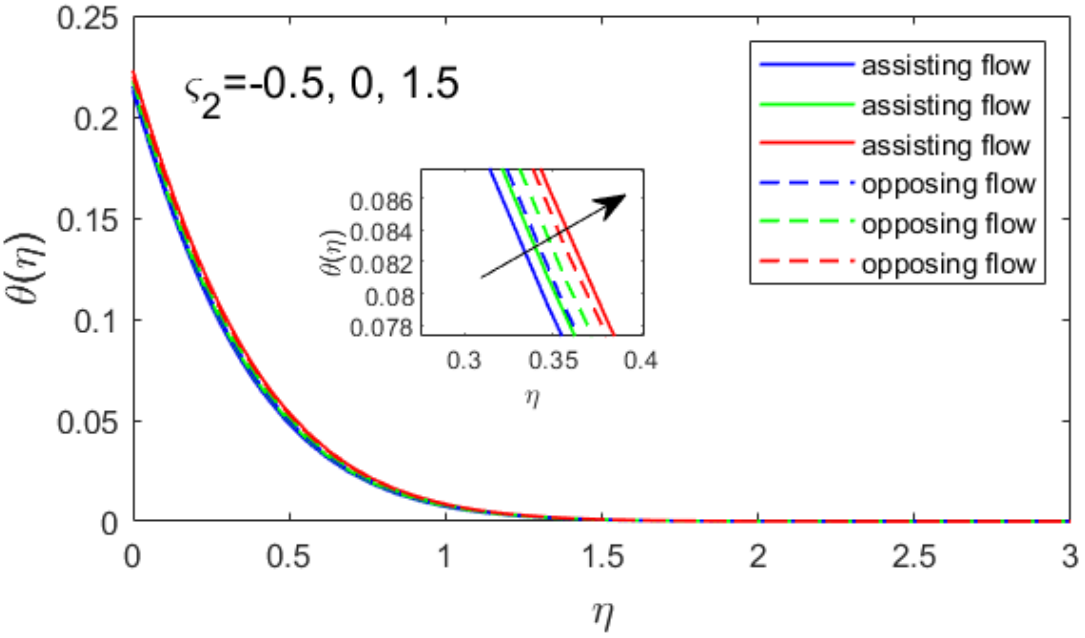

Figure 5.17. Conduct of ς_2 in terms of $\theta(\eta)$.

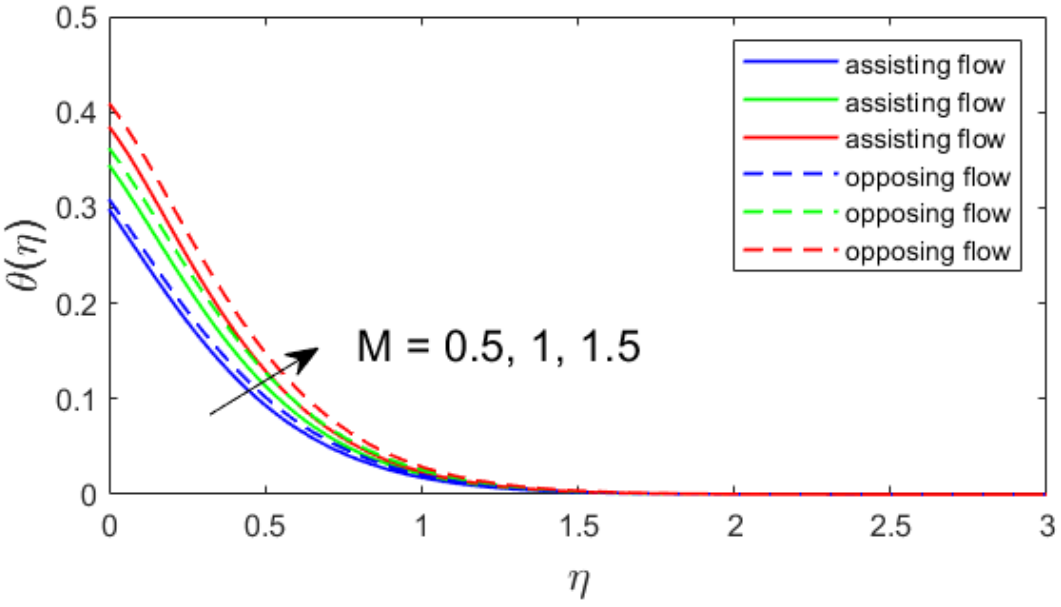

Figure 5.18. Conduct of M in terms of $\theta(\eta)$.

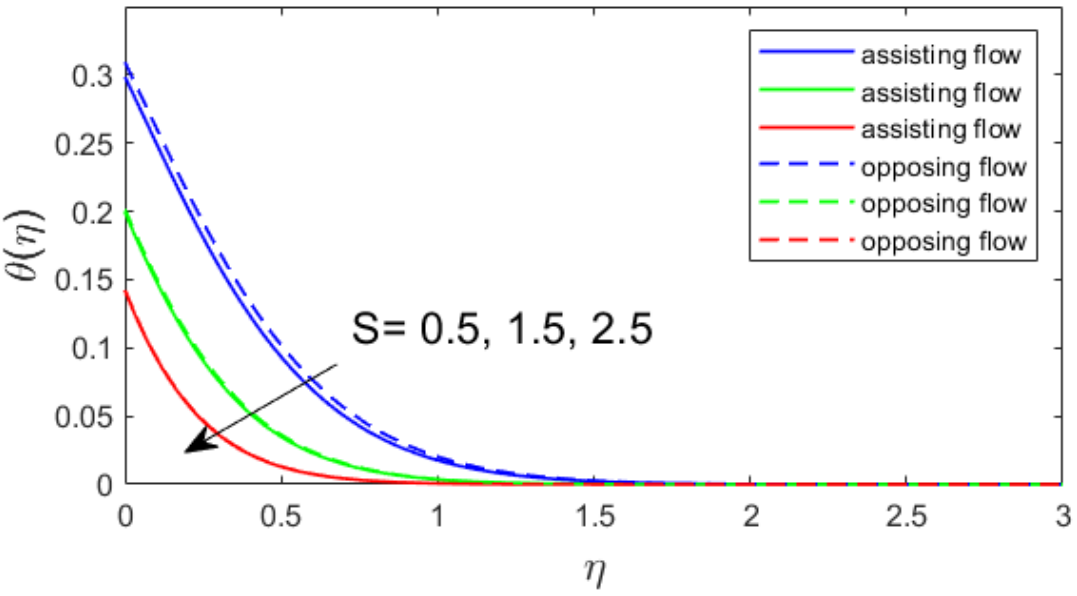

Figure 5.19. Conduct of S in terms of $\theta(\eta)$.

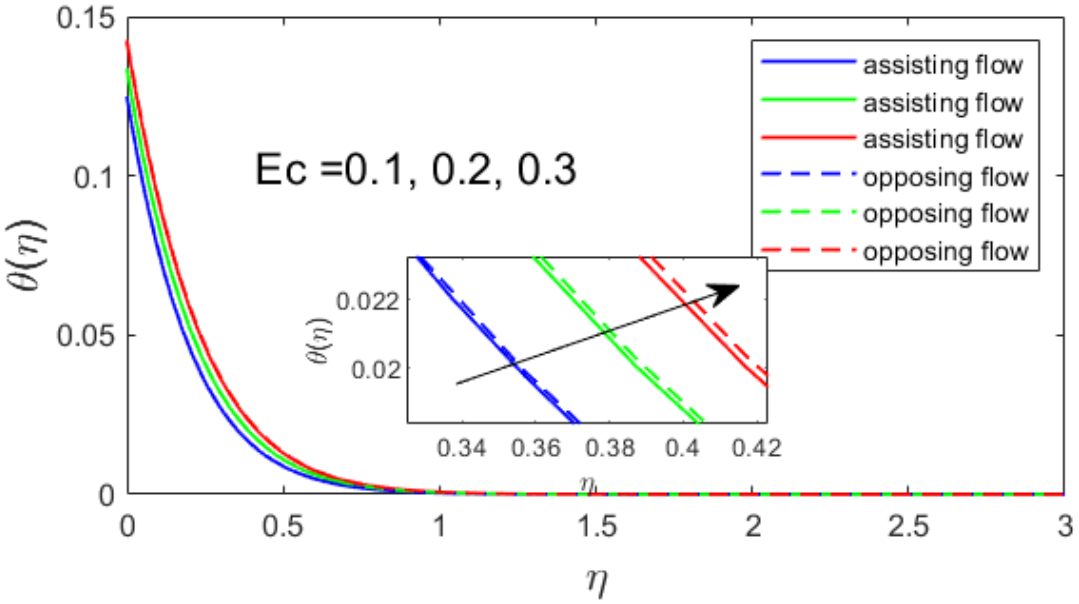

Figure 5.20. Conduct of Ec in terms of $\theta(\eta)$.

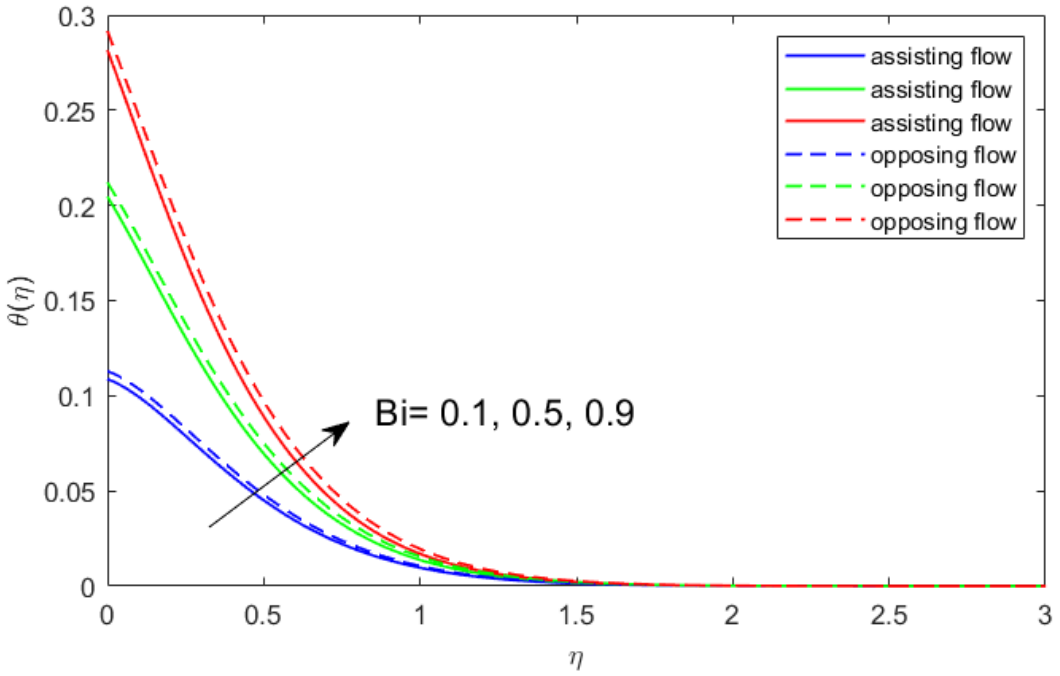

Figure 5.21. Conduct of Bi in terms of $\theta(\eta)$.

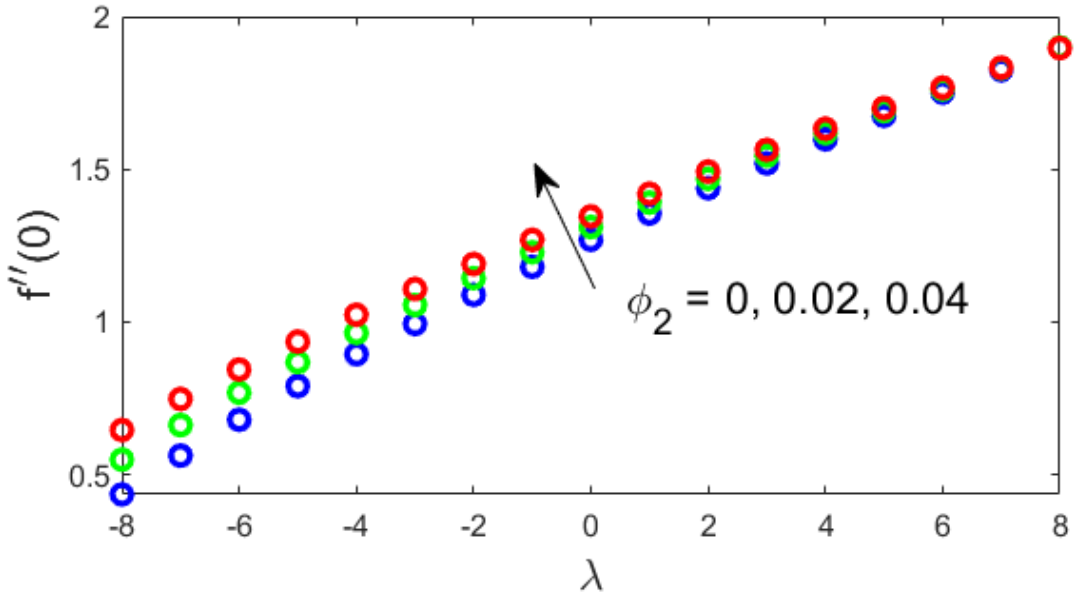

Figure 5.22. Conduct of λ and ϕ_2 in terms of $f''(0)$.

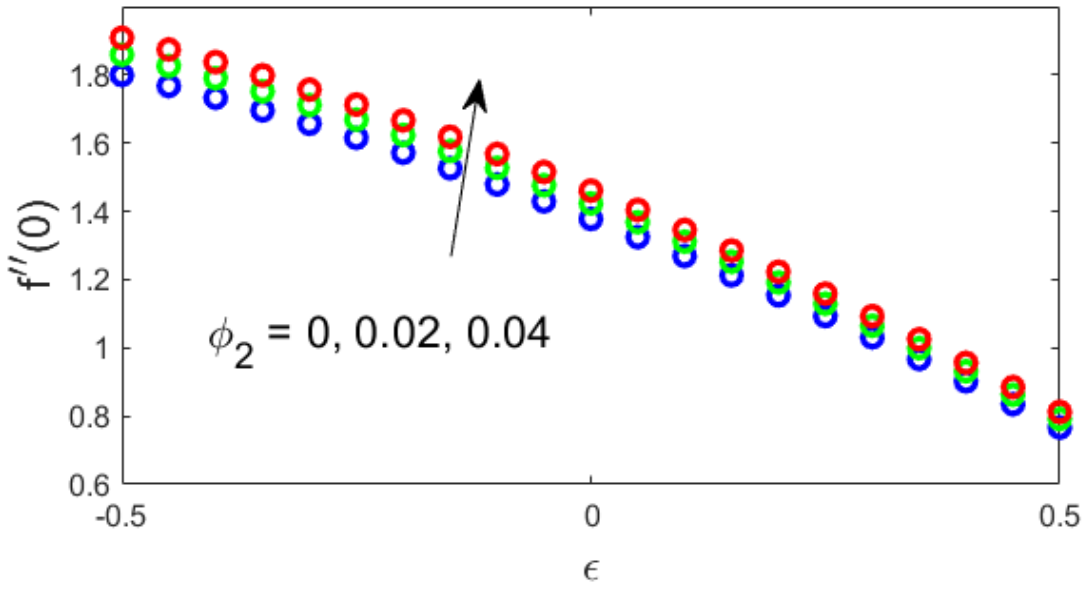

Figure 5.23. Conduct of ϵ and ϕ_2 in terms of $f''(0)$.

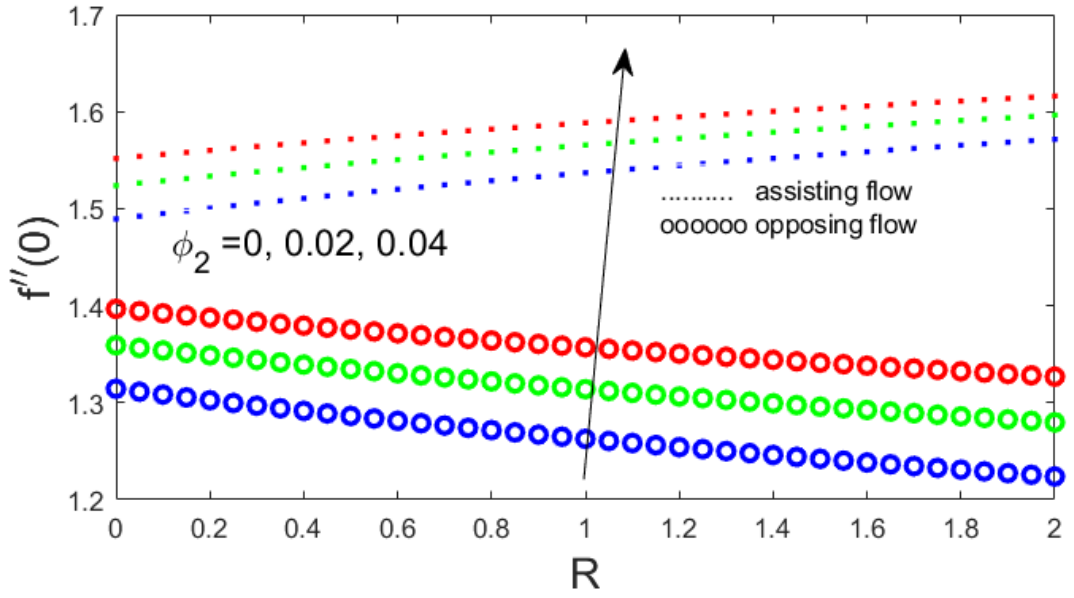

Figure 5.24. Conduct of R and ϕ_2 in terms of $f''(0)$.

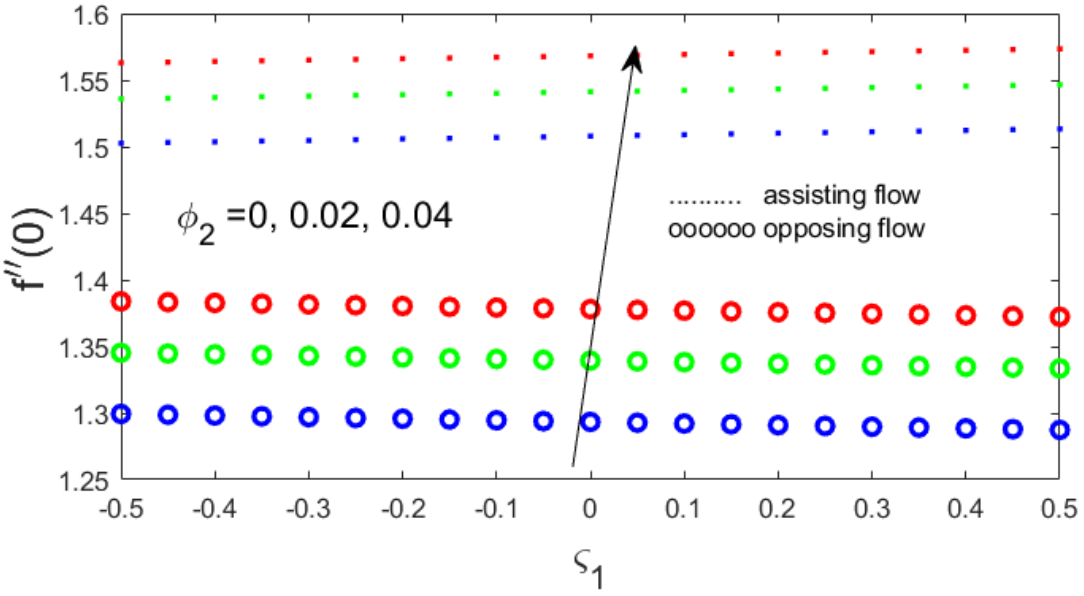

Figure 5.25. Conduct of ς_1 and ϕ_2 in terms of $f''(0)$.

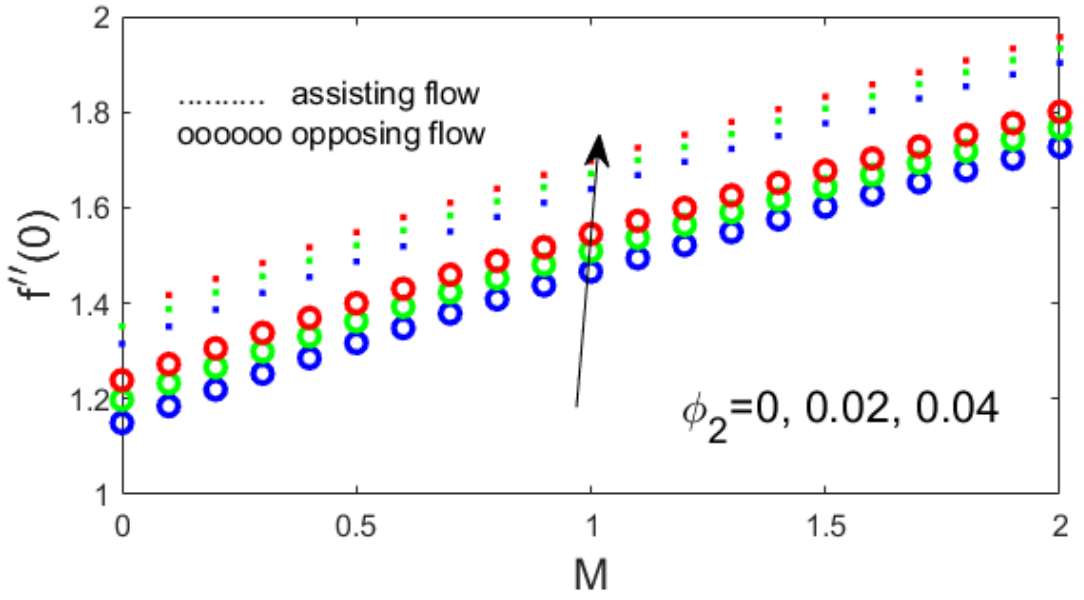

Figure 5.26. Conduct of M and ϕ_2 in terms of $f''(0)$.

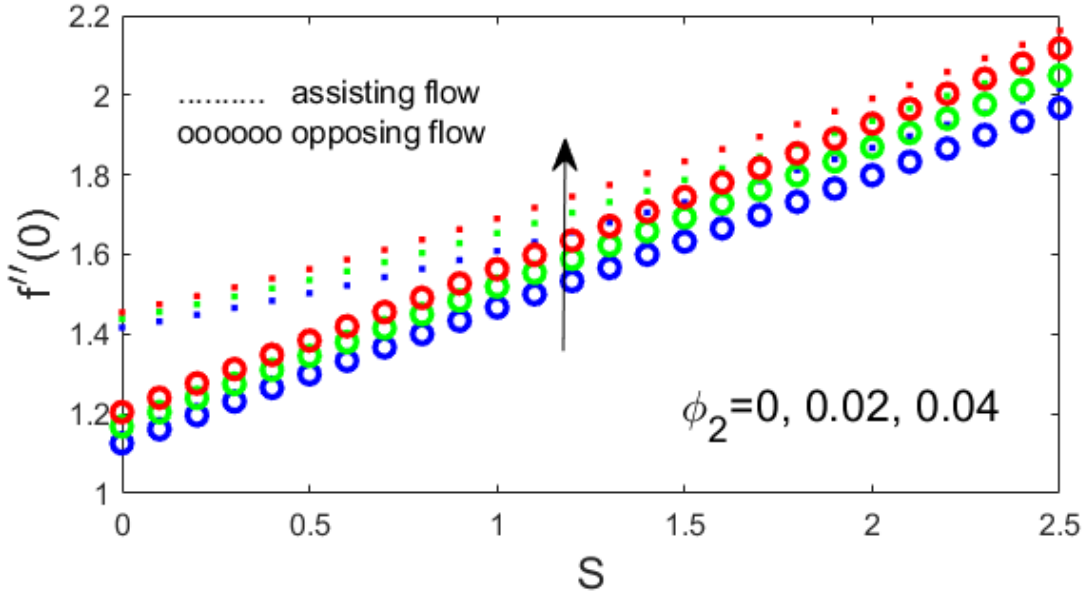

Figure 5.27. Conduct of S and ϕ_2 in terms of $f''(0)$.

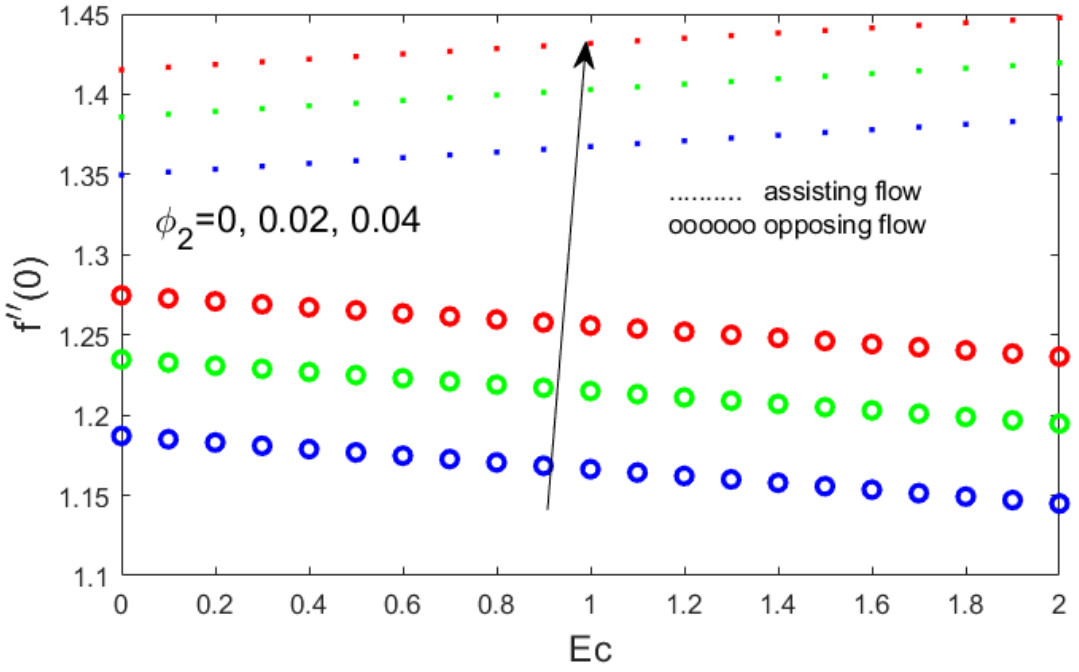

Figure 5.28. Conduct of Ec and ϕ_2 in terms of $f''(0)$.

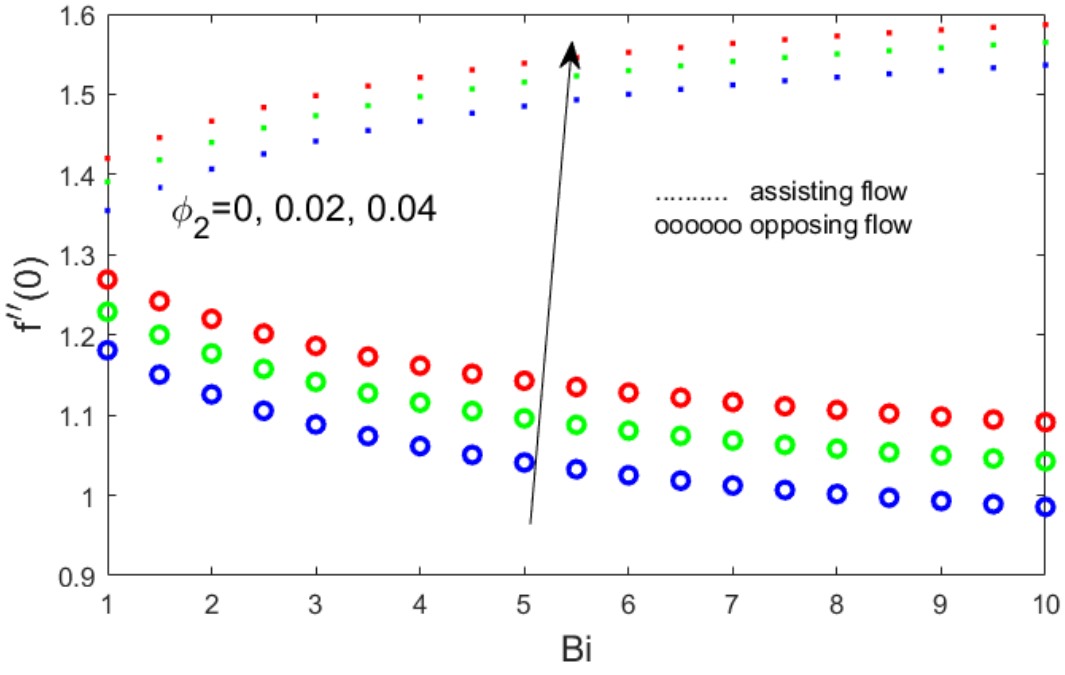

Figure 5.29. Conduct of Bi and ϕ_2 in terms of $f''(0)$.

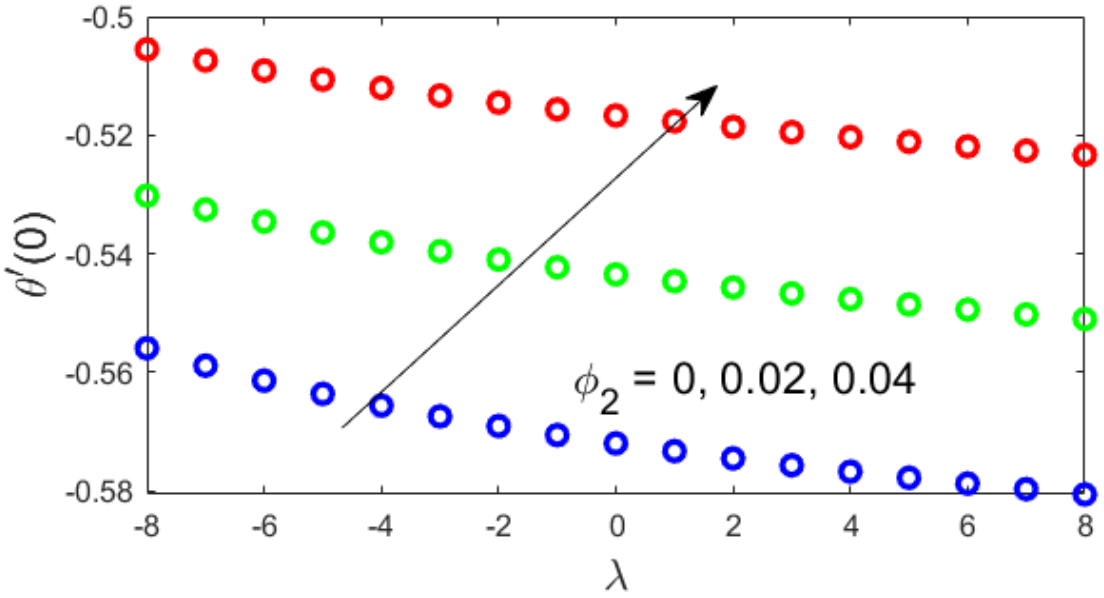

Figure 5.30. Conduct of λ and ϕ_2 in terms of $\theta'(0)$.

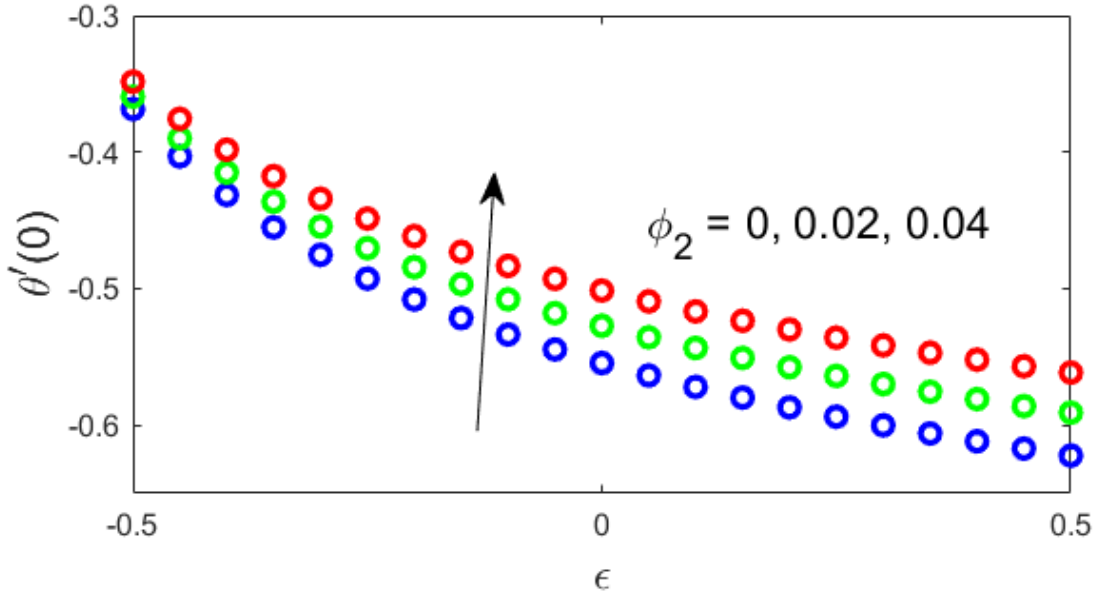

Figure 5.31. Conduct of ϵ and ϕ_2 in terms of $\theta'(0)$.

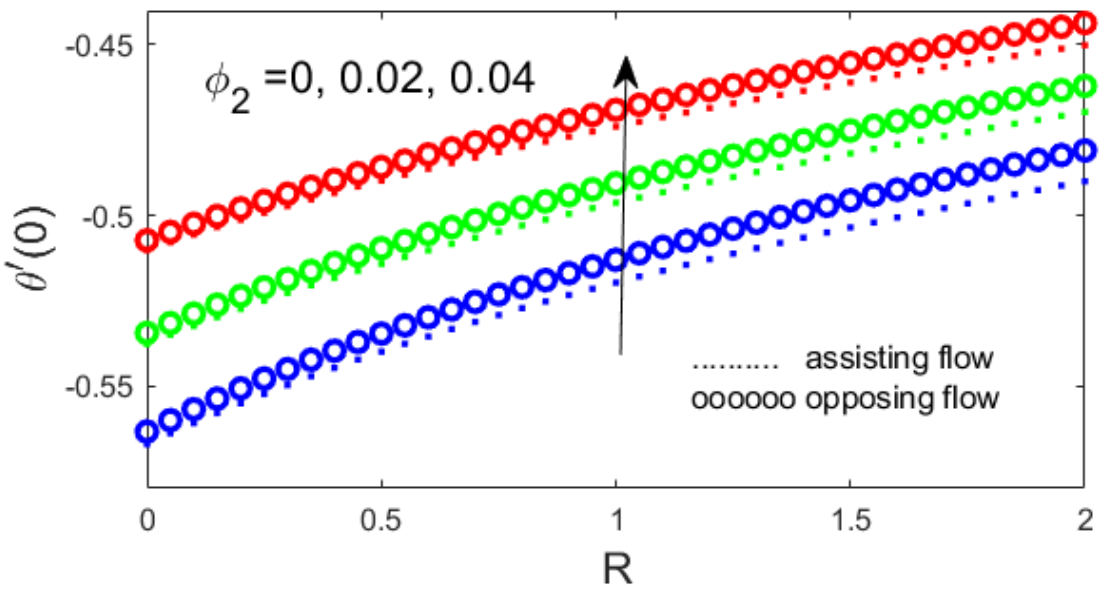

Figure 5.32. Conduct of R and ϕ_2 in terms of $\theta'(0)$.

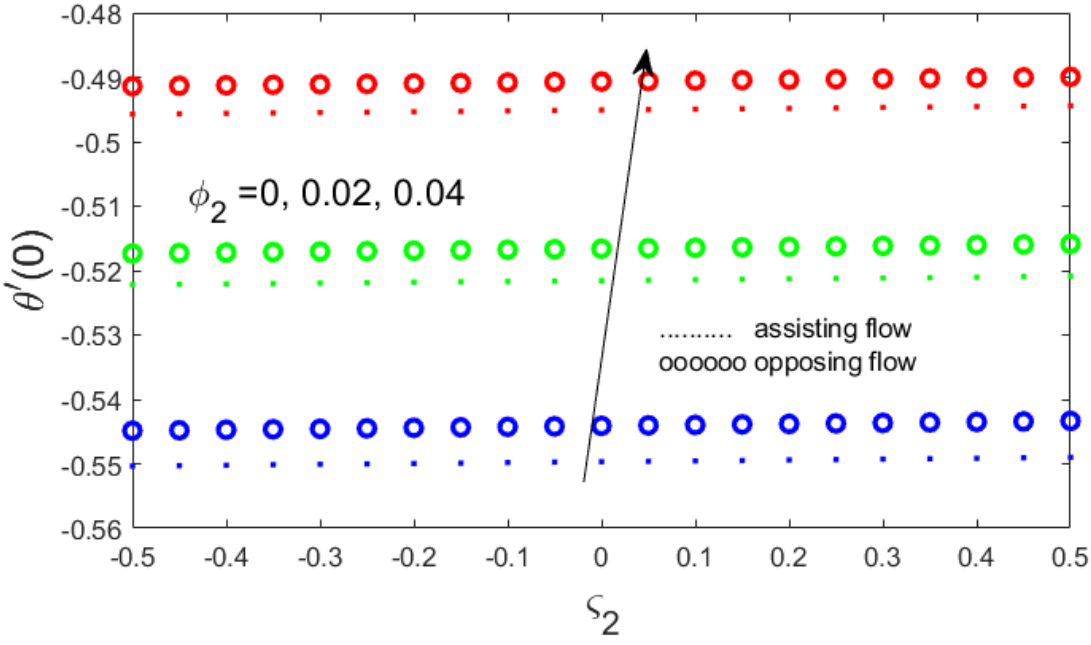

Figure 5.33. Conduct of ς_2 and ϕ_2 in terms of $\theta'(0)$.

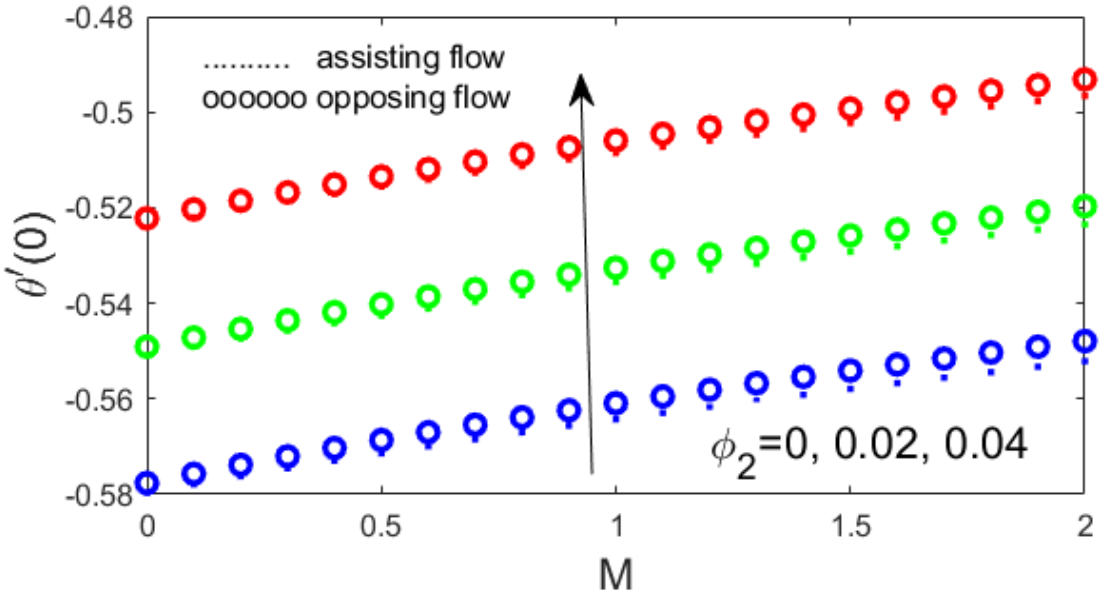

Figure 5.34. Conduct of M and ϕ_2 in terms of $\theta'(0)$.

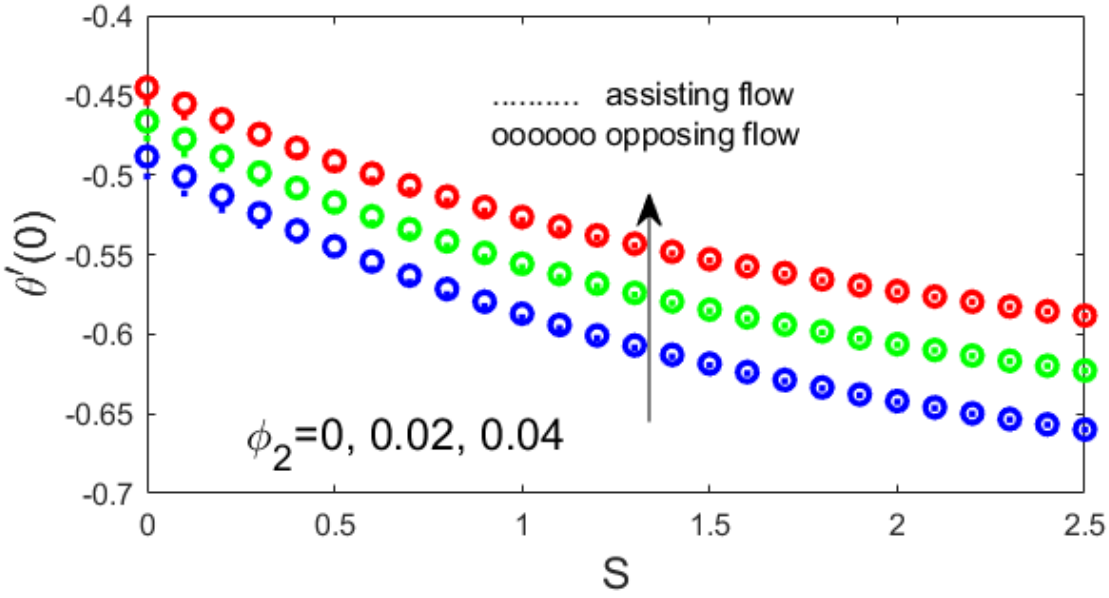

Figure 5.35. Conduct of S and ϕ_2 in terms of $\theta'(0)$.

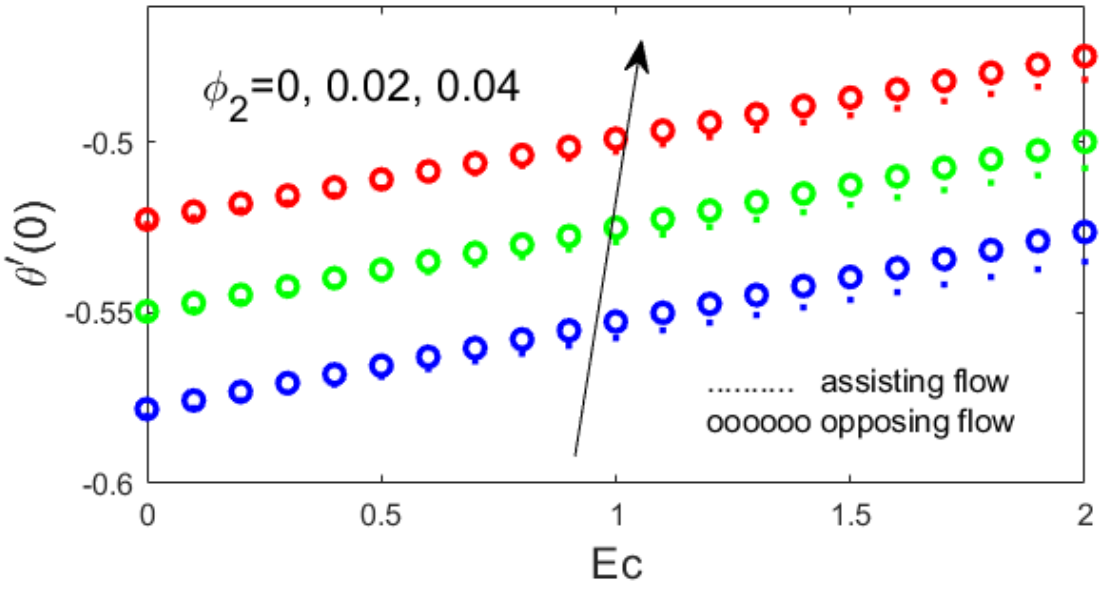

Figure 5.36. Conduct of Ec and ϕ_2 in terms of $\theta'(0)$.

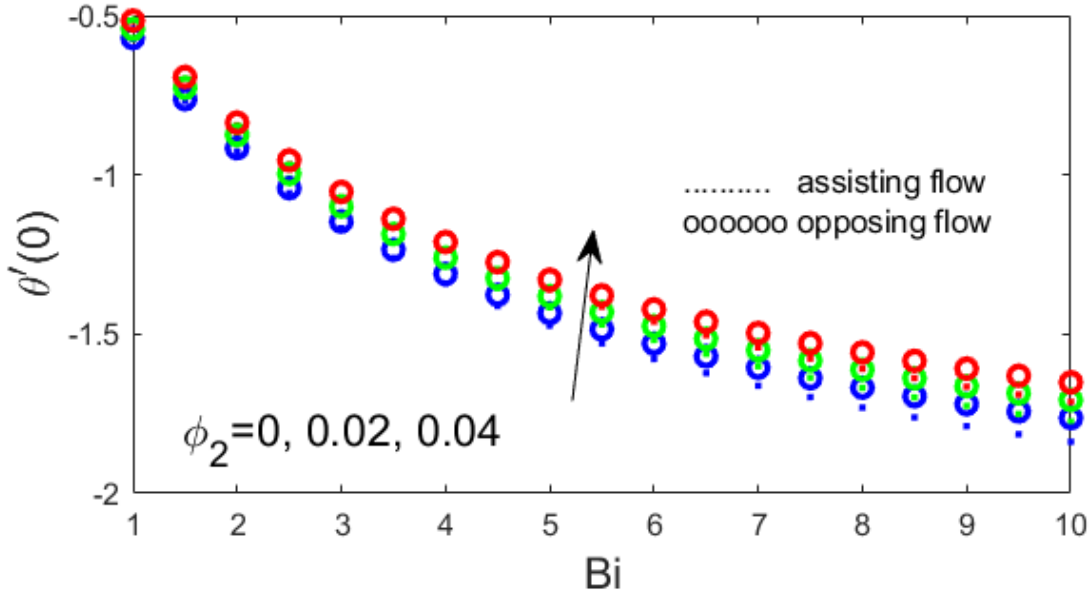

Figure 5.37. Conduct of *Bi* and ϕ_2 in terms of $\theta'(0)$.

Chapter 6

Conclusion and Future work

6.1 Concluded points

The applications and utility of hybrid nanofluids is manifested in numerous fields. The flow of a hybrid nanofluid flowing due to surface in light of magnetohydrodynamics is explored during the study. In order to further enhance the characteristics of flow model, the factors of uneven heat source/sink and thermal radiation are introduced. Initially, the adopted similarity transformations modifies the momentum and energy equations into ODEs. The deliberate solutions to the reformed ODEs have been revealed using the bvp4c. The upshots are obtainable as graphs for f', θ as well as for $f''(0)$ and $\theta'(0)$ using various values of the governing physical parameters. The study points towards useful results after the complete analysis of the considered flow. The velocity distributions is comprehended to upsurge with the elevated values of ϕ_2 and ε and the reverse drift is documented for the raised values of ϕ_2 while considering the supposed cases of opposing and also assisting flows. The assisting as well as the opposing flows reveal contrary trend for the boosted values of R, Pr and ζ_1. The velocity profile intensification is recorded as M values augments for the assisting and opposing flow case. The velocity also upturns for $\lambda = 1$ and also for $\lambda = -1$, as the suction parameter S shoots up. The mounted values of Ec shows opposite trend for the considered cases. $\lambda = 1$ corresponds to an enhancement whereas a decay is confirmed for $\lambda = -1$.The same behavior is noted as the Bi values are chosen to rise. The elevated values of the parameters ϕ_1, ϕ_2, R and ζ_2 supports the temperature distribution for assumed flow cases. The temperature declines with the rising values of M for $\lambda = 1$ and $\lambda = -1$. The temperature profile falls as the S values boost for both considered cases but while considering the boosted Ec values, the converse phenomena is prominent. The improved Bi values have an association with enhanced temperature profile for assisting and also opposing flow kinds. The drag force and also Nusselt number is affected due

to the variation in considered flow parameters. As M values increases, the drag force factor also surges, while the heat transfer rate reduces with both considered flows. The enlarged values of S escalates the drag force factor, however reduces the Nusselt number during both flow categories. The outcome of boosting Ec is dissimilar for the drag force factor in assisting flow and in addition opposing flow, while the Nusselt number cuts down in both cases. As the Bi values upturns, the drag force factor is augmented in assisting flow but declined in opposing flow, the Nusselt number instead amplified in both considered flow cases.

6.2 Future work expectations

The results of employing magnetic field and also thermal radiation for a hybrid nanofluid flowing with respect to a surface which is both permeable and stretching in an exponential trend are displayed in the inquiry. The substantial system of equations expressing the flow model is sought out using bvp4c tool through MATLAB software. The investigation points towards exciting upshots, however, there is still space to extend the current analysis and sightsee advanced results. Few of the thinkable researches are stated below.

- The heat and also mass transfer study for hybrid nanofluid moving due to curved surface.
- The radiative flow of viscoelastic hybrid nanofluid flowing over a rotating sphere by means of Cattaneo Christov model.
- The examination of double stratification for mixed convective flow of hybrid nanofluid moving over circular cylinder.

References

1. Choi, S. U. S. (1995). Enhancing thermal conductivity of fluids with nanoparticles. *Developments and applications of Non-newtonian flows, 231*, 99-105.
2. Turcu, R., Darabont, A., Nan, A., Aldea, N., Macovei, D., Bica, D., & Koos, A. (2006). New polypyrrole-multiwall carbon nanotubes hybrid materials. *Journal of optoelectronics and advanced materials,* 8 (2), 643-647.
3. Jana, S., Salehi-Khojin, A., & Zhong, W. H. (2007). Enhancement of fluid thermal conductivity by the addition of single and hybrid nano-additives. *Thermochimica Acta,* 462 (1), 45-55.
4. Huminic, G., & Huminic, A. (2020). Entropy generation of nanofluid and hybrid nanofluid flow in thermal systems: a review. *Journal of Molecular Liquids, 302*, 112533.
5. Waqas, H., Naqvi, S. M. R. S., Alqarni, M., & Muhammad, T. (2021). Thermal transport in magnetized flow of hybrid nanofluids over a vertical stretching cylinder. *Case Studies in Thermal Engineering*, *27*, 101219.
6. Aghamajidi, M., Yazdi, M., Dinarvand, S. and Pop, I., 2018. Tiwari-Das nanofluid model for magnetohydrodynamics (MHD) natural-convective flow of a nanofluid adjacent to a spinning down-pointing vertical cone. *Propulsion and Power Research*, *7*(1), .78-90.
7. Hiemenz, K. (1911).The Boundary Layer on a Straight Circular Cylinder Immersed in a Uniform Flow of Liquid, *Dingler's Polytechnisches Journal*, 326. 321-410.
8. Fay, J. A., & Riddell, F. R. (1958). Theory of stagnation point heat transfer in dissociated air. *Journal of the Aerospace Sciences, 25*(2), 73-85.
9. Rajeswari, G. K., & Rathna, S. L. (1962). Flow of a particular class of non-Newtonian visco-elastic and visco-inelastic fluids near a stagnation point. *Zeitschrift für angewandte Mathematik und Physik ZAMP, 13*, 43-57.
10. Beard, D., & Walters, K. (1964). *Elastico-viscous boundary-layer flows I. Two-dimensional flow near a stagnation point.* Paper presented at the Mathematical Proceedings of the Cambridge Philosophical Society.
11. Nath, G. (1975). Similar solutions for the incompressible laminar boundary layer with pressure gradient in micropolar fluids. *Rheologica acta, 14*(9), 850-857.

12. Hoogendoorn, C. (1977). The effect of turbulence on heat transfer at a stagnation point. *International Journal of Heat and Mass Transfer, 20*(12), 1333-1338.
13. Nazar, R., Amin, N., Filip, D., & Pop, I. (2004). Stagnation point flow of a micropolar fluid towards a stretching sheet. *International Journal of Non-Linear Mechanics, 39*(7), 1227-1235.
14. Anuar, N., Bachok, N., Arifin, N., Rosali, H., & Pop, I. (2019). *Stagnation-point flow and heat transfer over an exponentially stretching/shrinking sheet in hybrid nanofluid with slip velocity effect: stability analysis.* Paper presented at the Journal of Physics: Conference Series.
15. Khashi'ie, N. S., Md Arifin, N., & Pop, I. (2020). Mixed convective stagnation point flow towards a vertical Riga plate in hybrid Cu-Al_2O_3/water nanofluid. *Mathematics, 8*(6), 912.
16. Kandasamy, R., bt Adnan, N. A., & Mohammad, R. (2018). Nanoparticle shape effects on squeezed MHD flow of water based Cu, Al_2O_3 and SWCNTs over a porous sensor surface. *Alexandria Engineering Journal, 57*(3), 1433-1445.
17. Hussain, A., Hassan, A., Al Mdallal, Q., Ahmad, H., Rehman, A., Altanji, M., & Arshad, M. (2021). Heat transport investigation of magneto-hydrodynamics (SWCNT-MWCNT) hybrid nanofluid under the thermal radiation regime. *Case Studies in Thermal Engineering,* 27, 101244.
18. Khan, S. A., Waqas, H., Muhammad, T., Farooq, U., & Alghamdi, M. (2021). Recent progress in melting phenomenon for magnetized hybrid nanofluid flow over a stretching surface with temperature dependent viscosity: a comparative study. *Journal of Materials Research and Technology,* 15, 3965-3973.
19. Hassan, A., Hussain, A., Arshad, M., Awrejcewicz, J., Pawlowski, W., Alharbi, F. M., & Karamti, H. (2022). Heat and Mass Transport Analysis of MHD Rotating Hybrid Nanofluids Conveying Silver and Molybdenum Di-Sulfide Nano-Particles under Effect of Linear and Non-Linear Radiation. *Energies,* 15 (17), 6269.
20. Babu, M. J., Rao, Y. S., Kumar, A. S., Raju, C. S. K., Shehzad, S. A., Ambreen, T., & Shah, N. A. (2022). Squeezed flow of polyethylene glycol and water based hybrid nanofluid over a magnetized sensor surface: A statistical approach. *International Communications in Heat and Mass Transfer,* 135, 106136.
21. Sulochana, C., & Kumar, T. P. (2022). Regression modelling of hybrid nanofluid flow past an exponentially stretching/shrinking surface with heat source-sink effect. *Materials Today: Proceedings,* 54, 669-676.

22. Neethu, T. S., Sabu, A. S., Mathew, A., Wakif, A., & Areekara, S. (2022). Multiple linear regression on bioconvective MHD hybrid nanofluid flow past an exponential stretching sheet with radiation and dissipation effects. *International Communications in Heat and Mass Transfer*, 135, 106115.
23. Mustafaa, M., Hayat, T., & Obaidat, S. (2013). Boundary layer flow of a nanofluid over an exponentially stretching sheet with convective boundary conditions. *International Journal of Numerical Methods for Heat & Fluid Flow, 23*(6), 945-959.
24. Nadeem, S., Haq, R. U., & Khan, Z. H. (2014). Heat transfer analysis of water-based nanofluid over an exponentially stretching sheet. *Alexandria Engineering Journal, 53*(1), 219-224.
25. Ghalambaz, M., Roşca, N. C., Roşca, A. V., & Pop, I. (2020). Mixed convection and stability analysis of stagnation-point boundary layer flow and heat transfer of hybrid nanofluids over a vertical plate. *International Journal of Numerical Methods for Heat & Fluid Flow, 30*(7), 3737-3754.
26. Jamaludin, A., Naganthran, K., Nazar, R., & Pop, I. (2020). MHD mixed convection stagnation-point flow of Cu-Al_2O_3/water hybrid nanofluid over a permeable stretching/shrinking surface with heat source/sink. *European Journal of Mechanics-B/Fluids, 84*, 71-80.
27. Wahid, N. S., Md Arifin, N., Khashi'ie, N. S., Pop, I., Bachok, N., & Hafidzuddin, M. E. H. (2022). MHD mixed convection flow of a hybrid nanofluid past a permeable vertical flat plate with thermal radiation effect. *Alexandria Engineering Journal*, 61 (4), 3323-3333.
28. Khan, N. W., Khan, A., Usman, M., Gul, T., Mouldi, A., & Brahmia, A. (2022). Influences of Marangoni convection and variable magnetic field on hybrid nanofluid thin-film flow past a stretching surface. *Chinese Physics B,* 31 (6), 064403.
29. Yoo, D.-H., Hong, K., & Yang, H.-S. (2007). Study of thermal conductivity of nanofluids for the application of heat transfer fluids. *Thermochimica Acta, 455*(1-2), 66-69.
30. Chamkha, A. J., Dogonchi, A., & Ganji, D. (2019). Magneto-hydrodynamic flow and heat transfer of a hybrid nanofluid in a rotating system among two surfaces in the presence of thermal radiation and Joule heating. *AIP Advances, 9*(2), 025103.
31. Waqas, H., Farooq, U., Liu, D., Abid, M., Imran, M., & Muhammad, T. (2022). Heat transfer analysis of hybrid nanofluid flow with thermal radiation through a stretching

sheet: A comparative study. *International Communications in Heat and Mass Transfer,* 138, 106303.

32. Mahabaleshwar, U. S., Vishalakshi, A. B., & Andersson, H. I. (2022). Hybrid nanofluid flow past a stretching/shrinking sheet with thermal radiation and mass transpiration. *Chinese Journal of Physics,* 75, 152-168.
33. Salahuddin, T., Khan, M., Sakinder, S., & Al Alwan, B. (2022). A flow analysis of hybrid nanoparticles near a solid sphere. *International Journal of Hydrogen Energy,* 47 (37), 16640-16648.
34. Yasir, M., Hafeez, A., & Khan, M. (2022). Thermal conductivity performance in hybrid (SWCNTs-CuO/Ehylene glycol) nanofluid flow: Dual solutions. *Ain Shams Engineering Journal,* 13 (5), 101703.
35. Yahaya, R. I., Arifin, N. M., Nazar, R. M., & Pop, I. (2021). Oblique Stagnation-Point Flow Past a Shrinking Surface in a Cu-Al_2O_3/H_2O Hybrid Nanofluid. *Sains Malaysiana, 50*(10), 3139-3152.
36. Hussain, A., Alshbool, M. H., Abdussattar, A., Rehman, A., Ahmad, H., Nofal, T. A., & Khan, M. R. (2021). A computational model for hybrid nanofluid flow on a rotating surface in the existence of convective condition. *Case Studies in Thermal Engineering, 26*, 101089.
37. Othman, M. N., Jedi, A., & Bakar, N. A. A. (2021). MHD Flow and Heat Transfer of Hybrid Nanofluid over an Exponentially Shrinking Surface with Heat Source/Sink. *Applied Sciences, 11*(17), 8199.
38. Wahid, N. S., Arifin, N. M., Khashi'ie, N. S., Pop, I., Bachok, N., & Hafidzuddin, M. E. H. (2021). Flow and heat transfer of hybrid nanofluid induced by an exponentially stretching/shrinking curved surface. *Case Studies in Thermal Engineering, 25*, 100982.
39. Chu, Y.-M., Khan, M. I., Abbas, T., Sidi, M. O., Alharbi, K. A. M., Alqsair, U. F., Malik, M. (2022). Radiative thermal analysis for four types of hybrid nanoparticles subject to non-uniform heat source: Keller box numerical approach. *Case Studies in Thermal Engineering, 40*, 102474.
40. Khashi'ie, N. S., Waini, I., Wahid, N. S., Arifin, N. M., & Pop, I. (2023). Unsteady separated stagnation point flow due to an EMHD Riga plate with heat generation in hybrid nanofluid. *Chinese Journal of Physics, 81*, 181-192.
41. Chakraborty, T., Duari, P. R., & Acharya, N. (2023). Unfolding flow features of MHD hybrid nanofluid (Ag–Al_2O_3–H_2O) and mono nanofluid (Al_2O_3–H_2O) flow over exponentially expanded sheet soaked in a Darcy–Forchheimer absorbent medium co-

existing non-uniform heat generation/absorption. *Waves in Random and Complex Media*, 1-28.

42. Arani, A. A. A., & Aberoumand, H. (2021). Stagnation-point flow of Ag-CuO/water hybrid nanofluids over a permeable stretching/shrinking sheet with temporal stability analysis. *Powder Technology, 380*, 152-163.
43. Teh, Y. Y., & Ashgar, A. (2021). Three dimensional MHD hybrid nanofluid Flow with rotating stretching/shrinking sheet and Joule heating. *CFD Letters, 13*(8), 1-19.
44. Abbasi, A., Gul, M., Farooq, W., Khan, S. U., Aydi, A., Ayadi, B., Kolsi, L. (2022). A comparative thermal investigation for modified hybrid nanofluid model (Al_2O_3–SiO_2–TiO_2)/($C_2H_6O_2$) due to curved radiated surface. *Case Studies in Thermal Engineering, 37*, 102295.
45. Alqahtani, P. Hashim, Rehman, S., Kainat, Alshehery, S., (2023). Computional method for energy transport of MHD nanofluids flow near non-aligned stagnation point with non-linear thermal radiation and interface slip. *Results in Engineering*, 101383.
46. Sarfraz, M., Khan, M., Al-Zubaidi, A., & Saleem, S. (2023). Enhancing energy transport in Homann stagnation-point flow over a spiraling disk with ternary hybrid nanofluids. *Case Studies in Thermal Engineering*, 103134.
47. Aly, E. H., Roşca, A. V., Roşca, N. C., & Pop, I. (2021). Convective Heat Transfer of a Hybrid Nanofluid over a Nonlinearly Stretching Surface with Radiation Effect. *Mathematics, 9*(18), 2220.
48. Kumar, G. V., Rehman, K. U., Kumar, R., & Shatanawi, W. (2022). Unsteady magnetohydrodynamic nanofluid flow over a permeable exponentially surface manifested with non-uniform heat source/sink effects. *Waves in Random and Complex Media*, 1-19.
49. Unyong, B., Vadivel, R., Govindaraju, M., Anbuvithya, R., & Gunasekaran, N. (2022). Entropy analysis for ethylene glycol hybrid nanofluid flow with elastic deformation, radiation, non-uniform heat generation/absorption, and inclined Lorentz force effects. *Case Studies in Thermal Engineering, 30*, 101639.
50. Joshi, N., Upreti, H., & Pandey, A. K. (2022). MHD Darcy-Forchheimer Cu-Ag/H_2O-$C_2H_6O_2$ hybrid nanofluid flow via a porous stretching sheet with suction/blowing and viscous dissipation. *International Journal for Computational Methods in Engineering Science and Mechanics*, 1-9.
51. Khan, M. R., Mao, S., Deebani, W., & Elsiddieg, A. M. (2022). Numerical analysis of heat transfer and friction drag relating to the effect of Joule heating, viscous dissipation

and heat generation/absorption in aligned MHD slip flow of a nanofluid. *International Communications in Heat and Mass Transfer, 131*, 105843.

52. Babu, K. S. S., Parandhama, A., & Vijaya, R. B. (2022). Significance of heat source/sink on the radiative flow of Cross nanofluid across an exponentially stretching surface towards a stagnation point with chemical reaction. *Heat Transfer, 51*(4), 2885-2904.
53. Elattar, S., Helmi, M. M., Elkotb, M. A., El-Shorbagy, M. A., Abdelrahman, A., Bilal, M., & Ali, A. (2022). Computational assessment of hybrid nanofluid flow with the influence of hall current and chemical reaction over a slender stretching surface. *Alexandria Engineering Journal, 61*(12), 10319-10331.
54. Haq, I., Yassen, M. F., Ghoneim, M. E., Bilal, M., Ali, A., & Weera, W. (2022). Computational Study of MHD Darcy Forchheimer Hybrid Nanofluid Flow under the Influence of Chemical Reaction and Activation Energy over a Stretching Surface. *Symmetry, 14*(9), 1759.
55. Hansda, S., & Pandit, S. K. (2023). Thermosolutal hydromagnetic mixed convective hybrid nanofluid flow in a wavy walled enclosure. *Journal of Magnetism and Magnetic Materials, 572*, 170580.
56. Mamun, M. A. H., Prince, H. A., & Siam, M. M. H. (2023). Variations of MHD double-diffusive mixed convection and entropy generation in various nanofluids and hybrid nanofluids due to the deviation of the spinning of double rotating cylinders. *International Journal of Thermofluids, 20*, 100421.
57. Lone, S. A., Al-Essa, L. A., Al Bossly, A., Alduais, F. S., Eldin, S. M., & Saeed, A. (2023). Electrically conducting mixed convective flow of a hybrid nanoliquid over a rotating sphere with nonlinear thermal radiation. *Case Studies in Thermal Engineering*, 103165.
58. Wang, F., Khan, S. A., Khan, M. I., El-Zahar, E. R., Yasir, M., Nofal, T. A., & Malik, M. (2022). Thermal conductivity performance in propylene glycol-based Darcy-Forchheimer nanofluid flow with entropy analysis. *Journal of Petroleum Science and Engineering, 215*, 110612.
59. Zainal, N. A., Nazar, R., Naganthran, K., & Pop, I. (2022). Unsteady stagnation point flow past a permeable stretching/shrinking Riga plate in Al_2O_3-Cu/H_2O hybrid nanofluid with thermal radiation. *International Journal of Numerical Methods for Heat & Fluid Flow, 32*(8), 2640-2658.

60. Wahid, N. S., Arifin, N. M., Khashi'ie, N. S., & Pop, I. (2023). Mixed convection MHD hybrid nanofluid over a shrinking permeable inclined plate with thermal radiation effect. *Alexandria Engineering Journal, 66*, 769-783.
61. Arif, M., Kumam, P., Watthayu, W., & Di Persio, L. (2023). The proportional Caputo operator approach to the thermal transport of Jeffery tri-hybrid nanofluid in a rotating frame with thermal radiation. *Scientific Reports, 13*(1), 13802.
62. Pritchard, P. J., & Mitchell, J. W. (2016). *Fox and McDonald's introduction to fluid mechanics*: John Wiley & Sons.
63. Bansal, R. (2005). *A textbook of fluid mechanics*: Firewall Media.
64. Schetz, J. A., & Fuhs, A. E. (1999). *Fundamentals of fluid mechanics*: John Wiley & Sons.
65. Bansal, R. (2005). *A textbook of fluid mechanics and hydraulic machines:(in SI units)*: LAXMI Publications, Ltd.
66. Logan, D. L. (2022). *First Course in the Finite Element Method, Enhanced Edition, SI Version*: Cengage Learning.
67. Ahmed, J., & Rahman, M. S. (2012). *Handbook of food process design, 2 Volume Set*: John Wiley & Sons.
68. Fox, R. W., McDonald, A., & Pitchard, P. (2006). Introduction to fluid mechanics, 2004: John Wiley & Sons, Inc.
69. Reddy, J. N., & Gartling, D. K. (2010). *The finite element method in heat transfer and fluid dynamics*: CRC press.
70. Kunes, J. (2012). *Dimensionless physical quantities in science and engineering*: Elsevier.
71. Yahaya, R. I., Md Arifin, N., & Mohamed Isa, S. S. P. (2018). Stability analysis on magnetohydrodynamic flow of casson fluid over a shrinking sheet with homogeneous-heterogeneous reactions. *Entropy, 20*(9), 652.
72. Shampine, L., Gladwell, I., & Thompson, S. (2003). ODEs with MATLAB: Cambridge.
73. Waini, I., Ishak, A., & Pop, I. (2019). Hybrid nanofluid flow and heat transfer over a nonlinear permeable stretching/shrinking surface. *International Journal of Numerical Methods for Heat & Fluid Flow, 29*(9), 3110-3127.
74. Devi, S. A., & Devi, S. S. U. (2016). Numerical investigation of hydromagnetic hybrid Cu–Al_2O_3/water nanofluid flow over a permeable stretching sheet with suction.

International Journal of Nonlinear Sciences and Numerical Simulation, 17(5), 249-257.

75. Polu, B. A. R., & Reddy, S. (2020). Impact of thermal radiation and viscous dissipation on hydromagnetic unsteady flow over an exponentially inclined preamble stretching sheet. *Journal of Computational & Applied Research in Mechanical Engineering (JCARME), 10*(1), 171-181.
76. Waini, I., Ishak, A., & Pop, I. (2020a). Mixed convection flow over an exponentially stretching/shrinking vertical surface in a hybrid nanofluid. *Alexandria Engineering Journal, 59*(3), 1881-1891.
77. Waini, I., Ishak, A., & Pop, I. (2020b). Squeezed hybrid nanofluid flow over a permeable sensor surface. *Mathematics, 8*(6), 898.
78. Bachok, N., Ishak, A., & Pop, I. (2012). Boundary layer stagnation-point flow and heat transfer over an exponentially stretching/shrinking sheet in a nanofluid. *International Journal of Heat and Mass Transfer, 55*(25-26), 8122-8128.
79. Waini, I., Ishak, A., Pop, I., (2021). Hybrid nanofluid flow towards a stagnation point on an exponentially stretching/shrinking vertical sheet with buoyancy effects. *International Journal of Numerical Methods Heat Fluid Flow* 31, 216–235.
80. Rahman, M., Ferdows, M., Shamshuddin, M., Koulali, A., & Eid, M. R. (2022). Aiding (opponent) flow of hybrid copper–aluminum oxide nanofluid towards an exponentially extending (lessening) sheet with thermal radiation and heat source (sink) impact. *Journal of Petroleum Science and Engineering, 215*, 110649.
81. Alarifi, I. M., Abokhalil, A. G., Osman, M., Lund, L. A., Ayed, M. B., Belmabrouk, H., & Tlili, I. (2019). MHD flow and heat transfer over vertical stretching sheet with heat sink or source effect. *Symmetry, 11*(3), 297.
82. Sarfraz, M., Yasir, M., & Khan, M. (2023). Multiple solutions for non-linear radiative mixed convective hybrid nanofluid flow over an exponentially shrinking surface. *Scientific Reports, 13*(1), 3443.
83. Ahmad, S., Ali, K., Rizwan, M., & Ashraf, M. (2021). Heat and mass transfer attributes of copper–aluminum oxide hybrid nanoparticles flow through a porous medium. *Case Studies in Thermal Engineering, 25*, 100932.
84. Waini, I., Ishak, A., & Pop, I. (2021). Flow towards a stagnation region of a vertical plate in a hybrid nanofluid: Assisting and opposing flows. *Mathematics, 9*(4), 448.

85. Dulikravich, G., & Lynn, S. (1997). Unified Electro-Magneto-Fluid Dynamics (EMFD). A Survey of Mathematical Models. *International Journal of non-linear Mechanics*,32(5), 923-932